Engineering post-infarct extracellular matrix remodeling *in vitro* for understanding cardiac fibroblast fate and function

Peter Kim

A dissertation

Submitted in partial fulfillment of the

Requirements for the degree of

Doctor of Philosophy

University of Washington

2019

Reading Committee:

Deok-Ho Kim, Chair

Jennifer Davis Co-Chair

Michael Regnier

Program Authorized to Offer Degree:

Department of Bioengineering

University of Washington

Abstract

Engineering post-infarct extracellular matrix remodeling *in vitro* for understanding cardiac fibroblast fate and function

Peter Kim

Chair of the Supervisory Committee:

Associate Professor : Deok-Ho Kim, Ph.D.

Assistant Professor : Jennifer Davis, Ph.D.

Department of Bioengineering

Myocardial fibrosis is associated with vast majority of cardiovascular diseases which is one of the most common disease afflicting adults around the world. During myocardial infarction, myocytes die and are replaced by a specialized fibrotic extracellular matrix (ECM), otherwise known as scarring. The transdifferentiation to myofibroblasts is essential for wound healing of the heart. This cell type influences the secretion of cytokines, deposition of extracellular matrix proteins, structural support, and filling of the mechanical load caused by myocyte necrosis. However, the fibrosis influenced by myofibroblasts can lead to progressive heart failure. Fibrotic scarring presents a tremendous hemodynamic burden on the heart, as it creates a stiff substrate which resists diastolic filling. Fibrotic mechanisms result in permanent scarring which often leads to

hypertrophy, arrhythmias, and a rapid progression to failure. Despite the deep understanding of fibrosis in other tissues, acquired through previous investigations, the mechanisms of cardiac fibrosis remain unclear. Recent studies suggest that biochemical cues as well as mechanical cues regulate cells in myocardium. However, the steps in myofibroblast transdifferentiation, as well as the molecular mechanisms of such transdifferentiation *in vivo* are poorly understood. This dissertation is focused on addressing the limited understanding of myofibroblast transdifferentiation cues and pathways that transduce those cues for cellular response, especially those mechanical in nature. Previously p38 has been reported to govern cardiac myofibroblast fate in response to various cues such as TGFβ, substrate stiffness, and mechanical stretch. We investigated the myofibroblast fate regulation through p38 in response to topographic cue. Moreover, YAP was known to lend itself to heart regeneration and myofibroblast phenotype. In this dissertation, we show that p38 and YAP are also responsible for transducing mechanical signals related to topography and works in conjunction to tensin 1 to regulate transdifferentiation to myofibroblast. These results help to elucidate the pathway by which mechanical cues are transduced, leading to transdifferentiation. This study has addressed the limited understanding of myofibroblast transdifferentiation by identifying the novel topographic regulation and pathways that transduce such signals. Taken together, this research demonstrates the utility of bioengineering strategies to develop *in vitro* platforms to better understand the mechanism of cardiac fibrosis which would aid in discovering solutions to assist patients with hearts affected by fibrosis.

Table of Contents

List of Figures viivii

List of Tables ix

Chapter 1. Introduction 1

1.1 Myocardial remodeling during cardiac fibrosis 1

1.2 Cellular origins of cardiac fibrosis 3

1.3 Microenvironmental cardiac scar mechanics 6

1.4 Mechanical stress underlies fibroblast to myofibroblast differentiation 9

1.5 Substrate stiffness regulate myofibroblast fate 12

1.6 Matrix topography regulates myofibroblast fate 15

1.7 Unmet Needs and Future Perspectives 17

1.8 Dissertation Overview and Significance 19

Chapter 2. Development of Anisotropic Nanopatterned Substrates with Tunable Mechanical Characteristics Enhance the Cellular Alignment 20

2.1 Rationale 20

2.2 Scientific Methods 22

2.3 Results 27

2.4 Discussion 45

Chapter 3. Nanopatterned Human iPSC-based Model of a Dystrophin-Null Cardiomyopathic Phenotype 49

3.1 Rationale 49

3.2 Scientific Methods 50

3.3 Results....53
3.4 Discussion....56
Chapter 4. Combinatorial Maturation (ComboMat) Strategy for hPSC-CMs....58
4.1 Rationale....58
4.2 Scientific Methods....59
4.3 Results....61
4.4 Discussion....66
Chapter 5. Mature Cardiac DMD Model and Phenotypic Drug Screen....67
5.1 Rationale....67
5.2 Scientific Methods....69
5.3 Results....71
5.4 Discussion....77
Chapter 6. Summary and Future Directions....79
References....83

List of Figures

Figure 1.1. Illustration of cardiac fibrosis development..... 3

Figure 1.2. Myofibroblast characteristics during myocardial fibrosis..... 6

Figure 1.3. Extracellular matrix composition is remodeled post-infarction. 8

Figure 1.4. Myofiber and collagen direction is remodeled during cardiac fibrosis..... 8

Figure 1.5. Myofibroblast transdifferentiation is mechanically regulated..... 12

Figure 1.6. Schematic illustration of signaling pathways regulating fibroblast transdifferentiation into myofibroblast through mechanoregulation..... 19

Figure 2.1. Fabrication of nanopatterned PEG-GelMA substrates 28

Figure 2.2. Stiffness profile of various ratios of PEGDMA and GelMA 29

Figure 2.3. Degradation profile of various ratios of PEGDMA and GelMA..... 31

Figure 2.4. Enhanced cell adhesion on unpatterned and nanopatterned PEGDMA-GelMA composite and ability to reach confluency 32

Figure 2.5. Effect of nanostructures and the various compositions of PEGDMA and GelMA on cell morphology..... 34

Figure 2.6. Guided and enhanced HUVEC migratory behavior on nanopatterned PEG-GelMA substrates..... 36

Figure 2.7. Nanoengineered platform regulate vSMC differentiation. 38

Figure 2.8. Real time PCR analysis of vSMA-secreted inflammatory markers when cultured on the different substrates..... 39

Figure 2.9. Immunocytochemical analyses of the actin cytoskeleton 40

Figure 2.10. RhoA upregulation, along with the upregulation of the Rho-kinases 43

Figure 2.11. Yap/Taz nuclear localization is altered by nanopatterning and knockout of syndecan-1 44

Figure 3.1. Illustration of cardiac infarct matrix geometry during fibrosis.. 54

Figure 3.2. MEF cell culture on topographic platforms 56

Figure 4.1. Fibroblast proliferation and transdifferentiation are regulated by topographic cues 63

Figure 4.2. ECM secretion and synthesis are regulated by topographic cues 65

Figure 5.1. Topographic cues are transduced via p38 and YAP 74

Figure 5.2. Topographic cues are sensed through tensin 1 in focal adhesion complex 76

Figure 5.3. Schematics of mechanosensing of topographic cues for myofibroblast transdifferentiation 79

List of Tables

Table 1.1. Primer Sequence used for RT-PCR (5’ to 3’)..... 27

Acknowledgements

The research presented in this dissertation was the result of the devotion, support, and mentorship of many wonderful people I encountered during my graduate study. Firstly, I would like to thank Dr. Deok-Ho Kim for supervising me throughout my graduate studies even starting as an undergraduate intern, when I decided to pursue PhD after bachelor. Dr. Kim's support and encouragement to challenge myself with research vision even during struggling times has brought me to be able to reach this stage of study. His unwavering support throughout my time in the lab allowed me to design and develop new strategies to answer bioengineering questions. Secondly, I would like to thank Dr. Jennifer Davis whom equally supervised me with great ideas and superb mentorship. Without guidance of Dr. Davis, I would not have been able to dive deep into the field of cardiac engineering and explore cutting edge models of fibrosis. Dr. Davis' close supervision has enriched my rudimentary cardiac fibrosis background and allowed a bridging between bioengineering techniques and cardiac biology. I would also like to thank the esteemed members of my supervisory committee for all of their wisdom and tutelage: Dr. Michael Regnier, and Dr. Young Kwon. Also, I would like to thank all collaborators who helped me along the way and through the years. Kim Lab: Alex Jiao, Alec Smith, Jesse Macadangdang, Jonathan Tsui, Joy Su, Nisa Penland, Travis Moerk, Sam Frankel, Ki-Hwan Nam, Kshitiz Gupta, Eunpyo Choi, Koichiro Uto, Jongsub Choi, Changho Chun, Alex Yuan, Kevin Mun, and Nick Chiu. Davis Lab: Jagadambika J Gunaje, Emily Olszewski, Guy Wallace Everett, Darrian N Bugg, Danny El-Nachef, Kristin A. Zabrecky, Ross Bretherton, and Galina Flint.

Finally, I would like to thank my family and friends whose love and support kept me sane and allowed me to enjoy the most memorable times of my life in graduate school. I would like give special thanks to my wife, Soomin Song, who provided unlimited amount of support during good or bad periods of graduate study.

Chapter 1. Introduction

Parts of this chapter have been published in the following review manuscript:

- **Kim P**, Chu N, Davis J, and Kim D-H. Mechanoregulation of myofibroblast fate and cardiac fibrosis, *Adv. Biosys*. 2017; 1700172.

1.1 Myocardial remodeling during cardiac fibrosis

In the United States and many other nations, cardiac failure is the leading cause of death. Heart diseases account for over 800,000 deaths per year (1 of every 3 deaths), and economic expenses exceed $320 billion in direct and indirect costs [1]. Nearly all forms of cardiovascular disease are associated with myocardial fibrosis, which is primarily mediated by cardiac fibroblasts. While cardiac fibroblasts are responsible for extracellular matrix (ECM) maintenance in healthy myocardium, they can also transform into myofibroblasts. Post-transformation, they can contribute to the secretion of cytokines, deposition of ECM, structural support, and filling the mechanical load created by myocyte necrosis [2]. Myofibroblast transdifferentiation is essential in overcoming cardiac injury, but progressive fibrosis often leads to remodeling of both infarcted and residual non-infarcted myocardium. This remodeling results in reduced tissue compliance, increased matrix stiffness, irregular action potential propagation, and progressive heart failure [2] (Figure 1.1). The limited regenerative capacity of the mammalian myocardium intensifies the fibrotic and inflammatory response during cardiac wound healing [3-5]. These changes lead to disruption of overall tissue organization, critically damaging organ function through hypertrophy, chamber dilation, biochemical intracellular signaling factor secretion, and transdifferentiation of neighboring fibroblasts. Fibrosis is linked to ventricular arrhythmias, hypertension, diabetes, rheumatic heart diseases, hypertrophic cardiomyopathy, heart failure, and sudden cardiac death [6, 7]. Currently, clinical strategies to combat damage to the myocardium from fibrosis are essentially palliative. This is especially true due to the limited supply of hearts for transplantation

[2] and lack of understanding of the regulation of the remodeled cardiac environment on scar tissue formation.

Inhibition of heart scarring and fibrosis would be an ideal therapeutic strategy for treating heart diseases. One such disease is Ischemic fibrosis, where obstruction of the coronary arteries leads to a reduction of the oxygen supply to the myocardium. This can potentially result in infarction, where the lack of oxygen results in necrosis. The area of necrosis will eventually be replaced by fibrotic scar, greatly affecting the functionality of the myocardium.

Myocardium is a complex, highly ordered system, with a mix of cellular and acellular components, providing resident cells with strong structural organization as a whole [2-4]. Ultrastructural analysis of mammalian myocardial tissue highlights that the arrangement of aligned cells correlates strongly with the direction of the underlying ECM fibers [5]. In the myocardium, the ECM is aligned congruently, providing a natural direction for myocyte exertion of contractile forces and a defined axis for action potential propagation. In a healthy myocardium, the fibrous ECM provides several other functions as well. These include, providing a native myofascial plane between layers of muscle, a barrier to electrical activation of the atria and ventricles, and structural guidance to blood vessels. These functions are often disrupted after myocardial infarction [4]. Post-infarction remodeling such as ECM deposition, increased stiffness, and impaired contraction are known to be regulated by chemical, mechanical, and structure cues through myofibroblast transdifferentiation [8]. This suggests that ECM offers mechanical cues for cardiac cellular and macroscopic tissue organization and development.

There is a tremendous need for the development of effective interventions for cardiac fibrosis both clinically and economically. Currently, numerous publications have been made regarding myofibroblasts and cardiac wound healing. Recent publications have shown cell-matrix regulation to play a key role in cardiac wound healing. This dissertation will focus on the current status of

research revolving around the mechanical regulation of myofibroblasts in cardiac fibrosis and wound healing, as well as the future targets for possible therapeutic development.

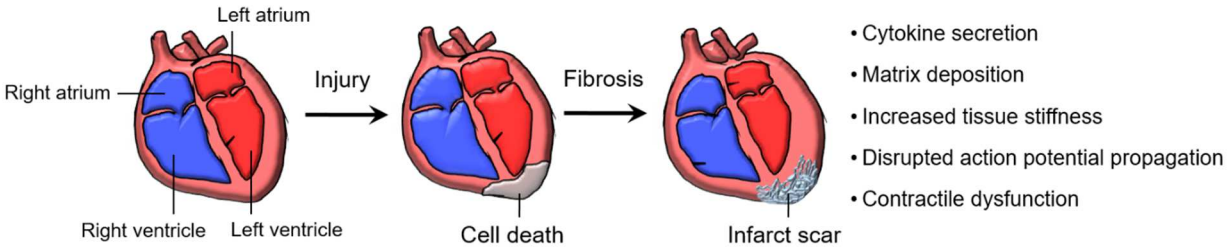

Figure 1.1. Illustration of cardiac fibrosis development. Cardiac infarction often results in myocyte necrosis which is replaced by infarct scar. Cytokine secretion, matrix deposition, increased tissue stiffness, disrupted action potential propagation, and contractile dysfunction are consequential events post-infarction and may lead to heart failure.

1.2 Cellular origins of cardiac fibrosis

Myofibroblasts are responsible for secreting a fibrotic matrix in response to injury signals. They can secrete large amounts of matrix proteins including collagen type I, collagen type III, collagen type IV, periostin, and fibronectin [1]. They play a critical role in wound healing in various organs including the lungs, liver, kidneys [2, 3], skeletal muscle [4], and heart [5, 6]. Their contribution to wound healing includes: migration, wound contraction, recruitment of inflammatory cells, and the remodeling/secretion of ECM to provide structural reinforcement [7, 8] (Figure 1.2). Morphologically, myofibroblasts are identified by ruffled membranes, a spindle shaped morphology, dendritic processes, and large endoplasmic reticulum organelles. The characteristics of myofibroblast are a cross between fibroblasts and smooth muscle cells, including the expression of alpha smooth muscle actin (αSMA) and the intermediate filament desmin. The contractile property of myofibroblasts originates from the electron dense smooth muscle myosin and αSMA. While these characteristics are all documented, the steps and molecular mechanisms in myofibroblast transdifferentiation *in vivo* are not well understood.

A few extracellular ligands which are involved in fibroblast to myofibroblast transdifferentiation include transforming growth factor β (TGFβ), endothelin 1 [9], angiotensin-II [10], nerve growth factor [11], thrombin [12], Wnt β catenin/fizz1 [13, 14], platelet-derived growth factor (PDGF) [15], and intracellular stress [16]. Previous studies *in vitro* suggest that in the early stage of transdifferentiation, fibroblasts exhibit an increase in focal adhesion proteins, which increase mechanical stress on the cells [17, 18]. As myofibroblast fully differentiate, smooth muscle actin expression increases [18]. Although the presence of αSMA is considered to be a marker for myofibroblasts; longer focal adhesions, paxillin, tensin, ED-A fibronectin, increased $\alpha_v\beta_3$ or $\alpha_v\beta_5$ integrin, and excessive secretion of collagen are all collectively used to identify myofibroblasts [7, 19]. However, many markers fail to specifically identify cardiac myofibroblasts. This remains a major challenge in cardiac tissue engineering [20]. It should also be noted that multiple factors including inflammatory cytokines such as TGFβ, are known to lead fibroblasts to a myofibroblast lineage. However, the factors that initiate and differentiate fibroblasts into myofibroblasts have not been confirmed *in vivo*.

While normally not present in healthy myocardium, myofibroblasts appear and transform the myocardium upon cardiac injury, in pathological responses, or aging. Importantly, myofibroblasts develop dense microfilaments and actin cytoskeletons that extend the membrane of the cell to an adhesion complex, fibronexus [21]. Altogether, a mature adhesion complex with internal stress fibers, generates a contractile force, which is then reinforced by deposition of collagen [22]. Despite this contractile machinery, myofibroblasts are non-excitable cells that do not directly participate in contractile behavior or conduction of action potentials through gap junctions of normal myocytes. Although Cx43 protein has been reported to be present between fibroblasts and myocytes in the sinus node of a normal rabbit heart, further investigation suggested that such coupling levels are very low, even slowing electrical conduction [23]. Overpopulation of myofibroblasts is likely to hinder myocyte to myocyte coupling and cardiac conduction via gap

junctions, while leading to over-stiffening of the myocardium by excessive ECM deposition [24]. Although multiple animal models have shown myofibroblasts play an important role in physiologic remodeling and wound closure, overexpression of the myofibroblasts phenotype often leads to uncontrolled fibrosis [25-27]. In the case of cardiac tissue, this results in pathological ventricular remodeling, hypertrophy, arrhythmia, and even heart failure.

Classes of cardiac fibrosis include reactive interstitial, replacement, and perivascular fibrosis [28]. Reactive interstitial and perivascular fibrosis are often observed in left ventricular pressure overload models or in hearts affected by hypertension, diabetes or aging [29, 30]. Reactive interstitial and perivascular fibrosis are characterized by progressive collagen accumulation in the perivascular and interstitial spaces in the absence of myocyte cell death. Such changes are accompanied by myocyte hypertrophy, and are reported to affect even remote non-infarcted myocardium. Progressive fibrosis is considered a hallmark of aging in many organs including the cardiovascular system. Although aged hearts may exhibit a normal ejection fraction and contractility, the myocardial compliance and ventricular mass is often increased due to deposited collagen from progressive fibrosis [31]. Different types of progressive fibrosis may have different causal mechanisms leading to cardiac fibrosis. Fibrosis induced from hypertension is caused by increased collagen synthesis, but age-induced fibrosis exhibits decreased collagen synthesis, but significant attenuation of matrix-degrading pathways accounting for cumulative collagen deposition [32]. Reactive interstitial and perivascular fibrosis are considered an intermediate marker of fibrosis as it precedes irreversible replacement fibrosis. Some therapeutic approaches were found to reverse such phenotypes [33]. In contrast, replacement fibrosis is observed in acute myocardial infarction and ischemic heart disease with no effective therapeutic approaches. In this case, necrotic myocytes are replaced with fibrotic scar through excessive matrix deposition, mainly type I collagen [34]. Interstitial and perivascular fibrosis ultimately lead to replacement fibrosis which then often leads to heart failure.

Recent studies suggest that myofibroblasts are primarily derived from resident fibroblasts which undergo programmed transdifferentiation. However; endothelial-derived fibroblasts [35], epithelial-derived fibroblasts [35, 36], circulating fibrocytes [37], perivascular cells [19] and mesenchymal cells from the Gli1 lineage, may also contribute to the population of myofibroblasts within injured tissue [7]. The diversity of myofibroblast precursor cells are one of the confounding factors in understanding myofibroblast function; as well as their role in fibrotic remodeling of the heart after injury or during disease progression.

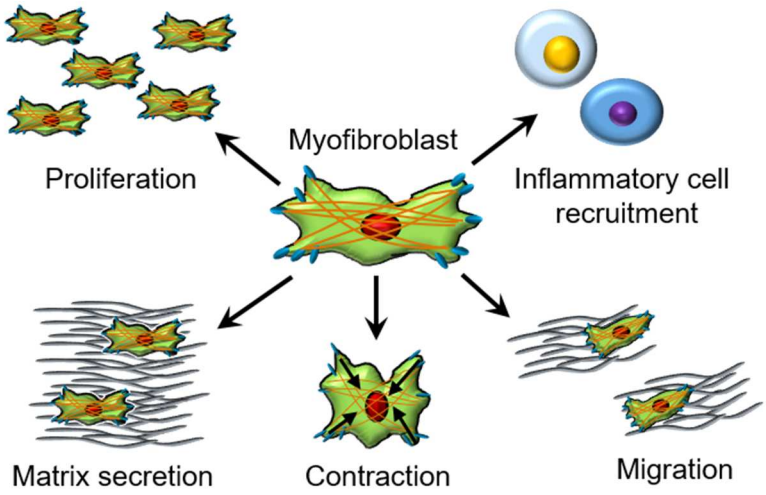

Figure 1.2. Myofibroblast characteristics during myocardial fibrosis. Cardiac myofibroblasts are transdifferentiated and proliferate to infarct region. Myofibroblasts are responsible for recruiting inflammatory cells via secretion of pro-inflammatory factors to the infarct region. Matrix secretion, contraction, and migration of myofibroblast all contribute to compensating tissue load, localization, and wound contraction during cardiac fibrosis.

1.3 Microenvironmental cardiac scar mechanics

Due to the recent findings of mechanical cues modulating myofibroblast transdifferentiation [18, 38-41], cardiac researchers are focusing on investigating the signaling pathways underlying the transduction of mechanical cues. Traditional understandings of the myofibroblast and its role in cardiac wound healing has mainly relied on an *in vitro* setting on flat tissue culture plastic. These settings are distant from the rich *in vivo* microenvironments, which myofibroblasts continuously interact with both before and after transdifferentiation.

In vivo, fibroblasts and myofibroblasts regulate the ECM dynamically, and concurrently receive environmental regulatory cues. The heart's ECM microenvironment is known to maintain the heart's electrophysiology, provide structural support to myocytes, and provide residing cells with signaling proteins [34]. Studies on ECM dynamics have found that ECM not only regulates fibrosis chemically, but also mechanically [39, 42-44]. The conversion of mechanical signals into biochemical signals plays a pivotal role in cellular differentiation. A large range of subcellular structures have been found to contribute to this process. Some of these include the ECM itself, cytoskeletal filaments, myosin motors, growth factors, integrins, and stretch activated ion channels.

The healthy heart is organized with various ECM proteins, which contribute to synchronized contraction, tight cell-cell coupling, and directional action potential propagation [42, 45]. Since directional ECM organization has been observed in many studies, cardiac tissue engineering has been attempting to recapitulate the native heart ECM to understand the mechanisms of cell-ECM interactions [42, 44-47]. A major protein in the ECM of the heart is planar laminin. It is reported that healthy adult myocardium is comprised of about 35% laminin, however as an infarct develops, collagen, specifically type I collagen, a fibrillary protein that provides tensile strength and stiffness to myocardium, dominates [48] (Figure 1.3). The increase in fibrillar type I collagen content, resulting in increased rigidity, is generally a hallmark of fibrosis [49]. Both collagen content and tissue stiffness in the microenvironment are known to be regulated by myofibroblasts. Fibrillar collagen, which is often absent in healthy myocardium, develops on the border of an infarct in congruent direction to myocytes upon injury [50]. Notably, the core of an infarct displays random orientation of collagen fibers (Figure 1.4). The mechanoregulation of remodeled microenvironments in infarct scaring has not been investigated in depth. Cyclic stretch [51-53], rigidity [43, 51], ECM orientation [54], infarct location [39], and topographic cues [42, 45] are beginning to be examined for roles in cardiac scar formation and myofibroblast regulation. Studies suggest these environmental mechanical cues are key regulators in cardiac remodeling. Attempts

made to recapitulate *in vivo* microenvironments, in order to investigate effects of exogenous mechanical cues, would advance effective study of cellular biomechanical function.

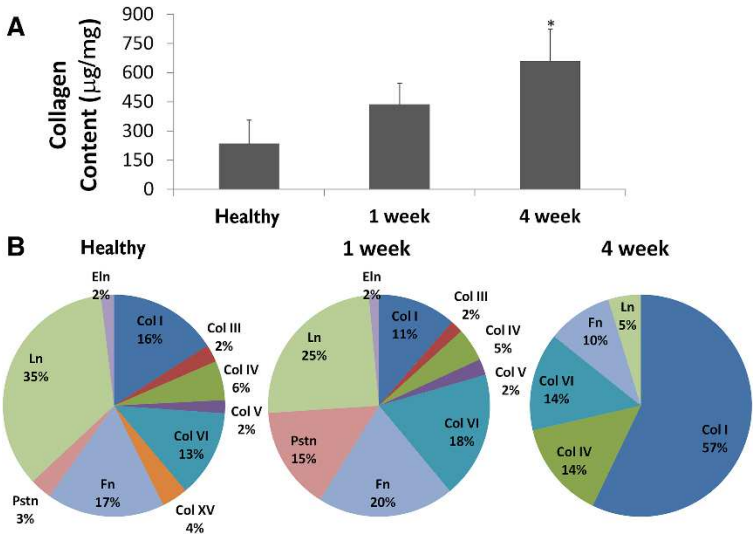

Figure 1.3. Extracellular matrix composition is remodeled post-infarction. (A) Total collagen content within the 4-week infarct is significantly greater than the both healthy and 1-week conditions. (B) LC-MS/MS spectrum count analysis has shown the relative percentages of each matrix protein content within the decellularized heart. Note that Pstn is periostin, Ln is laminin, Eln is elastin, Fn is fibronectin, and Col is collagen. Reproduced with permission from Reference [48].

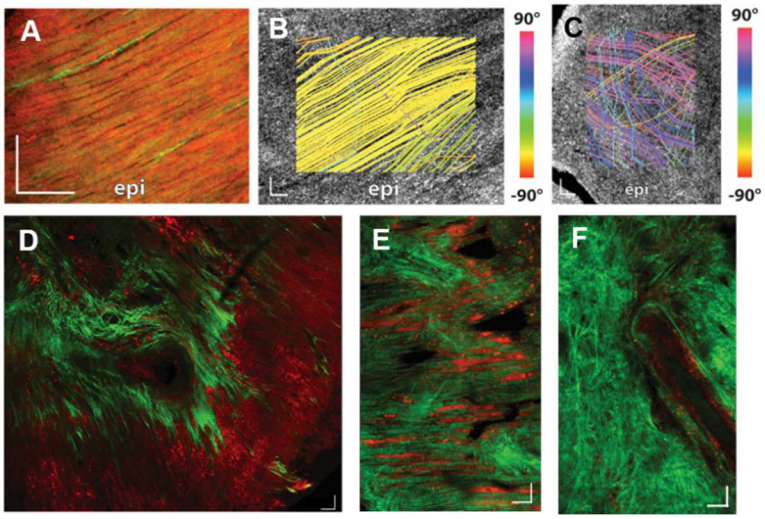

Figure 1.4. Myofiber and collagen direction is remodeled during cardiac fibrosis. Myofiber direction was analyzed for (A, B) heathy and (C) infarcted heart. (A) Two-photo microscopy and tractography streamline analysis of (B) healthy and (C) infarcted heart displayed a significant disruption of myofiber direction on infarcted heart. (D) Collagen (green) direction was regionally remodeled on the infarct site. (E) Collagen fibers were congruently aligned to cardiomyocytes (red) on the border of the infarct. (F) Core of infarct exhibited randomly oriented collagen fibers. Reproduced with permission from Reference [50].

1.4 Mechanical stress underlies fibroblast to myofibroblast differentiation

Myofibroblasts are highly sensitive to mechanical force, and can generate contractile tension on their surroundings during wound healing. Mechanical forces are known to induce increased proliferation, reduced collagenolytic activity, and increased collagen production [55]. A number of studies are starting to report congruent effects of mechanical and chemical signals on myofibroblast transdifferentiation [1, 56, 57]. Evidences suggest cyclic tension itself (15%, 1 Hz) can transdifferentiate fibroblasts into myofibroblasts, without any secondary soluble growth factors [51-53, 55]. On the contrary, a number of studies also report that cyclic strain has an inhibitory effect on myofibroblast transdifferentiation [58-61]. Here, the inhibitory effect was reverted with increased anisotropy, suggesting that fibroblasts can also sense the directionality of cyclic strain [58]. Moreover, infarcts induced on the equator of hearts, where myocytes contract in a circumferential direction, change the orientation of ECM fibers. This was not observed when the infarct was restricted to the apex, where myocytes induce circumferential and longitudinal contraction of the heart [39].

Integrins are well-established mechanosensors in fibroblasts and myofibroblasts that connect the ECM and cytoplasmic actin cytoskeleton. These mechanosensors are heterodimer membrane receptor proteins. They are composed of an alpha and a beta chain which confer specificity to certain ECM components. Integrins link the actin/myosin cytoskeleton within fibroblasts to the ECM, allowing cells to exert and sense mechanical forces in the external environment. These mechanosensors have been shown to play a role in myofibroblast transdifferentiation.

Myofibroblast differentiation and cell specific markers have been shown to increase with mechanical tension [55, 62]. Such increased transdifferentiation events were effectively reduced with the inhibition of integrins, specifically integrin α_v, in liver, kidneys, and lungs via suppression of latent TGFβ activation [63]. Stretch-mediated mechanical signals have also been shown to alter ECM-integrin interactions and vary cellular responses [64]. Thus, strategies to modulate

myofibroblast integrin inhibition with small molecules or antibodies are emerging as a novel method of combating fibrotic cardiac diseases [65].

One significant pathway that transduces mechanical stress, is the mitogen-activated protein kinases (MAPK). All three MAPK kinases (ERK, JNK, and p38) were activated with cell stretch, and inactivated with cell contraction [66]. A number of results suggest there exists a selective activation pathway of MAPK during mechanical force stimulation [55, 67, 68]. Interestingly, passive biaxial stretching has shown an increase in ERK and JNK activity, but not the p38 kinase pathway [69, 70]. Conversely, tensile forces were shown to increase activity of p38, but not ERK and JNK [71]. Recent findings have shown that increases in myofibroblast transdifferentiation induced by cyclic strain were inhibited with p38 knockout, suggesting the regulatory effect of p38 on transducing mechanical cues for fibrotic response [59] (Figure 1.5A, 1.5B).

Unlike myocytes, myofibroblasts do not produce cyclic tension. However, studies suggest that static tensile forces can also regulate myofibroblast fate. A static tensile force of 0.65 pN/μm^2 resulted in a 2-fold increase in αSMA protein levels within a short period for low basal levels of αSMA. While a decrease in αSMA for high basal levels of αSMA through MAPK occurs [55]. It was found that stress worked synergistically with TGFβ causing activation of latent TGFβ1, which in turn induces myofibroblast differentiation [40, 72]. Activation of TGFβ1 by release from the latency associated peptide, has been found to require as low as 40 pN of integrin-transmitted force [72]. Mechanical force induces myofibroblast differentiation, setting up a positive feedback loop, in which newly differentiated myofibroblasts exert force on the surrounding microenvironment. This positive feedback is assisted by TGFβ1 activation, amplifying the inductive signals for a fibroblast to differentiate.

Incorporation of αSMA into stress fibers is significant, as it leads to myofibroblast contractility. The contractile stress fibers, comprised of mature actin microfilaments and non-muscle myosin

are regulated by myosin light-chain (MLC) phosphorylation [44]. This phosphorylation is regulated by Rho kinase. RhoA, a small GTPase protein of the Rho family, is known to enhance actin reorganization and activate TGFβ responses. This kinase is another major factor in myofibroblast transdifferentiation [73, 74]. Inhibition of RhoA significantly reduces contractile force, as well as wound granulation in tissue contraction [75].

RhoA/Rho-associated kinase (ROCK) regulates not only the phosphorylation status of MLC, but also underlies the remodeling of the actin cytoskeleton into stable stress fibers [76]. Although both ROCK1 and ROCK2 have been implicated in cardiac hypertrophy and ventricular remodeling, ROCK1 is central to the development of cardiac fibrosis. In the context of mechanical signaling the ROCK kinases are critical for mechanosensing in both fibroblasts and myofibroblasts [76]. The close relationship between external mechanical tensions, myofibroblast induced tension, the pathways involved, and fate changes all suggest that focus on these areas may represent a new strategy in preventing maladaptive scar formation and in developing an anti-fibrotic therapeutic strategy [77].

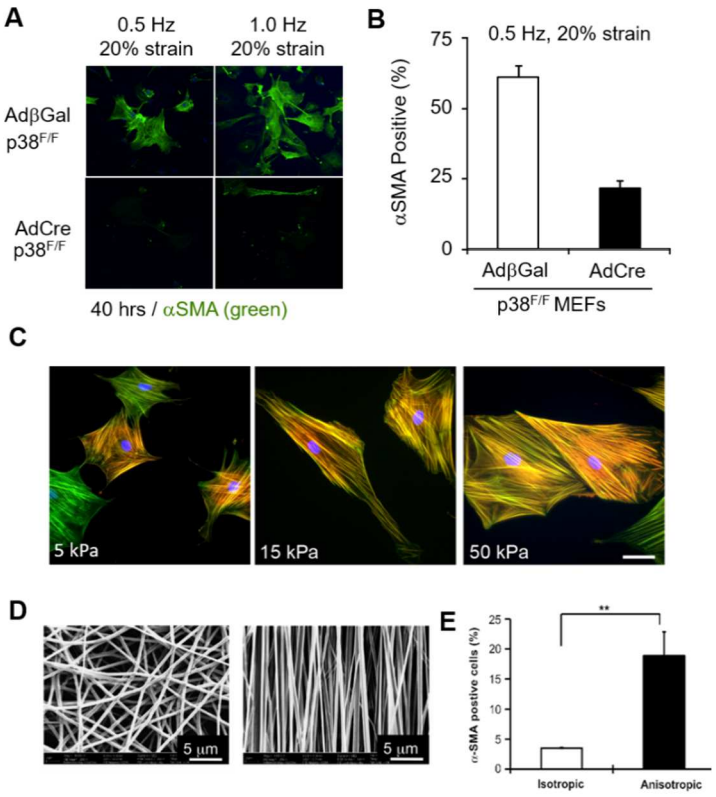

Figure 1.5. Myofibroblast transdifferentiation is mechanically regulated. (A, B) Cyclic strain has shown regulatory effect on myofibroblast transdifferentiation. Recent findings suggest p38 play a key role in mechanoregulation of cyclic strain. Reproduced with permission from Reference [59]. (C) Stiffness has shown to regulate fibroblast transdifferentiate into myofibroblast. Increase in elastic modulus has shown increased expression of αSMA. Reproduced with permission from Reference [78]. (D) Myofibroblasts are also sensitive to alignment cues imposed by electrospun fibers in isotropic (left) and anisotropic (right) fibers. (E) Fibroblasts cultured on anisotropic fibers have expressed higher αSMA signals. Figures (D, E) reproduced with permission from Reference [79].

1.5 Substrate stiffness regulate myofibroblast fate

Recent findings demonstrate that myofibroblast fate is also regulated by substrate stiffness [78, 80, 81]. Fibroblasts cultured on low stiffness planar substrates do not form stress fibers or express αSMA, in contrast to fibroblasts cultured on high stiffness substrate or tissue culture plastic [78, 82] (Figure 1.5C). It has been discovered that tissue stiffness or loading have a close relationship to wound healing and scar formation. However, the understanding of the molecular mechanism of how myofibroblasts transduce mechanical elasticity is still at an elementary stage. Various models have been suggested to understand how myofibroblasts sense external stiffness. One

model is detection through mechanosensitive membrane ion channels, which change conformation in response to external tension.

Mechanosensitive ion channels were shown to detect rapid changes in tension induced by magnetic beads [83]. Mechanosensitive ion channel models are appealing, however they have drawbacks. This model does not reflect *in vivo* fibrotic response, as matrix dynamics occur over a period of weeks to even months, while the ion channel models are limited to short term changes. Thus, in order to understand the process of myofibroblast fate change mediated by substrate stiffness, the current focus is on investigating ECM-cell adhesion dynamics and cytoskeletal regulation through mechanotransduction.

Formation of enlarged focal adhesions has been found to be a key step in a feedback loop of external stiffness to actin stress fiber organization that regulates myofibroblast transdifferentiation. Fibronexus, a myofibroblast-specific extensive ECM-cell adhesion complex is formed in fibrotic tissue by myofibroblasts [7]. *In vitro*, enlarged focal adhesion complexes ("supermature focal adhesion") are often observed in high stiffness substrates. Limiting myofibroblasts focal adhesion formation on arrays of restricted islets led to the rapid loss of αSMA expression [84]. Moreover, increasing the size of the islets to allow supermature focal adhesion formation on extendable membranes reincorporated αSMA regardless of the stretch variable [84]. However, it is not clear whether formation of supermature focal adhesions is the primary event which determines myofibroblast fate post injury.

Approaches using three-dimensional model systems with loaded ECM, may provide the most relevant environment for simulating *in vivo* interaction between myofibroblasts and ECM [84]. However, the unrestrained ECM gels with loaded fibroblasts do not provide a continuous positive feedback of increased stiffness and myofibroblast interaction [85]. When collagen gel loses its elasticity, myofibroblasts lose their stress fibers and fibronexus adhesion complexes, which adhere myofibroblasts to collagen fibrils [86]. This is similar to the case when myofibroblasts

cultured on stiff substrates are treated with actin-myosin inhibitors [21]. Thus, it is believed that substrate stiffness dynamically and continuously regulates myofibroblast transdifferentiation.

This hypothesis of substrate stiffness regulating myofibroblasts is backed by recent findings which indicate Yes-associated protein (YAP) and transcriptional coactivator with PDZ binding domain (TAZ), which are transcriptional coactivators of the Hippo pathway, may be closely involved in myofibroblast transdifferentiation in response to ECM stiffness [41]. Where YAP and TAZ are not expressed in healthy tissue, they have been found to be expressed in fibrotic tissue. YAP and TAZ are unique in that their responses are mediated by nuclear translocation of the YAP/TAZ complex followed by altered gene expression [87, 88] . YAP and TAZ have been found to regulate various cell fates in response to mechanical cues [87, 88]. In stiff substrate cultures *in vitro*, YAP and TAZ accumulate in the nuclei of fibroblasts. This accumulation results in pro-fibrotic matrix synthesis, contraction, and proliferation. This response is through plasminogen activator inhibitor (PA-1) regulation, independent of TGFβ signaling [41]. Knockdown of YAP and TAZ has been found to suppress the myofibroblastic response. Utilization of a ‘smart polymer’, with the ability to change stiffness, has also revealed that a switch in substrate stiffness regulates YAP and TAZ activation [87]. Although the role of YAP and TAZ in cardiac fibrosis has not been investigated in depth, YAP activation was shown to increase cardiac function and enhanced regeneration [89, 90].

Not only does mechanical stiffness regulate enhanced transdifferentiation of fibroblasts, it also synergistically modulates various stimulus induced responses. It is reported that matrix stiffness modulates TGFβ induced transdifferentiation, with a significantly higher response to TGFβ on stiffer substrates [80]. It has also been found that contraction of myofibroblasts promote latent TGFβ activation on a stiffened matrix; where the activation of TGFβ via integrin-mediated myofibroblast contraction could be a critical point in fibrosis [73]. Traditionally, mechanical activation of myofibroblast differentiation was perceived as an acute process that is limited to

contractile force of cells. However, evidences suggest that even pre-stressed ECM can mechanically prime late stage transdifferentiation [40].

It has been found that in response to matrix stiffening, actin dynamics change causing filamentous actin polymerization to be more favorable. This results in nuclear translocation of myocardial related transcription factor (MRTF), a marker for myofibroblast differentiation, which has a part in regulating expression of αSMA [81]. In this case, both actin and MRTF may mediate an intrinsic mechanotransduction pathway, that regulates fibroblasts differentiating to myofibroblasts induced by matrix stiffening [81]. Increased expression of actin in response to matrix stiffness is thought to be sufficient in driving myofibroblasts to generate contractile force [44]. Identified as a mechanosensitive protein, αSMA localizes to stress fibers under external mechanical load. Although mechanisms underlying αSMA dynamics on myofibroblast stiffening is not known, evidence shows intracellular inhibition of αSMA increases motility, and reduces contraction both *in vitro* and *in vivo* [18]. Substrate stiffness reduction also leads to disassembly of αSMA from stress fibers, suggesting an interactive nature to stiffness regulation.

1.6 Matrix topography regulates myofibroblast fate

The heart is an organ that exhibits exceptionally high anisotropy of both myocytes and fibroblasts. This anisotropy and cell-cell junctions contribute to synchronized electric signal propagation and contraction [45]. Previously, ECM topography and anisotropy have shown to play a critical role in controlling cell and tissue function [45]. Electron microscopy of the myocardium has confirmed a directional ECM underlying cells [45]. Not only does the ECM supply cells with chemical cues to adhere, it also physically provides mechanical structures for cells to bind. While the mechanisms of chemical binding have been studied carefully, the role of ECM and its ability to impart regulatory mechanical cues, through variations such as the dimension of fiber bundles, orientation, and density, have not been thoroughly studied in the field of cardiac fibrosis.

The traditional method of culturing myofibroblasts often utilizes a smooth surface substrate, with uncontrolled ECM organization. The fundamental properties and functions of fibroblasts such as migration and cell fate can be affected by engineering mechanical properties of the culture matrix [91-94]. In this context, mechanically modifying the matrix to establish a physiologically relevant environment is critical to creating cardiac scar tissue models to study cardiac fibrosis.

The native anisotropic morphology is lost when cardiac cells are maintained *in vitro* using standard cell culture substrates and techniques. Infarcted hearts have shown disrupted matrix organization when compared to healthy hearts which consists of a left handed helix matrix [50]. Moreover, the heart matrix content shifts from sheet-like laminin-dominant condition to a fibrous collagen-dominant condition [48]. This loss of matrix organization disrupts the structural organization of ECM cues with adverse consequences for cardiac cell physiological properties.

Analysis of infarct scar remodeling has shown that matrix directionality is regionally regulated on the border and core of the infarct scar [50]. The core of the infarct consisted of matrix oriented in random directions, while the border of the infarct scar displayed an aligned fibrous matrix. To develop relevant model systems to study fibrosis, several engineering approaches have been attempted to recapitulate the dimensions, directionality, and spacing of native ECM fibers in healthy and scarred tissues. [92, 94, 95].

Clinically, the location of the infarct has been reported to affect ECM orientation in scar tissue [39]. In contrast, initial infarct size or orientation did not have a significant effect on ECM remodeling. Infarcts induced near the equator of the left ventricle resulted in scar ECM remodeling in a circumferential direction, whereas infarcts induced near the apex resulted in isotropic organization of the ECM [39]. These results suggest that mechanical regulation in infarct scars is a complex system with outcomes related to the location of infarcts. The fibroblast cells exhibited more directional and higher cell migration speeds on anisotropic nanoscale fibers over isotropic nanofibers and 3D models of wounds [79, 96]. Moreover, anisotropic cues also regulate

fundamental fibroblast cell fate by differentiating to a myofibroblastic lineage [40, 79] (Figure 1.5D, 1.5E). Specifically, the integrin β1 signaling pathway was activated, and phosphorylation of focal adhesion kinase was observed in response to anisotropic cues [79].

It is well known that myofibroblasts are capable of remodeling their surrounding ECM. Recent studies have found that this remodeled ECM mechanically induces a myofibroblastic response [40]. In these studies, myofibroblasts deposited similar levels of latent TGFβ as fibroblasts, while the organization of latent transforming growth factor beta binding protein-1 (LTBP-1) differed. Myofibroblasts were found to organize LTBP-1, an integral component of the ECM that stores and presents latent TGFβ, to denser and straighter fibrils. Pathologically organized ECM's ability to trigger enhanced latent TGF activation, may explain how decellularized ECM from fibrotic tissue lead *de novo* seeded cells to fibrotic properties even in the absence of TGFβ treatment, while decellularized ECM from normal tissue did not [97].

Although not as thoroughly investigated as other mechanical regulatory cues, directionality of ECM indeed plays a critical role in myofibroblast transdifferentiation. In this context, mechanically modifying the matrix to establish a physiologically relevant environment is essential. It aids in developing a fibrotic scar tissue model for understanding mechanisms underlying myofibroblast fate mapping. This may enable development of new therapeutic approach, targeting ECM directly for alleviating fibrosis.

1.7 Unmet Needs and Future Perspectives

Myofibroblasts are an essential cell type in the heart, heavily involved in both damage repair and maintenance of cardiac function. In this dissertation, we discussed the microenvironmental control of myofibroblast fate and fibrosis (Figure 1.6). Both chemical and mechanical signaling were highlighted in comparing healthy hearts to damaged hearts. Fibroblasts as well as their transdifferentiated myofibroblast cells have shown sensitivity to various mechanical signals, and

quite a few signaling pathways have been proposed to transduce such signals. Previous studies have been conducted to investigate the chemical regulation of fibroblast differentiation, garnering some level of understanding. However, our understanding of the mechanoregulation of myofibroblast transdifferentiation and fibrosis regulation remains limited. What is known, is that during fibrosis, heart tissue experiences a number of mechanical changes, and such changes act in synergy with chemical cues to induce various fibrotic responses through various signaling pathways. The complex chemical and mechanical signals that interplay *in vivo* presents great challenges to therapeutic cardiac engineering. Recent transgenic studies show promising results in understanding the origins [98, 99] and mechanics [25, 26, 77, 100] of myofibroblast transdifferentiation. Such approaches with mechanically engineered platforms could synergistically contribute to accurate assessment of myofibroblast regulation during fibrosis. Emergence of biomedical microelectromechanical technology may contribute to the field by developing mechanically engineered constructs, to simulate an accurate microenvironment, allowing for the study of the mechanics behind cardiac fibrosis. Decellularized matrix analysis with biomimetic scaffold designs may enable cell culture systems that could recapitulate microenvironmental cues of the *in vivo* myocardium, and may provide a faithful model to increase our understanding of the mechanical regulation of cardiac fibrosis. Moreover, 3D systems which offer explicit control over factors such as, cyclic stretch, rigidity, and topographic cues, would be a valuable asset, providing insights to combat cardiac diseases, as most forms are associated with myocardial fibrosis. A patient-derived stem cell culture in conjunction with a mechanically regulated microenvironment may contribute to personalized-therapy development. With a greater understanding of mechanical regulation, inhibition of heart scarring and fibrosis could become a realistic therapeutic strategy for treating heart diseases.

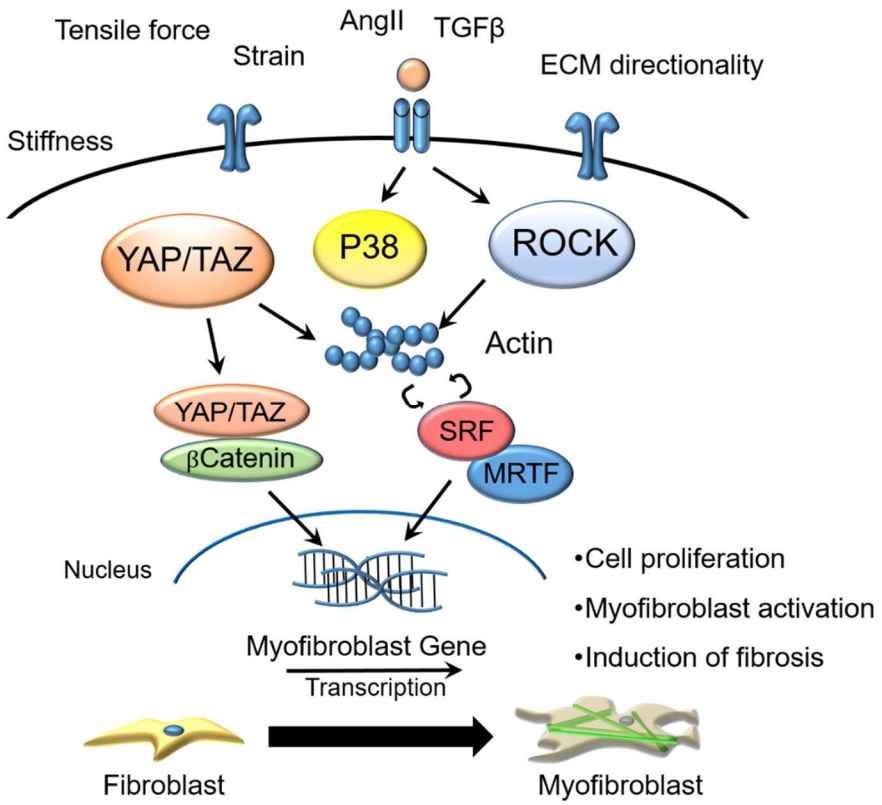

Figure 1.6. Schematic illustration of signaling pathways regulating fibroblast transdifferentiation into myofibroblast through mechanoregulation. Various pathways such as YAP/TAZ, p38, ROCK, SRF, and MRTF have been identified to transduce external mechanical cues such as stiffness, tensile force, strain, and ECM directionality.

1.8 Dissertation Overview and Significance

The research presented in this dissertation sought to address the challenges of regulating myofibroblast transdifferentiation during fibrosis, current understandings of effects of mechanical cues, and potential topographic as a novel mechanical regulator of cell fate throughout Chapter 1. Chapters 2 through 5 describe the rationale, scientific methods, and results of the following three specific aims:

Aim 1: Develop nanoengineered *in vitro* platforms with tunable mechanical characteristics to simulate cell response *in vivo*. (Chapters 2 & 3)

Aim 2: Identify a mechanotransduction pathways that transduce topographic cues for fibroblast transdifferentiation (Chapter 4)

Aim 3: Establish a pathway map of topographic cue sensing during cardiac fibrosis. (Chapter 5)

Chapter 2. Development of Anisotropic Nanopatterned Substrates with Tunable Mechanical Characteristics Enhance the Cellular Alignment

Parts of this chapter have been published in the following manuscripts:

- **P. Kim**, A. Yuan, and D. H. Kim, "Fabrication poly(ethylene glycol): gelatin methacrylate composite nanostructures with tunable stiffness and degradation for vascular tissue engineering" *Biofabrication* 2014
- S. Chaterji, **P. Kim**, S.H. Choe, D. S. Ho, J. H. Tsui, A. B. Baker, and D.H. Kim. "Synergistic Effects of Matrix Nanotopography and Stiffness on Vascular Smooth Muscle Cell Function" *Tissue Engineering,* 2014
- V. Le, J. Lee, S. Chaterji, A. Spencer, Y-L, Liu, **P. Kim**, H-C. Yeh, D.H. Kim, and A.B. Baker. "Syndecan-1 in mechanosensing of nanotopological cues in engineered materials" Biomaterials. 155 (2018) 13-24.

2.1 Rationale

Although synthetic polymers are desirable in tissue engineering applications for the reproducibility and tunability of their properties, synthetic small diameter vascular grafts lack the capability to endothelialize *in vivo*. Thus, synthetically fabricated biodegradable tissue scaffolds that reproduce important aspects of the extracellular environment are required to meet the urgent need for improved vascular grafting materials. In this chapter, we have successfully fabricated well-defined nanopatterned cell culture substrates made of a biodegradable composite hydrogel consisting of poly(ethylene glycol) dimethacrylate (PEGDMA) and gelatin methacrylate (GelMA) by using UV-assisted capillary force lithography. The elasticity and degradation rate of the composite PEG-GelMA nanostructures were tuned by varying the ratios of PEGDMA and GelMA. Human umbilical vein endothelial cells (HUVECs) cultured on nanopatterned PEG-GelMA substrates adhered

more than those cultured on unpatterned PEG-GelMA substrates. Additionally, HUVECs cultured on nanopatterned PEG-GelMA substrates displayed well-aligned, elongated morphologies similar to those of native vascular endothelial cells and demonstrated rapid and directionally persistent migration. The ability to alter both substrate stiffness and degradation rate as well as culture endothelial cells with increased elongation and alignment is a promising next step in recapitulating the properties of native human vascular tissue for tissue engineering applications.

Moreover, vSMC differentiation is modulated by a complex array of microenvironmental cues which include the biochemical milieu of the cells and the architecture and stiffness of the extracellular matrix (ECM). In this chapter, we demonstrate that by using UV-assisted capillary force lithography (CFL) to engineer a polyurethane substratum of defined nanotopography and stiffness, we can facilitate the differentiation of cultured vSMCs, reduce the inflammatory signature of the cells, and potentially promote the optimal configuration of the vSMC contractile and cytoskeletal machinery. Specifically, we found that the combination of medial tissue-like stiffness (11 MPa) and anisotropic nanotopography resulted in significant upregulation of calponin, desmin, and smoothelin, as well as the downregulation of ICAM-1, tissue factor, interleukin-6, and MCP-1. Further, our results allude to the mechanistic role of the RhoA/ROCK pathway and caveolin-1 in altered cellular mechanotransduction pathways via differential matrix nanotopography and stiffness. Notably, the nanopatterning of the stiffer substrata (1.1 GPa) resulted in the significant upregulation of RhoA, ROCK1, and ROCK2. This indicates that nanopatterning an 800_800_600nm (ridge width_groove width_ridge height) pattern on a stiff substratum may trigger the mechanical plasticity of vSMCs resulting in a hypercontractile vSMC phenotype, as observed in diabetes or hypertension. Given that matrix stiffness is an independent risk factor for cardiovascular disease and that CFL can create different matrix nanotopographic patterns with high pattern fidelity, we are poised to create a combinatorial library of arterial testbeds, whether they be healthy, diseased, injured, or aged. Furthermore, syndecan-1 was

identified as a mechanosensor for vSMC in response to nanotopogological cues. A syndecan-1 knockout model was used to confirm increased nuclear localization of YAP in response to nanotopographies as well as elevated levels of Rho-state in the cells. Such high-throughput testing environments will pave the way for the evolution of the next generation of vascular scaffolds that can effectively crosstalk with the scaffold microenvironment and result in improved clinical outcomes.

2.2 Scientific Methods

2.2.1 GelMA synthesis

GelMA was synthesized as previously described [101-103]. Briefly, Dulbecco's phosphate-buffered saline (DPBS; Gibco) was prepared at 60°C under a constant stirring condition of 400 rpm. Gelatin (type A, 300 bloom from porcine skin; Sigma-Aldrich) was added at 10% (w/v) to DPBS stirred for 2 h until a clear mixture was formed. Then methacrylic anhydride (MA; Sigma-Aldrich) was added at 20% (w/v) in the same stirring condition at 50°C. 500μL methacrylic anhydride was added every 30 s until the desired volume was added to ensure the full reaction as shown previously [101]. The solution was allowed to react for 2 h under the stirring condition at 50°C. After a 5× dilution of the solution with warm DPBS at 40°C to stop the reaction, the mixture was dialyzed using distilled water in 12-14 kDa cutoff dialysis tubing (Spectrum Laboratories) at the stirring condition at 40°C. Distilled water was changed regularly for 4 days until the salts and methacrylic acid was removed. The dialyzed solution was passed through a 0.2 μm filter (Corning) and lyophilized for 4 days to produce a sponge-like foam. GelMA not immediately used for polymerization was stored at -80°C.

2.2.2 Fabrication of PEG-GelMA hydrogel nanopatterns

Lyophilized GelMA and PEGDMA (PEGDMA MW 1000 Da; Polyscience) were dissolved in DPBS at 80°C with a UV crosslinker at a ratio of 5 μL crosslinker per 1 mL of solution. The UV crosslinker was prepared by dissolving 2,2-dimethoxy-2-phenylacetophenone (Aldrich) into 1-vinyl-2-pyrrolidinone (Aldrich) at 30% (w/v). The UV crosslinker was stored protected from light to prevent photochemical reaction. PEGDMA was used at 5%, 20% (w/v) concentrations and GelMA concentration was varied among 0%, 5%, 10%, and 20% (w/v). The solution was stored at 40°C to prevent gelation and used within 7 days. A silicon wafer with ridge and groove width of 800 nm and height of 600 nm nanopatterned features were fabricated via ion etching as described in [95]. The features were transferred to a polyurethane (PUA) mold on polyester film prior to the fabrication of PEG nanopatterns on the glass by a UV-assisted nanomolding method used previously [104]. To prepare the glass coverslips for nanopatterning, glass coverslips were first rinsed in isopropyl alcohol in a sonicated bath at 35°C for 20 min and dried under a stream of compressed air. The coverslips were then oxygen-plasma treated for 5 min. An adhesion promoter (Glass Primer, Minuta Tech) was then applied to the 35 mm glass coverslips by spin-coating at 2000 rpm for 20 s. Once spin-coated, the coverslips were baked at 65 °C for 20 min and then treated with UV light (365 nm) for 60 s. Treated glass coverslips were stored up to 7 days in a desiccator before usage. PEGDMA and GelMA solutions were drop dispensed on the coverslips and a PUA master mold was placed over the solution. The pattern was UV cured (365nm) for 5 min, resulting in a polymer of 35mm in diameter, ~100μm in thickness on top of the coverglass. After polymerization, the nanopatterned PUA master mold was removed. The sample was kept under UV for 12 h to complete the UV curing. Unpatterned substrates were fabricated from an unpatterned polyester film instead of a PUA copy of the nanopatterned substrates. Fidelity of the nanopattern was confirmed by scanning electron microscope (JEOL) at 15 kV, 4000 x magnification after sputter coating gold on the surface.

2.2.3 Characterization of PEG-GelMA nanopattern: mechanical stiffness

Atomic force microscopy (Dimension 3000, Bruker) was used to measure the stiffness of various concentrations of nanofabricated PEG-GelMA substrates. Nanopatterned substrates were hydrated in DPBS for 24 h period and were air dried right before the measurement of substrate stiffness. The ridge portion of the nanopatterned substrates was carefully scanned to generate a force curve. To calculate Young's modulus from the force curve, the cantilever's spring constant and deflection sensitivity was calibrated prior to the force curve measurement. The Derjaguin-Muller-Toporov (DMT) model was used to calculate the Young's modulus of the samples [105, 106]. A total of five samples were measured for each concentration of PEGDMA and GelMA.

2.2.4 Characterization of PEG-GelMA nanopattern: biodegradability

Washable glue stick was applied to an ultra-sonicated coverglass to easily detach the nanopatterned substrates from the coverglass prior to nanofabrication of the hydrogel substrates. The hydrogel was then detached from the coverglass by the addition of deionized water and rinsed thoroughly with deionized water. The sample's dry mass prior to degradation was weighed after using lyophilization (Freezone; Labconco). The enzymatic degradation rates of various PEG-GelMA compositions were then determined as previously described [103, 107]. The hydrogel substrate was submerged in a 1.5 mL tube with 1 mL of 2.5 U/mL collagenase type II (Worthington Biochemical) solutions in DPBS. The hydrogel and enzyme were incubated at 37°C for one, three, and seven days. After each set, the sample was centrifuged to remove only supernatant. The remaining PEG-GelMA was washed 3 times with deionized water for 5 min to remove DPBS and residual enzymes, and lyophilized overnight for dry mass measurement.

2.2.5 Cell culture

Human Umbilical Vein Endothelial Cells (HUVEC; Lonza) were cultured under 37°C, 5% CO_2 in a cell culture incubator (VWR). Endothelial Cell Growth Medium (Lonza) was mixed with 20% fetal bovine serum (FBS; Sigma) and 1% Penicillin Streptomycin (Gibco). Passage was conducted at 50% confluency, and only the cells with passage numbers between 3 and 6 were used for experiments. Each experiment was conducted by plating 500,000 HUVECs on a multi-well device with the fabricated nanopatterned and unpatterned substrates adhered on the bottom and allowing 4 h of initial incubation for attachment.

2.2.6 Quantitative analysis of cellular adhesion

Following the initial incubation, unattached cells were washed away with DPBS and only remaining cells that were adhered to the nanopatterned and unpatterned substrates were counted for each group. Number of cells was converted to cell/cm^2.

2.2.7 Quantitative analysis of cell morphology

Cell morphology was measured by washing unattached cells with DPBS and taking images by microscope (Axiovert200; Zeiss) after initial incubation. Cell morphology was studied by outlining the cell boundary using ImageJ. Cell alignment, elongation, and spreading area were measured. Alignment was measured by the angle between the direction of the nanopattern and cell's major axis. Major and minor axis length was measured by fitting ellipses to the cell borders. Elongation was calculated by dividing major axis length by minor axis length. Cell area was a converted value of the pixel to area in the cell boundary region.

2.2.8 Quantitative analysis of cell migration

After initial incubation, cell motility was measured by taking images of multiple locations every 20 min for 5 h using automated live cell microscope (Eclipse Ti, Nikon) at 37°C and 5% CO_2. Cell nucleuses were tracked at each time point. A custom-made MATLAB code was used to analyze cell migration. Migration speed was measured by calculating displacement per time, and persistence time was calculated from the rate of mean-square displacement in comparison to the random walk model [108].

2.2.9 Cell Culture, Seeding, and Stimulation of vSMC Differentiation.

Aortae were harvested from 6 to 10 week old male syndecan-1 knockout (S1KO) and wild type (WT) mice. Following harvest, the aortae were minced and a glass coverslip was placed over the tissue fragments. The cells were then cultured in DCDB-131 culture medium (Life Technologies) with 20% fetal bovine serum (FBS), L-glutamine and antibiotics. The vSMCs migrated out of the tissue and were allowed to proliferate. After the first passage, the cells were grown in MCDB-131 with 10% FBS, L-glutamine and antibiotics. The vSMCs were seeded onto the substrates at 50% confluence. Cells were seeded onto the substrates and treated 24h later with 1% DMSO, 10 μM Y-27632 (Sigma), or 10 μM verteporfin (Tocris) in culture medium for 48h. For differentiation of vSMCs, differentiation media containing a smooth muscle differentiation supplement (SMDS) comprising of 1% FBS and 30 μg/mL heparin (heparin sodium, Sigma) was used

2.2.10 Gene Expression Analysis.

Following differentiation treatments, as described above, mRNA was isolated from vSMC cultures using the RNAeasy Kit (Qiagen, Valencia, CA). The cDNA were obtained using the Taqman cDNA Reverse Transcription Kit (Life Technologies). Real time PCR was performed using the ViiA™ 7 Real-Time PCR System (Applied Biosystems, Foster City, CA) using a SYBR Green Master Mix

(Life Technologies). All PCR results were normalized to the expression levels of GAPDH prior to further analysis. The custom-synthesized primer pairs (Sigma) used for real time reverse transcription-PCR are listed in Table 1.

Gene	Forward Primer	Reverse Primer
Collagen 1a2	TTGTGGATACGCGGACTCTG	CTGAGCAGCAAAGTTCCCAG
Periostin	AAGGAAAAGGGTCATACACGTACTTC	CCTCTGCGAATGTCAGAATCC
ED-A Fibronectin	CCCACCGTGGAGTATGTGG	AGCCCTGACACAATCACGGA

Table 1.1. Primer Sequence used for RT-PCR (5' to 3')

2.2.11 Statistics

Statistical analysis was carried out by two way ANOVA test and Pearson chi-square test. Statistical significance was indicated for p-values less than 0.05.

2.3 Results

2.3.1 Fabrication of PEG-GelMA composite polymer nanopattern

UV-assisted capillary force lithography (CFL) is a cost-effective, easy-to-use, scalable, and highly reproducible technique which can fabricate polymeric nanofeatures. The PEG-GelMA was synthesized by a method similar to that previously described [101]. Figure 2.1A shows a reaction scheme of composite hydrogel of PEGDMA and GelMA. Gelatin was reacted with methacrylic anhydride (MA) to make GelMA, which was shown to possess tunable stiffness and biodegradability in bulk sample [103]. In order to model a vascular tissue environment, this PEG-GelMA was patterned with the CFL nanofabrication technique. Ion etching was used to fabricate a nanopatterned master mold with ridge and groove width of 800 nm and height of 600 nm on a silicon wafer [95]. Nanopatterned master features were then easily transferred to the PUA copy

by CFL, resulting in a negative feature of nanopatterns as defined in the silicon master molds. UV-assisted capillary force lithography [109, 110] was used to fabricate a large area (> 10 cm^2) of nanopatterned substrates. The mixture of PEGDMA and GelMA was kept in water bath at 37°C until it was cured under PUA stamps with UV light to functionalize acrylate groups to form a complete nanofabricated PEG-GelMA hydrogel as shown in Figure 2.1B. SEM images confirmed that various concentrations of PEGDMA and GelMA were successfully polymerized to both unpatterned and conformal nanopatterned substrates (Figure 2.1C). PEGDMA alone did not polymerize at 5% w/v as previous work has shown [103]. Only one representative SEM image of the unpatterned substrates of 5% w/v PEGDMA and 20% GelMA is shown.

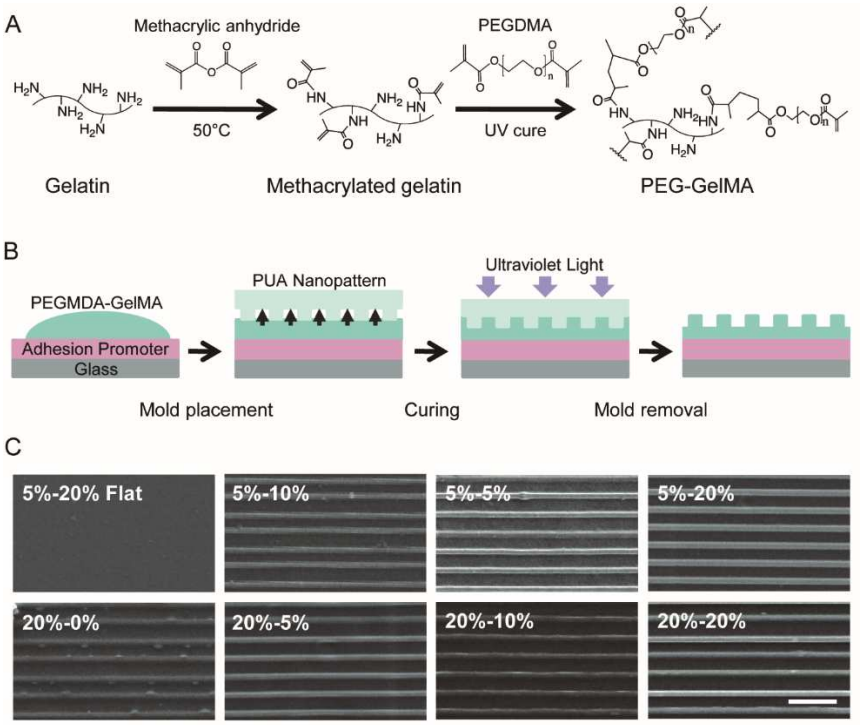

Figure 2.1. Fabrication of nanopatterned PEG-GelMA substrates. (A) Synthesis of Poly(Ethylene Glycol)-Methacrylated Gelatin (PEG-GelMA) composite. GelMA was first synthesized by methacrylating amine groups of gelatin with methacrylic anhydride (MA). The mixture of GelMA and PEGDMA was photocrosslinked under UV light (365nm) for 5 min in the presence of 2,2-Dimethoxy-2-phenylacetophenone and 1-Vinyl-2-pyrrolidinone mixture as a photoinitiator. (B) Schematic illustration of the fabrication process of nanostructures. Various compositions of PEG-GelMA were drop dispensed onto adhesion promoter coated coverglass. Then the coverglass was embossed with PUA master mold (ridge and groove of 800nm, height of 600nm). UV-assisted capillary force lithography polymerized the PEG-GelMA into a groove and ridge pattern. Careful removal of the master completed the fabrication.(C) Representative SEM images of unpatterned substrates (top left) and nanopatterned substrates of various

conditions. The number indicates each percentage (w/v) of PEGDMA and GelMA. Replication of constant topography was successful for various concentrations of PEGDMA and GelMA. Scale bar: 10□m.

2.3.2 Characterization of substrate mechanical properties: Tunable stiffness of hydrogel.

Cell morphology, skeletal assembly, migration, adhesion, and differentiation are affected by substrate stiffness [111-116]. As various moduli are required to model different types of tissue, it is clear that tunable stiffness would be advantageous in material used in engineered tissue grafts. Compared to PEGDMA, GelMA has relatively low material stiffness. A wide range of material rigidities were achieved by varying ratios of PEGDMA and GelMA. For higher concentrations of PEGDMA and GelMA, high viscosity was apparent even from the polymerization process. Young's moduli of the samples were calculated from the AFM by DMT model [105, 106]. Figure 2.2 indicates that the nanostructure fabricated by varying PEGDMA and GelMA have tunable stiffness. The stiffnesses achieved were in the range of sub-megapascal, which was significantly lower than the gigapascal range of standard polystyrene surfaces where typical cell culture studies are held. The profiled stiffness range indicates that PEGDMA and GelMA ratio could be adjusted depending on the desired substrate stiffness. For both 5% and 20% PEGDMA group, stiffness increased as w/v of GelMA increased. Interestingly, 5% PEGDMA samples with 20% GelMA resulted in similar stiffness (0.88 ± 0.06 MPa) as 20% PEGDMA and 5% GelMA (0.87 ± 0.06 MPa).

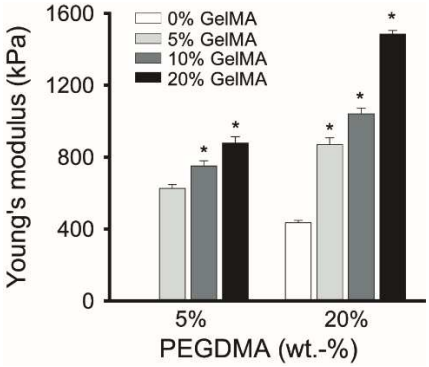

Figure 2.2. Stiffness profile of various ratios of PEGDMA and GelMA. Mechanical properties of the fabricated nanopattern made of various compositions of PEGDMA and GelMA were measured. Young's modulus was measured by using atomic force microscope by Derjaguin-Muller-Toporov model. n=5 for each group. Error bars indicate standard error of mean, *p<0.05

2.3.3 Characterization of substrate mechanical properties: Degradation profile of various ratios of PEG-GelMA

An appropriate amount of degradation in implantable scaffolds may minimize inflammation and improve biocompatibility. Crosslinking GelMA with PEGDMA to form PEG-GelMA composite was conducted in order to overcome the limitation of PEGDMA's inability to degrade. Figure 2.3A and 3B shows the percent mass remaining of samples of various ratios of PEGDMA and GelMA over 7 days of degradation with collagenase II. All samples showed exponential decay pattern with the fastest decay rate in the earlier time. Interestingly, for 5% PEGDMA samples, degradation was faster for low GelMA groups, and for 20% PEGDMA samples, degradation was faster for higher GelMA group. This might be due to the degree of crosslinking between PEGDMA and GelMA for higher and lower PEGDMA samples. Visually, the samples synthesized with low PEGDMA and GelMA were porous and were broken into pieces indicating that collagenase type II activity degraded the PEG-GelMA composite (data not shown). Notably, substrates of similar stiffness, 5% PEGDMA and 20% GelMA and 20% PEGDMA and 5% GelMA resulted in a significant difference in degradation rate. Results from stiffness of hydrogel and degradation profile exhibit that the substrates could be tuned independently of stiffness and degradation. By varying ratios of PEGDMA and GelMA, a substrate of desired stiffness or degradation could be achieved without altering the other variable.

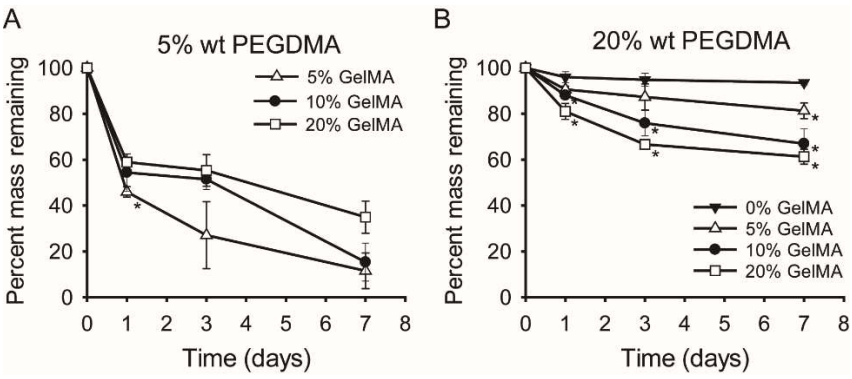

Figure 2.3. Degradation profile of various ratios of PEGDMA and GelMA. Degradation was measured as the percent mass remaining of PEG-GelMA in DPBS solution with collagenase II (2.5 U/mL) for 1, 3, and 7 days. Various concentrations of GelMA were tested with 5% PEGDMA (A) and 20% PEGDMA (B). Statistical analysis showed that for lower concentration of PEGDMA, degradation was significantly faster ($p<0.05$). n=3 for each group. Error bars indicate standard error of mean, *$p<0.05$.

2.3.4 Increased cellular adhesion by nanopatterning

Cellular adhesion to a culture substrate is important to enhance efficiency of transferred cells for experiments and avoid apoptosis. However, commercial plastic, glass, or even PEG surfaces have been shown to exhibit low cellular adhesion, causing portions of cells to be lost through passaging or transferring. Cellular adhesion was measured by culturing HUVECs on various concentrations of polymerized PEG-GelMA that were unpatterned and nanopatterned, allowing for attachment, and then counting the number of cells adhered after DPBS washing. HUVEC adhesion to various substrates was obtained by calculating number of cells per cm^2 at same culture conditions. Figure 2.4A shows that HUVEC-substrate adhesion was significantly enhanced for patterned substrates for every ratios of PEG-GelMA when compared to unpatterned substrates. Increasing the w/v ratio of GelMA exhibited a general increase of HUVEC adhesion for all conditions. The effect of GelMA on HUVEC adhesion was amplified on nanopatterened surface. For 5% PEGDMA condition, increasing GelMA from 5% to 10% and 20% resulted in 3 and 5.4 times more HUVECs adhered respectively on nanopatterened substrate whereas on flat condition, the increase in HUVEC adhesion was only 1.7 and 4.8 times more. This trend was

observed on 20% PEGDMA group as well, but in smaller scale. On nanopatterned 20% PEGDMA substrate, increasing GelMA from 0% to 5%, 10%, and 20% resulted in 1.2, 1.2, and 1.5 times increased HUVEC adhesion whereas for flat 20% PEGDMA substrates, the same increase resulted in only 1.1, 1.1, and 1.3 times increased HUVEC adhesion. On average, nanopatterning enhanced cell adhesion by 2.8 times for 5% PEGDMA group, and 1.8 times for 20% PEGDMA group, indicating that the effect of nanopatterning on cell adhesion was more enhanced when PEGDMA ratio was low. Overall, the cellular adhesion was optimal at nanopatterned substrates with 5% PEGDMA and 20% GelMA. After the initial attachment, HUVECs were allowed to reach confluency for 7 days. F-actin and DAPI as shown in Figure 2.4B and 2.4C. The result indicates that both flat (Figure 2.4B) and nanopatterned (Figure 2.4C) substrates in x-direction could be populated with endothelial cells to form a monolayer to be utilized in vascular tissue engineering. Interestingly, polarization of nucleus and F-actin fibers of HUVEC was observed on nanopattern. HUVEC on flat substrate showed random anisotropy of nucleus and F-actin.

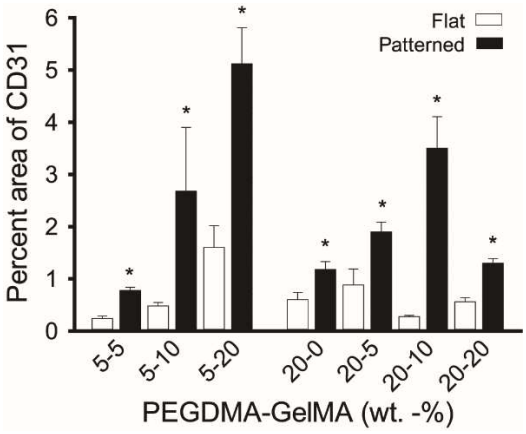

Figure 2.4. Enhanced cell adhesion on unpatterned and nanopatterned PEGDMA-GelMA composite and ability to reach confluency. (A) Adhesion was measured in cell/cm^2. Numbers on x-axis indicate the ratio of PEGDMA (w/v)-GelMA (w/v). Varying concentration of PEGDMA and GelMA affected cellular attachment significantly. For all cases, statistical analysis shows that cellular attachment was enhanced for patterned PEG-GelMA substrates compared to unpatterened substrates. Error bars indicate standard error, *p<0.05. (B,C) Adhered cells were allowed to reach confluency for 7 days. Representative images are HUVECs with F-actin stained (red) and DAPI (blue) on flat (B) and nanopatterned (C) substrates of 20% PEGDMA and 10% GelMA. Scale bars : 50 μm

2.3.5 Effects of nanopatterning of PEG-GelMA on cell physiology

Endothelial cells *in vivo* show highly organized anisotropy and an elongated shape aligned along the direction of flow [117]. However, endothelial cells cultured *in vitro* on a standard culture dish often appear unlike the highly organized morphology of endothelial cells *in vivo*; that is, they are randomly oriented, not fully spread, and rounded. A scaffold or a graft must be able to provide *in vivo* like environment to enhance effectiveness of the device. It has been shown previously that cells show strong contact guidance with nanopatterned substrates [95, 109]. We found that on PEG-GelMA fabricated nanopatterned substrates, the morphology of HUVEC was significantly affected by nanotopographical cues for all compositions of PEGDMA and GelMA as shown in Figure 2.5. As expected, for all ratios of PEGDMA and GelMA samples, HUVECs on the nanopatterned PEG-GelMA substrates showed higher anisotropy (Figure 2.5A, 2.5B), more cell spreading (Figure 2.5C), and greater elongation (Figure 2.5D) than HUVECs on the unpatterned substrates. Alignment was calculated by measuring the angle between the direction of the nanopattern and each cell's major axis. Over 72% and 85% of cells were aligned within ±10 degree range of the direction of the 5% PEGDMA and 20% PEGDMA nanopattern respectively. For unpatterned substrates, only 18% and 12% of cells were in the range of the same orientation for 5% PEGDMA and 20% PEGDMA respectively. Nanopatterning also increased cell spreading area by 29% on average, with cell area increased significantly overall for all compositions of PEGDMA and GelMA. Among the nanopatterned substrates, composition of PEGDMA and GelMA did not affect cell spreading area as significantly as the patterning did. However, for unpatterned substrates groups, cell spreading area was minimal at the lowest composition of PEGDMA and GelMA, and increased with higher GelMA composition with 20% PEGDMA and 20% GelMA group as an exception. For nanopatterned groups, cell spreading area is not significantly different among different compositions of PEGDMA and GelMA. The effect of nanopatterning of PEG-GelMA was even more significant for cell elongation. Cell elongation was

calculated by dividing major axis length by minor axis length. Each composition of PEGDMA and GelMA resulted in significantly elongated cell morphology. On average, cells on nanopatterned PEG-GelMA substrates were over 2.6 times more elongated than the cells on the unpatterned PEG-GelMA substrates. The concentrations of PEGDMA and GelMA respectively did not have a significant effect on cell elongation as nanopatterning did, indicating the cell elongation was topographically regulated, not strongly by compositions of the substrates.

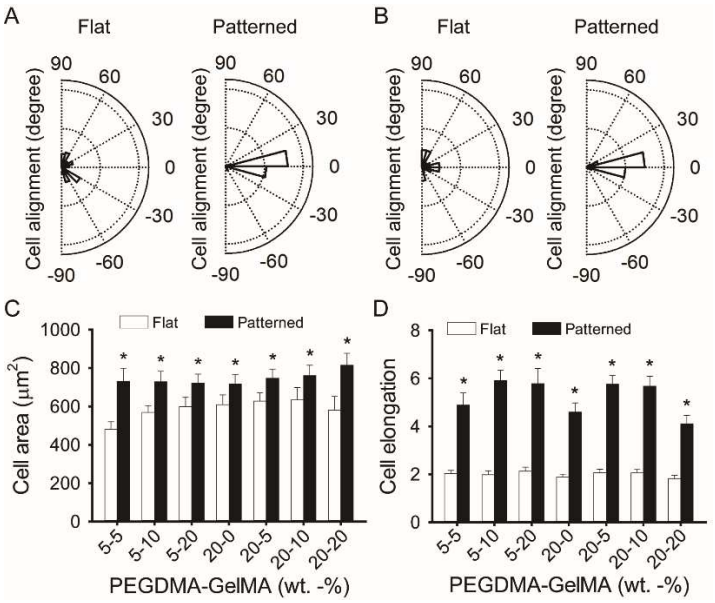

Figure 2.5. Effect of nanostructures and the various compositions of PEGDMA and GelMA on cell morphology. (A) Cell alignment was measured by plating HUVEC on unpatterned (left) and nanopatterned substrates (right) for 5% PEGDMA and 10% GelMA (A) and 20% PEGDMA and 10% (B). Alignment was measured by the angle of major axis in a range of -90 to 90 degree. For nanopatterned substrates, the groove was in the direction of x-axis. (C) HUVEC had larger cell area on nanopatterned substrates ($p<0.05$) for same ratio of PEGDMA and GelMA. (D) Elongation was measured by dividing major axis length by minor axis length of individual cell. The statistical analysis showed that HUVECs were much elongated on nanopatterned substrates than on unpatterned substrates. Varying concentration of both PEGDMA and GelMA had no statistical significance. Elongation was measured by dividing length of major axis by length of minor axis. Error bars indicate standard error of mean. $n>45$ for each experiment *$p<0.05$.

2.3.6 Guided and increased cell migration.

For biomimetic graft designs, not only is the anisotropy and morphological resemblance important for promoting endothelialization, but so is the migratory behavior of endothelial cells on the graft.

Directional guidance is important to control endothelial cells' behavior and enhanced recovery after a device is administered. For quantitative analysis of cell migration, hydrogel composition of 5% PEGDMA and 20% GelMA was selected for its optimal adhesion. HUVECs were seeded on unpatterned and patterned substrates fabricated and after 4 h of incubation, their migratory behavior was tracked every 20 min for 4 h. One representative image showing individual HUVEC nucleus tracking on unpatterned substrates (Figure 2.6A) and patterned substrates (Figure 2.6B) is shown. Cell boundary was indicated by red line to show cell movement. The center of HUVEC nucleus at 0 h (purple), 1 h (blue), 2 h (green), and 4 h (yellow) is shown to display overall migration (Figure 2.6A, 2.6B). The method used is able to track any cellular migration precisely over long periods of time. HUVECs on the unpatterned substrates exhibited random migration not biased to any specific direction, whereas HUVECs on nanopatterned PEG-GelMA substrates showed strong guidance of migration along the nanopattern in the y-axis direction (Figure 2.6D, 6E). Both trajectories of HUVECs not only suggested that endothelial cells resulted in guided migration along the direction of the nanopattern, but also persistent and faster migration. In order to confirm the enhanced migration, the persistence time and migration speed of HUVECs per every interval time was calculated. Persistence time, a measure to determine how persistent a cell maintains its directions of migration of the cell track, was determined from the rate of mean squared displacement measurements in comparison to random walk model [108]. Figure 2.6C shows that HUVECs on unpatterned substrates exhibited a significantly shorter persistence time than HUVECs on the nanopatterned PEG-GelMA substrates, indicating the direction of HUVEC on the unpatterned substrates was altered more frequently. As directed migration was observed for HUVEC on the patterned substrates, migration speed was measured to verify that HUVEC exhibited both guided and enhanced migration speed on nanopatterned substrates. Figure 2.6F shows that the migration speed of HUVECs was significantly higher (over two fold) on the nanopatterned substrates (38.6 ± 7.6 μm/hr) than that of the unpatterned substrates (18.7 ± 6.1 μm/hr). Thus, these results demonstrate that the nanopatterned PEG-GelMA substrates

contributed to guided migration along the groove direction as well as the enhanced migration speed and persistent movement of HUVECs.

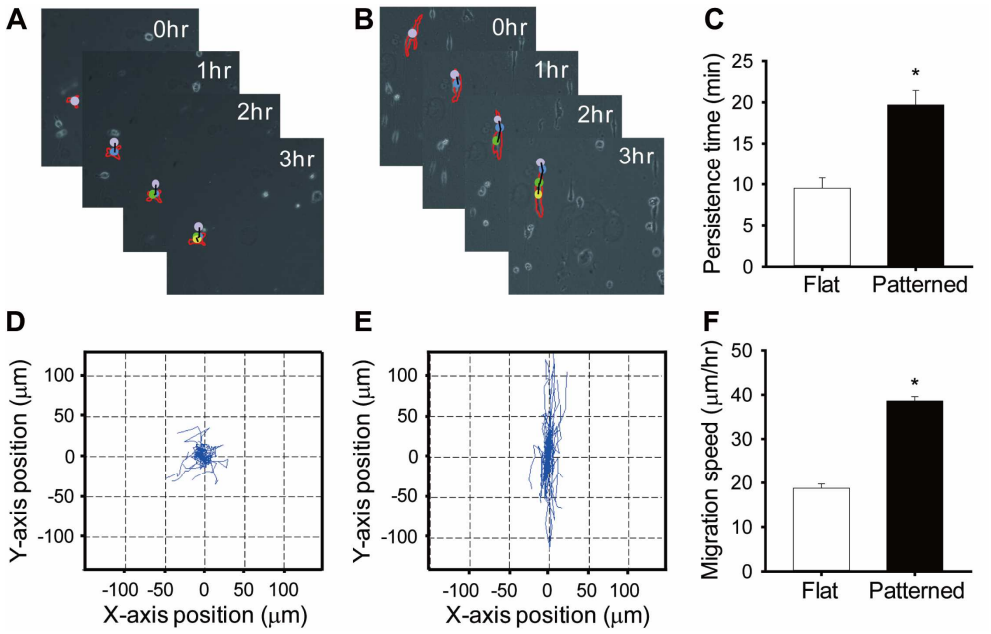

Figure 2.6. Guided and enhanced HUVEC migratory behavior on nanopatterned PEG-GelMA substrates. Representative migration trajectories of HUVEC were tracked on unpatterned (A) and patterned (B) substrates fabricated by 5% PEGDMA and 20% GelMA every 20 min for over 4 h. One representative nucleus positions at 0 h (purple), 1 h (blue), 2 h (green), and 4 h (yellow) are indicated as colored dots. Cell boundary was shown in dotted red line. (C) HUVEC on unpatterned substrates exhibited significantly shorter persistence time compared to cells on patterned substrates. Trajectory of HUVEC indicates a random migration on unpatterned substrates (D) and guided migration along the direction of nanopatterned substrates (E). X and Y axis are in the unit of □m. (F) Migration speed for HUVEC was significantly faster on patterned substrates than unpatterned substrates. (*p<0.05) n>60 for each experiment. Error bars indicate standard error of mean.

2.3.7 Analysis of vSMC Differentiation on Differentially Engineered Substrata.

In addition of HUVEC culture, we tested the synergetic effect of engineered nanotopography and stiffness on the gene expression of multiple markers of vSMC. Nanopatterning the substrata resulted in increase in calponin gene expression, with the expression of calponin being higher in the case of vSMCs cultured on the soft ANFS than on the stiff ANFS (Figure 2.7A), highlighting the beneficial effect of physiologically-relevant compliance and of nanopatterning the substratum.

In addition, nanopatterning the stiff substratum resulted in higher smooth muscle α-actin (α-SMA) gene expression relative to the unpatterned stiff substratum (Figure 2.7B), indicating that even in the absence of an optimally-stiff substratum, patterning the substratum could enhance vSMC contractility. Further, desmin was also upregulated on the soft ANFS (Figure 2.7C), and was significantly lowered on the stiff substratum even when nanopatterned. While desmin is an early marker of muscle cell differentiation, the presence of desmin in vSMCs indicates high functional activity since it links myofibrils to the cell membrane [118]. Desmin has been found greatly diminished in vascular lesions such as in a pig model of directional atherectomy [119]. In addition, the levels of tropomyosin-1 were higher on the nanopatterned substrata relative to the unpatterned substrata (Figure 2.7D). While tropomyosin-1 is an established marker for vSMC phenotype, erratic levels of this marker have been associated with hypertension in some tissues [120]. Finally, given that smoothelin is a very sensitive marker for vSMC differentiation [121], we also tested the synergistic effect of nanopatterning and stiffness on smoothelin gene expression. While the nanopatterning did not statistically alter the expression of smoothelin individually for the unpatterned and patterned substrata, the soft ANFS had statistically higher smoothelin expression relative to the stiff ANFS (Figure 2.7E). Since smoothelin has been exclusively found in fully-differentiated vSMCs and is absent in myofibroblasts, the upregulation of smoothelin in vSMCs cultured on soft ANFS is particularly interesting. Overall, our findings illustrated the synergetic effect of anisotropic nanopatterning and vascular tissue-like compliance of engineered PUA substrata, with ANFS specifically upregulating the expression of vSMC-restricted contractile protein genes.

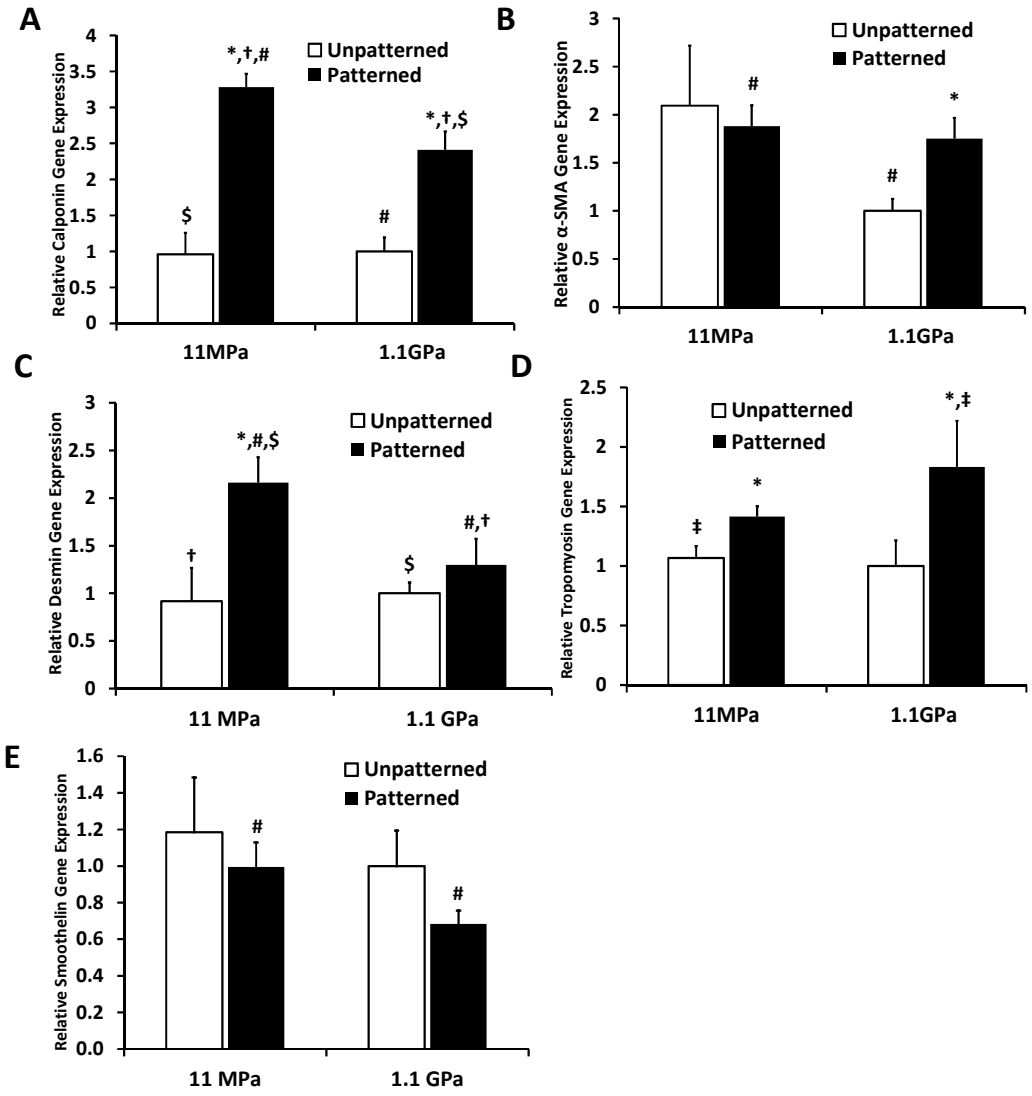

Figure 2.7. Nanoengineered platform regulate vSMC differentiation. Real time PCR analyses of vSMC differentiation-related markers when cultured on the different substrata. Interestingly, for the intermediate filament-related markers calponin and desmin and for the smooth muscle-specific cytoskeletal protein smoothelin, soft ANFS resulted in statistically higher gene expression ($p < 0.05$). This highlights the synergetic effects of substratum nanotopography and elasticity on vSMC differentiation, with ANFS resulting in a more profound effect of vSMC-restricted contractile protein marker genes. Interestingly, for the less stringent marker α-SMA (also found in myofibroblasts), there was no statistical difference between soft and stiff ANFS. For tropomyosin, found to be erratically upregulated in hypertension, stiff ANFS expressed statistically higher levels. Statistically significant difference between nanopatterned and unpatterned substrata ($p < 0.05$) for the same substratum stiffness is indicated with an asterisk. For all other substrata-type combinations, the identical signage indicates statistically significant difference for that pair.

2.3.8 Analysis of vSMC Activation on the Fabricated Substrata

Nanopatterning the soft and stiff substrata decreased the gene expression of inflammatory mediators (Figure 2.8) such as intercellular adhesion molecule-1 (ICAM-1), tissue factor (TF), and interleukin-6 (IL-6). However, monocyte chemoattractant protein (MCP-1 or CCL2) expression, known to be upregulated in hypertensive individuals [122], remained high on nanopatterned stiff substrata. This indicated that a stiffer matrix may trigger the homing of inflammatory cells with the activation of the inflammatory NF-κB pathway [123].

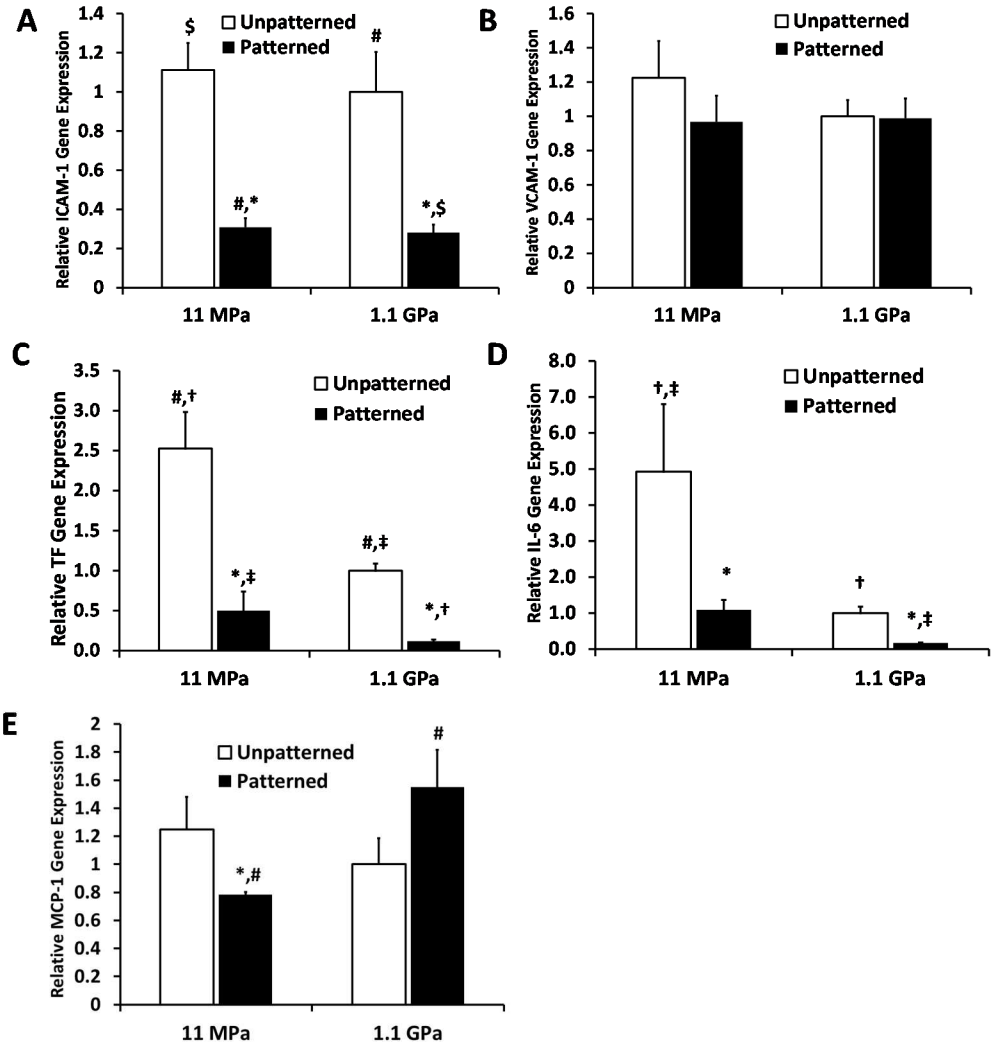

Figure 2.8**.** Real time PCR analyses of vSMC-secreted inflammatory markers when cultured on the different substrata. ANFS, for the most part, decreased the gene expression of inflammatory cytokines for both the soft and stiff substrata ($p < 0.05$) and thus made ANFS more biomimetic. Notably, the levels of MCP-1 expression increased around twofold on stiff ANFS relative to soft ANFS. Statistically significant difference

between nanopatterned and unpatterned substrata ($p < 0.05$) for the same substratum stiffness is indicated with an asterisk. For all other substrata-type combinations, the identical signage indicates statistically significant difference for that pair.

2.3.9 Analysis of the F-actin Cytoskeleton of vSMCs on the Substrata.

The cytoskeletal F-actin stress fibers were clearly different for all four types of substrata (Figure 2.9), with the stress fibers forming a diffuse meshwork of fibers on the unpatterned substrata. Further, the stress fibers were directionally aligned by the nanopatterning on both soft and stiff substrata and demonstrated a higher intensity on the nanopatterned stiff substrata. Given that the dynamic remodeling of the actin cytoskeleton plays a prominent role in vSMC proliferation and migration [124], it follows from the altered F-actin cytoskeleton that the different substrata would confer different proliferative and migratory states to the vSMCs.

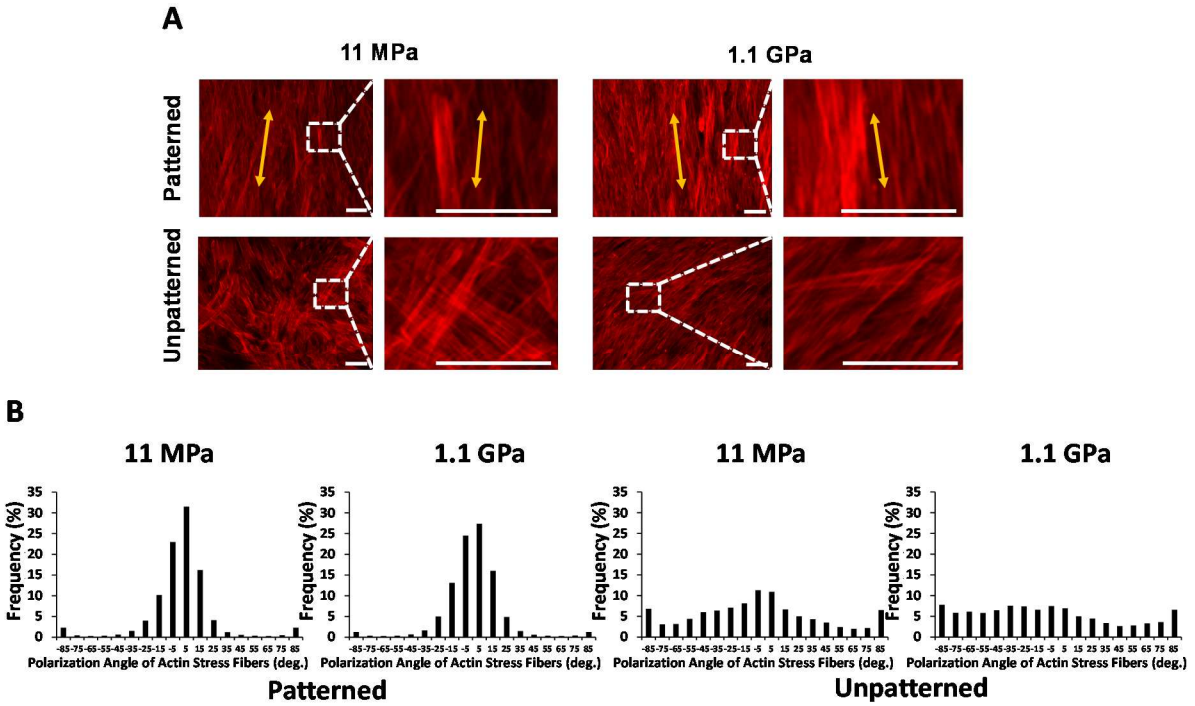

Figure 2.9. Immunocytochemical analyses of the actin cytoskeleton in vSMCs cultured on the different substrata. Clearly, the stress fibers were directionally aligned by both the soft and stiff ANFS, as demonstrated by the histograms. Scale bar: 100 μm.

2.3.10 Potential Mechanistic processes Involved in Cell-Sensing of the Substratum Micromechanics.

The Rho pathway has been implicated in the hypercontractility of vSMCs which could result in vasospasms or hypertension, as reviewed in [125]. In addition, the Rho pathway has also been demonstrated to be involved in rigidity sensing and lineage commitment in stem cells [126]. Given that the vSMCs cultured on nanopatterned stiff substrata recapitulated some of the phenotypic characteristics of hypercontractile vSMCs, we explored the gene expression of components of the Rho-ROCK pathway, specifically RhoA, ROCK1, and ROCK2 gene expression; ROCKs or Rho-associated kinases being the immediate downstream targets of RhoA [127]. As per our prediction, we found statistically higher levels of RhoA, ROCK1, and ROCK2 in the vSMCs cultured on stiff ANFS (Figure 2.10A-C). Our hypothesis was based on the fact that vSMCs on stiff ANFS were longer, less circular, and contractile, expressing higher levels of α-SMA, tropomyosin, and F-actin stress fibers, and high levels of the inflammatory cytokine MCP-1. This points to the possibility that stiffer substrata (such as conventional stents), when "nanopatterned" after *in vivo* deployment via the natural deposition of ECM proteins, could potentiate phenotypic switching (triggering mechanical plasticity [128]) of vSMCs, especially in the case of deep medial injury [129], or, in abnormally reactive smooth muscle stemming from diabetes [130]. This points toward the potential therapeutic benefit of ROCK-inhibitors, such as statins, prior to or post stent deployment. In fact, some of the pleiotropic effects of statins are now attributed to ROCK-inhibition [131]. We also found some of the downstream targets of the Rho-ROCK pathway to be upregulated, the gene expression of which have been well correlated with protein expression and their upregulation found to be associated with the hypertensive vSMC phenotype in pulmonary vSMCs [132, 133]. Thus, nanopatterning the stiff substrata appears to alter gene expression in the Rho-ROCK-LIMK-cofilin pathway in vSMCs, which has been shown to modulate actin assembly in a variety of cell types [134]. Importantly, activation of the Rho pathway has been

associated with the hypertensive vSMC phenotype, as outlined here [135] and fits well with our findings.

We also found caveolin-1, expressed by plasma membrane invaginations (caveolae) and associated with the differentiated vSMC phenotype [136], to be significantly upregulated in vSMCs on nanopatterned soft substrata (Figure 2.10D). Notably, caveolin-1 suppression has been associated with the proliferative airway smooth muscle phenotype [137]. Of particular relevance to this study is also the fact that caveolin-1 has been shown to confer cell polarity [138] which makes our finding that caveolin-1 is upregulated in more polarized cells, specifically those on soft ANFS, interesting. Finally, we also found that the levels of profilin-2 were upregulated in cells on nanopatterned substrata (Figure 2.10E), profilin-2 being affiliated to the Rho pathway and capable of suppressing cell motility and invasiveness via an actomyosin contractility-driven mechanism [139].

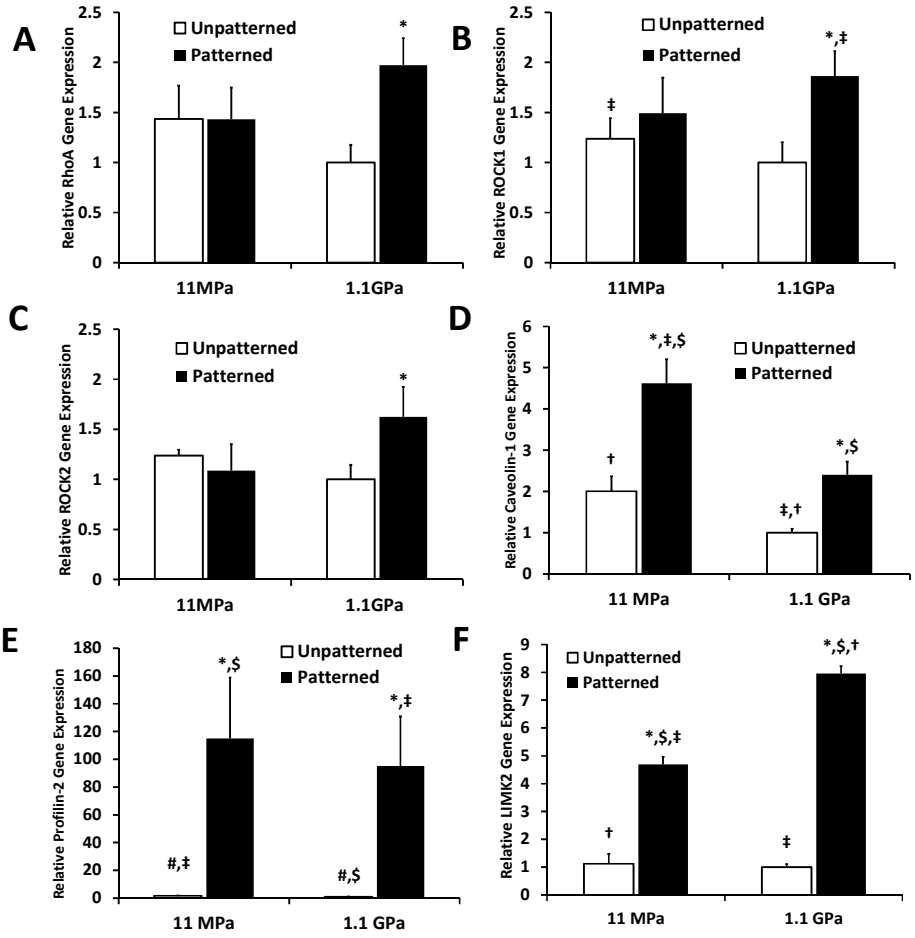

Figure 2.10. RhoA upregulation, along with the upregulation of the Rho-kinases – ROCK1 and ROCK2 ($p < 0.05$), the serine-threonine downstream effectors of RhoA, indicate that the activity of RhoA could be upregulated in the stiff ANFS potentially resulting in overly contractile vSMCs. This phenotype is reminiscent of hypertensive vSMCs and of asthmatic airway smooth muscle cells. Given that the vSMCs on the stiff ANFS are longer (higher EFF), stain higher for F-actin stress fibers, and express high levels of smooth muscle α-actin and tropomyosin and lowered levels of caveolin-1 ($p < 0.05$), it is probable that the phenotype of the vSMCs on the stiff ANFS is distinct from the others. Profilin-2, which has been found to decrease invasiveness and migratory tendencies of cells, was higher in vSMCs cultured on ANFS ($p < 0.05$). Statistically significant difference between nanopatterned and unpatterned substrata ($p < 0.05$) for the same substratum stiffness is indicated with an asterisk. For all other substrata-type combinations, the identical signage indicates statistically significant difference for that pair.

2.3.11 Loss of syndecan-1 increases nuclear localization of Yap/Taz in response to nanopatterned substrates

The Hippo signaling pathway and its intermediates Yap and Taz have been linked to mechanosensing in many cell types [51]. Immunostaining on vSMCs grown on the patterned and nonpatterned substrates demonstrated that S1KO vSMCs had increased nuclear localization of

Yap/Taz on all of the substrates. In addition, on the 2.4 GPa substrates nanopatterning led to increased nuclear localization of Yap/Taz (Figure 11). Cytoplasmic Yap/Taz was similar between genotypes on equivalent substrates, both soft and stiff. Overall, the nuclear/cytoplasmic ratio of Yap/Taz increased in response to nanopatterning on 2.4 GPa substrates and this increase was significantly enhanced with SDC-1 knockout. Treatment with Verteporfin (Hippo pathway inhibitor) or Latrunculin A (disruptor of actin cytoskeletal organization) eliminated differences in Yap/Taz localization between WT and S1KO vSMCs (Figure 11E).

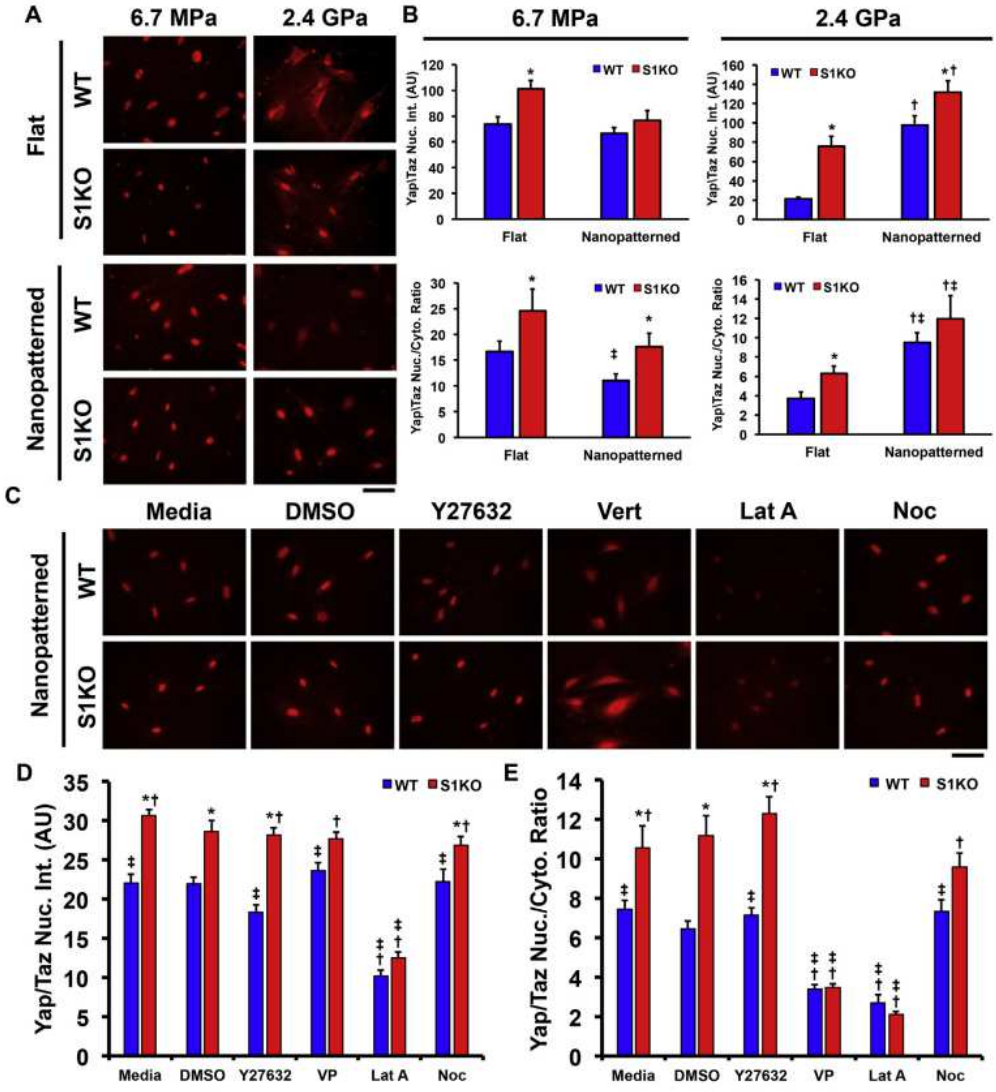

Fig. 2.11. Yap/Taz nuclear localization is altered by nanopatterning and knockout of syndecan-1. Wild type (WT) and syndecan-1 knockout (S1KO) vascular smooth muscle cells (vSMCs) were grown on engineered

substrates for 48 h and then immunostained. (A) Images of immunostaining for Yap/Taz. Scalebar: 200 μm. (B) Quantification of nuclear localization of Yap/Taz in response to the materials. *p < 0.05 versus WT group on the same substrate. y p < 0.05 versus same genotype grown on a nonpatterned substrate. z p < 0.05 between cells with a different genotype grown on a different substrate. (C) WT and S1KO vSMCs were grown 2.4 GPa nanopatterned substrates for 24 h, treated with media only, 0.1% DMSO, 10 mM Y27632, 10 mM Verteporfin (Vert), 1 mM Latrunculin A (Lat A) or 10 mM Nocodazole (Noc) for 2 h and immunostained. Images of immunostaining for Yap/Taz. Scalebar: 200 μm. (D) Quantification of nuclear localization of Yap/Taz in response to the materials and treatments. * p < 0.05 versus WT group of same treatment. y p < 0.05 versus DMSO-treated WT group. z p < 0.05 versus DMSO-treated S1KO group.

2.4 Discussion

The results of our study demonstrated the tunability of the material properties of a PEG-GelMA copolymer while being able to produce high-fidelity, large scale nanotopographies useful for altering cellular function. The incorporation of a reproducible and robust nanofabrication method to a material with variable properties could be highly useful in many applications such as vascular tissue engineering. In particular, we found that the biodegradation profile and stiffness measurements of PEG-GelMA suggest that independently tuning the stiffness and degradation is possible.

The nanopatterned substrates made of 5% PEGDMA and 20% GelMA and the nanopatterned substrates fabricated with 20% PEGDMA and 5% GelMA displayed similar stiffnesses. However the 5% PEGDMA and 20% GelMA samples were degraded significantly faster than the 20% PEGDMA and 5% GelMA samples. This is an indicator that two mechanical material properties, stiffness and degradation, could be controlled independently. Moreover, the PEGDMA to GelMA ratio could be independently tuned to desired levels without affecting cellular morphology because nanofabrication is used as a separate variable to control cell alignment, cell area, and cell elongation related phenotypic changes with cellular adhesion. This is advantageous when designing grafts for tissues with stiffness. The high anisotropy of endothelial cells on nanopatterned substrate suggests that PEG-GelMA nanopatterning could be utilized in designing highly organized tissues by mimicking mechanical, structural properties found *in vivo*.

Physiological enhancement would allow a better model to study endothelialization control, biomimetic platform for drug screening, and better recovery for operations.

The *in vitro* tissue engineering for *in vivo* implantation requires an appropriate scaffold which has mechanical, structural properties mimicking those found *in vivo*. Cell morphology, skeletal assembly, migration, adhesion, and even differentiation are affected by substrate stiffness [111-116]. It has been shown that various moduli are required to model different types of vascular tissues such as artery, vein, and capillary, ranging from 10 kPa to 10 MPa [140]. It is clear that a tunable stiffness would be advantageous in materials used in graft construction. Standard polystyrene or glass culture environment has the substrate elastic modulus on the order of gigapascals which is dramatically higher than real tissue [116, 141, 142]. Although many synthetic polymers have been proposed, their elastic modulus is still in a wide range of mega/gigapascal. Results show that when compared to gigapascals of standard cell culture substrate stiffness, nanopatterned PEG-GelMA was able to provide a substrate stiffness of submegapascal range. This range is more relevant to materials designed to mimic the *in vivo* environment [141]. Compared to PEGDMA, PEG-GelMA has a relatively low material stiffness. A wide range of material stiffness was achieved by varying ratios of PEGDMA and GelMA. High viscosity of the solution was apparent in the polymerization process for high composition of PEGDMA and GelMA groups. The result of PEG-GelMA stiffness indicates that both PEGDMA composition and GelMA composition can be adjusted to achieve a desired stiffness of the substrate. PEGDMA and GelMA composition of 5% and 20%, respectively, and 20% and 5% show an overlapping stiffness, which leads to the possibility that multiple ratios of the composition could be used to fabricate a nanotopography of certain stiffness. Two degrees of freedom enables other mechanical properties such as degradation to be tuned independent of the stiffness. Moreover, by altering the molecular weight of the PEGDMA used in copolymerization, an

additional variable affecting substrate stiffness can be used to provide a further degree of material property control.

In addition to material properties of the PEG-GelMA scaffolds, our robust fabrication method allows for many versatile and cost effective applications. The current design features have a dimension of 600nm in height, 800nm in ridge 800nm in groove length. As our results suggested that HUVECs sensed the directional nanotopographic cues strongly and respond by exhibiting a high anisotropy, desired cellular anisotropy could be successfully mimicked for various vascular tissue engineering purposes with modified nanostructures. The nanostructures could be altered to various topographies with simple lithographic designing. The simple UV-assisted polymerization scheme of PEG-GelMA described here would enable the material to be fabricated in various features, such as a wire form [143, 144]. An ability to fabricate features down to the nanometer scale will allow the PEG-GelMA material to be an excellent material for tissue engineering scaffold designing. As an affordable biomaterial that is non-cytotoxic, biodegradable, tunable, and able to be topographically engineered, PEG-GelMA could be utilized in myriad of applications such as graft, culture platform, and tissue model designing. The next steps toward a clinically viable product will involve fabricating PEG-GelMA in a conduit structure for further assessment. One approach to fabricating this structure might be to cure the monomer solution on a flexible biodegradable substrate and roll this underlying substrate into a tube. An alternative strategy might be to cure the monomer solution while it is shaped below by a mold to have a macroscopic half-pipe shape and while the solution is simultaneously molded by a PUA mold with nanoscale grooves placed on top of the solution. Two half-pipes (or sides of the rolled-up tube) could then be combined into a single conduit with some biocompatible adhesive material or perhaps by a final polymerization step carried out while the two halves are assembled into the tube shape [145]. In addition to synthetic grafts, the optimization of a nanofabricated PEG-GelMA scaffold could also be used in stents, a synthetic material inserted into a patient's blood vessel to

expand a disease-induced, localized flow constriction. Most stents today are made from metals, such as titanium, platinum-irridium, tantalum, and nickel-titanium [146]. The stent metal substrate is sometimes left bare, but is often coated with a drug or biomolecule in an attempt to increase biocompatibility. Unfortunately, many stents occlude after implantation due to stent thrombosis or, more commonly, in-stent restenosis. Stent thrombosis is often caused by hypersensitivity to the coating material and incomplete endothelialization, while in-stent restenosis is caused by a reaction to mechanical injury and the formation of neotintimal hyperplasia [146, 147]. Gelatin-coated metal stents have shown promise in avoiding stent thrombosis and in-stent restenosis as well as facilitating re-endothelialization *in vitro* [148]. However, precise control is challenging and metal is non-degradable. Hence, biocompatible and biodegradable materials that promote the appropriate amount of endothelialization may also improve stent technology and patient outcomes. Bioactive molecules such as peptides, proteins, enzymes, cell growth factors, oligonucleotides, and DNAs are easily conjugated into PEG based hydrogel [101, 107, 149] to increase individual mechanical properties and biocompatibility. Our findings suggest that nanopatterned PEG-GelMA, a biocompatible, biodegradable material with a tunable stiffness and the ability to promote geometrically organized endothelial cell migration, may additionally offer biocompatible materials which could additionally be used as a novel stent material.

Additionally, this chapter provides insight into the mechanisms by which vSMCs respond to the matrix-modulated mechanical environment, recapitulating the architecture of the basement membrane underlying the smooth muscle layers. It also points to the importance of controlled topographical and micromechanical cues in vascular mechanotransduction studies. This study further presents a simple reproducible method to alter the nanotopography of the substrata using CFL that can be exploited to mimic nanostructural changes in collagen or elastin fibril architecture in disease, aging, or vascular remodeling. Moreover, the chapter also have shown that nanotopography can alter signaling through the TGFβ and Hippo pathways through regulating the

generation of cytoskeletal tension with the cells. In addition, SDC-1 knockout creates a contractile state within the vSMCs leading to increased cell stiffness, changes in the response to contractile stimuli and regulating signaling through Yap/Taz. Thus, nanotopology and SDC-1 knockout appear to have synergistic effects on the activation of the Yap/Taz and Rock-1 mediated pathways. These findings add to our understanding of the mechanisms of mechanosensing in vSMCs and provide guidance for the creation of novel biomaterials that can regulate vascular cell function.

Chapter 3. Development of a nanoengineered model of regional ECM alignment in the infarcted heart.

3.1 Rationale

Fibroblasts are highly sensitive to their microenvironment. The chemo-mechanical cues in the injured environment induce the conversion of a fibroblast into a highly specialized cell called the myofibroblast, which is a cell required for fibrotic matrix secretion during the wound healing process. Because the fibroblast is mesenchymal in nature, it still retains a highly plastic phenotype and thus it may be possible to more readily reprogram the fibroblast into different cell types with the right microenvironmental guidance in tandem with the appropriated molecular constituents. Mechanical properties of infarct scar ECM dynamically change over time. Stiffness increases from the kilopascal range to low megapascal range, matrix fibers thickens, collagen content increases, and matrix orientation alters [34, 48, 150]. Current *in vitro* studies which utilize flat tissue culture plastic are significantly stiffer than native scars, and studies on soft gels are failing to consider topographic properties of infarct scars. Electron microscopy (EM) analysis of ECM organization of infarcted mouse myocardium has revealed a striking difference in the directionality of matrix fibers in the healthy myocardium, border zone, and fibrotic region. (Figure 1.3). Healthy myocardium is composed of heavily packed cardiomyocytes with a laminin-heavy matrix in

between. Heavily fibrotic regions consisted of a compacted fibrous matrix in random orientation. Notably, the infarct border zone exhibited a rich fibrous matrix, but in aligned orientation. This significant difference in infarct ECM topography may have a regulatory role in fibrosis progression. However, the complexity of cell types, matrix, and chemical signals in the infarct scar *in vivo* confounds determination of whether cardiac cells respond to specific topographic cues. Thus, a reductionist approach of modeling microenvironmental topographic cues would help investigate how cardiac cells respond to the altered ECM topography in the infarcted heart in the absence of confounding variables present *in vivo*. Altogether, development of a nanoengineered model of regional ECM alignment similar to the post-infarct heart will allow effective infarct model development to investigate topography-specific regulation in fibrosis.

3.2 Scientific Methods

3.2.1 Transmission electron microscopy for assessing ECM organization in healthy and infarcted myocardium

An adult myocardial infarction model was produced adhering to IACUC protocols. Mice were anesthetized, shaved and then intubated for ventilation during surgery. An incision was made on the left pectoralis major followed by exposure of the ribs blunt dissection of the tissue. The 4^{th} and 5^{th} ribs were cut to expose the heart. The pericardium was then removed from the infarct area and the LAD was ligated using an 8-0 non-absorbable suture. The chest was then closed and the mouse was extubated for recovery for 1 month. Myocardium samples were collected for both healthy and infarcted regions and were prepared for TEM imaging. Collagen fiber orientation on the border and core of infarct were then compared with aligned topographies and random topographies developed in this study.

3.2.2 Development of mechanically engineered nanotopographic platform

To develop mechanically engineered nanotopographic platforms, incorporation of a nanofabrication technique termed capillary force lithography was used as in the previous study [110, 151]. An anisotropic nanopattern master was developed by photolithography with a photoresist patterning via using stepper, photoresist development, deep reactive ion etching of exposed silicon, removal of the remaining photoresist, and dicing into silicon masters for polymer fabrication as described previously [95]. Isotropic nanopattern masters were fabricated by utilizing anisotropic patterns. To accomplish this elastic polydimethylsioxane (PDMS) copies of anisotropic patterns were developed by treating silicon masters with trichlorosilane and pouring slygard 184 at 10:1 ratio. PDMS copies were stretched in biaxial direction and ozone plasma treated. Slow, controlled release of the strain resulted in deformation of anisotropy. Isotropic PDMS patterns were then used as a master for desired polymer fabrication. It has been shown that UV-assisted capillary force lithography (CFL) is exceptionally advantageous in fabrication. It could be utilized for fabricating scalable, inexpensive, conformal nanostructures for cell culture substrates in the scale of tissue level (>25 cm^2), while the resolution of lithography is preserved down to a 50 nm scale [95, 152-154]. Through UV-assisted CFL, isotropic and anisotropic nanotopographies were copied onto flexible polyester film and then applied to circular cover glass of 18 mm diameters. This was accomplished by drop dispensing UV-curable Norland Optical Adhesive (NOA) 76 on to the chosen template and then joining it with the polyester film. NOA 76 was chosen for its ability to culture cells, optical transparency, and young's modulus of 6.7MPa. This allowed the polymer solution to form nanotopography copies by capillary force. Together they were cured under UV and then separated by hand. With a copy of the nanopattern on the polyester film, it was designated as a workable template to be used for the fabrication of nanopatterned cover glass. The template was left under UV overnight. The template was then coated with NOA 76 and pressed onto cover glass that had been treated in ozone, coated in glass primer, and dried. The

joined template and treated cover glass were cured under UV, and then separated. The cover glass stamped with the nanopattern was cured overnight under UV. Patterned cover glass was then adhered to the bottom of a glass bottom dish using NOA76 to cover up the microwell. The patterned side was exposed in the microwell for use in cell culture. The device was then left under UV overnight. Random patterns were developed through biaxial stretch, ozone treatment, then shrinking of PDMS patterns as previously described [155]. Devices lacking nanopatterns were also constructed in this way by using nonpatterned polyester film as the template. Fidelity and reproducibility of the fabricated topography were then confirmed by SEM.

3.2.3 Culturing cardiac fibroblast on nanotopographic platforms

Mouse Embryonic Fibroblasts (MEF) were isolated from the fetus of pregnant mice at 14 days post-coitum. MEF cells were then expanded in culture media (DMEM + 10% FBS + 1% p/s) until passage number 3 and were frozen down for future experiments. MEF cells were then thawed and stabilized through 1~2 passage at 1:3 split ratio at 75% confluency to ensure all experiments were conducted with equal conditions. For each experiments, fibroblasts between passage number 4~5 were used for consistency. Nanotopographic platforms used in experiments were sterilized with 70% alcohol and left under UV overnight. The nanotopographies were then coated with gelatin at 2% (w/v) to enhance cell attachment while avoiding matrix protein initiated transdifferentiation. Gelatin was aspirated and topographies were allowed to dry for 2 hours. MEF cells were added to the engineered platform at 100,000 cells/mL and incubated in 37°C, 5% CO_2 with experimental media (DMEM + 1% FBS + 1% p/s) for 72 hours. The TGFβ treatment group received TGFβ (R&D systems) at 10 ng/mL.

3.2.4 Assessment of cell culture capability on nanotopographic platforms

Cell attachment, proliferation, and viability is critical in assessing the topographic regulation on cardiac cells. To assess cell attachment to nanotopographic platforms, fibroblasts were cultured

at 100,000 cells/mL and allowed to attach for 6 hours. Attached cells were counted after a gentle wash with DPBS. Cell proliferation was assessed via ki67 staining. MEF cells were co-stained for DAPI and αSMA. Fluorescence images were analyzed to assess proliferation for both anisotropic and isotropic nanopatterns. Morphological analysis was completed after culturing MEF cells for 72 hours on each platforms as described above. Samples were fixed, and ImageJ software was used to assess cell morphology for each condition. Cell proliferation rate, area, directionality and elongation were assessed to evaluate the engineered post-infarct topography's ability to recapitulate fibrotic cell responses.

3.3 Results

3.3.1 Nanoengineered platform development for recapitulating infarct geometry

Myocardial infarction significantly remodels the myocardium matrix and residing cells. As shown in the schematics in Figure 3.1A, the infarct zones are identified by densely packed fibrous collagen. As previously shown, myocardium of healthy or remote zone was mostly occupied by cardiomyocytes. The border zone of infarct was where myocyte necrosis occurs and myofibroblast population was observed along with dense vessels. Interestingly, myofibroblast population was only localized on the infarct border zone and the core of infarct zone lacked myofibroblast population [156]. Researchers have also found that the geometry of deposited matrix on the infarct site is also significantly different in the infarct zone and border zone [50, 156]. A heart infarction induced with LAD ligation for 1 month were observed through TEM microscopy to assess matrix geometry. Collagen deposited in the infarct zone exhibited random orientation (Figure 3.1B left). Collagen fibers deposited on the border zone of the infarct was anisotropically aligned (Figure 3.1C left). Such differences in the topographic orientations were recapitulated *in vitro* through nanofabrication techniques (Figure 3.1D) as described previously [94]. Coverglass was first treated with primer, then UV-curing polymer was dispensed for capillary force lithography.

NOA76 was chosen to recapitulate the infarct elasticity of low megapascal range. Recent studies have revealed that myofibroblast transdifferentiation are closely governed by stiffness. Moduli of standard tissue culture plastic or coverglass ranges at hundreds of gigapascal, which would be unsuitable for investigating specific variable-dependent transdifferentiation. Master pattern film was placed on top of UV-curing polymer, and cured to complete the pattern development. Random patterns were developed through biaxial stretch, ozone treatment, then shrinking of PDMS patterns as previously described [155]. The UV-curing polymer was then used to develop random platform devices. Unpatterned surfaces were developed by using flat silicon surface as a master. Resulting random (Figure 3.1B right) and anisotropic (Figure 3.1C right) topographies recapitulating infarct zone and border zone respectively were imaged through SEM to confirm fidelity and reproducibility.

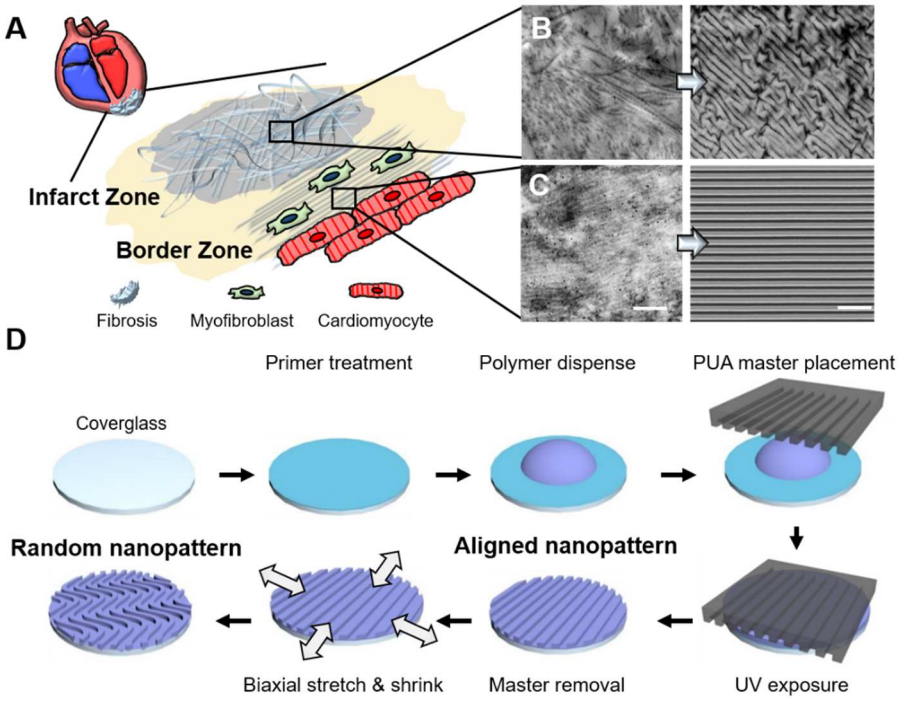

Figure 3.1. Illustration of cardiac infarct matrix geometry during fibrosis. (A) During fibrosis, myofibroblast population rise on the border of the infarct site resulting in deposition of matrix. Matrix organization in infarcts are dynamically remodeled, exhibiting random orientation in the core of infarct (B, left), and aligned orientation in the border of infarct (C, left) as shown by TEM image of 8-week LAD ligation-infarcted mouse myocardium. An *in vitro* model was designed to recapitulate regional matrix topographies in fibrotic infarct. SEM images of random (B, right) and aligned (C, right) nanotopographies were developed to match matrix

organization of core and border of fibrotic infarct respectively. (D) Schematics of *in vitro* nanopatterns fabrication is shown. Coverglass was first primer coated, and UV-curable polymer was drop-dispensed. Nanotopography master was placed, and UV was exposed to cure nanoengineered platform. Removal of master mold completed aligned nanopatterns. Random platform was developed by utilizing PDMS. PDMS aligned nanopattern was biaxially stretched and slowely shrunk to produce random topographies. Random PDMS topography was utilized as a master mold to develop random topographic platform. Scale bar: 2 μm Scale bar: 5 μm

3.3.2 Nanoengineered infarct platform were able to align cells without altering cell attachment and viability

The nanoengineered infarct platform were tested for its capability to culture cells through culturing mouse embryonic fibroblasts (MEF). As the study attempted to observe topographic regulation on fibroblast fate and function, cell alignment, initial cell attachment, and cell viability on different topographies were tested as these factors could affect transdifferentiation of fibroblasts. Cell alignment was assessed by culturing MEF cells on unpatterned, aligned, and random platform and allowing MEF cells to employ topographic cues for 72 hours. Brightfield images were taken and using imageJ software, cell alignment was quantified. Quantitative analysis of cell alignment revealed that MEF cells did not express directionality on unpatterned and random platform. On aligned platform, MEF cells expressed directionally aligned morphology congruent to the underlying nanotopographies showing directional cues were able to regulate MEF cell phenotypically (Figure 3.2A). Cell attachment to each topographic substrates were observed by first coating each substrates with 2% gelatin and seeding each platforms with cell density of 100,000 cells/mL After 6 hours, unattached cells were washed away, and the number of cells attached were counted (Figure 3.2B). Cell attachment to unpatterned, aligned, and random patterns were not significantly different suggesting our topographies did not affect cell-platform interactions and can achieve relatively equal cell density while culturing. Cellular viability was assessed through live-dead stain after 72 hours of culture in conditions described in the method section. As TGFβ treatment was a golden standard for observing transdifferentiated myofibroblasts, cell viability with and without TGFβ treatment on unpatterned, aligned, and

random topographies were assessed (Figure 3.2C). Results exhibited that no significantly cell deaths were resulted on our platform, and each topographies were not affecting cell viability. It was noticed that the morphology of MEF cells were affected by each patterns significantly over time. Previously, fibroblasts transdifferentiated to myofibroblast were reported to have larger cell area [1, 157, 158]. As expected, TGFβ treatment resulted in larger cell area (Figure 3.2D). Interestingly, aligned pattern resulted in larger cell area even without TGFβ, and with TGFβ the effect was synergistic. MEF cells on random was generally smaller as reported previously [155].

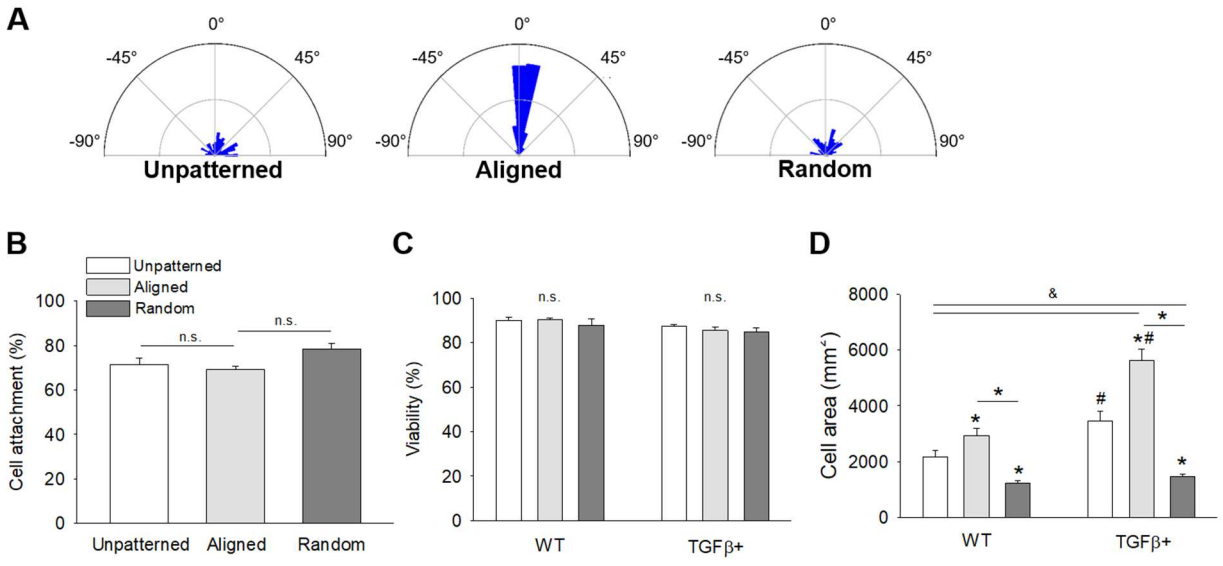

Figure 3.2. MEF cell culture on topographic platforms (A) Mouse Embryonic Fibroblast (MEF) cell was cultured on unpatterned (A, left), aligned (A, middle), and random (A, right) platform. Cell alignment was quantitatively analyzed to confirm effect of alignment cue. (B) Cell attachment was assessed by seeding MEF on each platform for 6 hours and counting attached cells. (C) Cell viability was assessed by live/dead assay after 72 hour culture on each platform with and without TGFβ treatment. (D) Cell area was quantitatively analyzed to observe increased cell area on aligned pattern and synergistic effect with TGFβ.

3.4 Discussion

Utilizing the techniques optimized from the Chapter 2, a recapitulation of post-infarct ECM geometry was conducted in this Chapter 3. Heart engineering often focus on myocytes and contractile function of the heart. However, fibroblasts are undoubtedly as important in maintaining structural integrity and are responsible for fibrosis, which most populations experience through

myocardial infarction, hypertension, diabetes, genetic disorders, and even with age [157-159]. As fibroblasts take up about 15% of cell population of the healthy heart and critically regulate infarct scar formation and fibrosis, understanding the regulation of fibroblasts would allow the field to better assist impacted hearts [160]. Previous studies have found that myofibroblasts population rise upon injury, and were localized on the border of the infarct zone [156]. Moreover, the infarct border ECM topography dynamics were reported to be significantly altered throughout the fibrosis [50]. Although myofibroblasts were reported to regulate infarct scar preventing initial heart rupture, assist in wound regeneration, and responsible for uncontrolled fibrosis, the regulation of myofibroblast in response to infarct ECM topographies has not been investigated [161, 162]. Chapter 3 attempted to develop an *in vitro* model to mimic ECM topographies of post-infarct scar. TEM images of fibrotic mouse myocardium affected by LAD ligation has revealed that ECM dense infarct region are regionally regulated. Infarct border zone expressed aligned organization of fibrous ECM, and infarct core expressed randomly organized ECM. Such geometric cues were recapitulated via nanoengineering techniques. SEM images were used to confirm fidelity and reproducibility of each platforms. MEF cells were chosen to model infarct scar fibrosis for their plasticity. Nanoengineered platforms were tested for their ability to provide alignmental cues and maintain cell culture conditions. We were able to alter topographies without altering cell attachment, and cell viability. Only on aligned platform, cells exhibited directional morphology and enlarged cell area which is one phenotypic marker for transdifferentiated myofibroblasts.

Taken together, the Chapter highlighted the striking difference in ECM organization in infarct scar region. Developed platforms were able to modulate nanotopographies independent of cell attachment and viability, and was confirmed to provide alignmental cues to regulate cell morphology.

Chapter 4. Investigate cardiac cell fate in response to topographic cues found in posti-infarct ECM topography.

4.1 Rationale

In vivo, fibroblasts and myofibroblasts regulate ECM dynamically, and remaining cardiomyocytes respond to environmental cues simultaneously. Heart microenvironmental ECM is known to maintain the heart's electrophysiology, allow functional cardiomyocyte configuration, and provide residing cells with appropriate signaling proteins [34]. Fibroblasts transdifferentiate into myofibroblasts when tissue injury occurs through increased mechanical load and secretion of cytokines such as TGFβ. Moreover, myofibroblast localized on the border of infarcts exhibit elongated morphology congruent to the direction of ECM [17], suggesting the fibrotic microenvironment and ECM topography have a close relationship. Recently, mechanical cues such as cyclic stretch [51-53], rigidity [43, 51], micropatterned proteins [54], infarct location [39], and topographic cues [42, 45] were identified and elucidated for roles in cardiac scar formation and myofibroblast regulation. Our group has shown that cardiomyocytes are sensitive to anisotropic nanotophographies and express mature sarcomere structure [163] on anisotropic topographies. However, current understanding of microenvironmental regulation on fibroblasts and cardiomyocyte interactions in the context of fibrosis are limited. Traditional understanding of myofibroblasts' role in cardiac wound healing was mainly from *in vitro* experiments on flat tissue culture plastic. These settings are distant from rich *in vivo* microenvironments with which cardiac cells continuously interact. Recent structural analysis of infarcted myocardium exhibiting regional differences in ECM topography raise the question of how cardiac cells respond to such remodeled topography. Specifically, with our ability to develop nanoengineered topographies that recapitulate infarct border and core ECM and previous findings of cardiac cells showing topography induced responses *in vitro*, this Aim will investigate how fibroblasts and cardiomyocytes respond to infarct topographies via myofibroblast marker assessment,

cardiomyocyte behavior analysis, and co-culture modeling. Assessment of myofibroblast markers on post-infarct topography platform will highlight the importance of topographic regulation during fibrosis. Once certain topographies are identified to transdifferentiate myofibroblasts, a therapeutic approach to remediate ECM topography might be possible. Few studies have attempted to inject stem cell-derived cardiomyocytes to remuscularize infarcted myocardium, but such techniques are limited by low engraftment and lack of understanding on cell fate imposed by post-infarct ECM. The proposed platform could successfully model how cardiomyocyte proliferation, maturation, and contraction are altered in response to fibrotic ECM topography. Moreover, a co-culture of fibroblasts with cardiomyocytes will be able to model cell injection therapy, and may explain why cardiomyocytes do not repopulate infarct region even though anisotropic topographies have been found to maturate them previously, and that attempts to remuscularize infarcted myocardium must focus on fibroblast and matrix topographies.

4.2 Scientific Methods

4.2.1 Fluorescent staining for myofibroblast transdifferentiation in response to various mechanical cues

Mechanical regulation of MEF transdifferentiation was investigated using various forms of mechanical cues. Myofibroblast transdifferentiation is primarily identified through αSMA expression. By observing αSMA expression in fibroblasts cultured in engineered nanotopographies, we were able to investigate how remodeled infarct ECM regulates myofibroblast transdifferentiation. MEF cells were cultured at 100,000 cell/mL on the device. MEF cells were fixed at 72 hours after seeding and stained with antibodies such as αSMA (1:1000, Sigma), YAP (1:500, Cell Signaling), and tensin 1 (1:200, Sigma). Using the same exposure and LUT settings, fluorescent images were quantitatively analyzed to assess the ratio of αSMA

expressing cells over total cells. The role of topographic organization in recapitulating infarct topography was investigated by analyzing αSMA expression levels of fibroblast cultured on unpatterned, aligned, and random substrates.

4.2.2 Assessment of matrix secretion in response to post-infarct geometries

Matrix secretion is one of the key features of fibroblast and myofibroblast function, and excessive deposition of ECM leads to fibrotic scarring. Investigation of how the microenvironment regulates residing fibroblasts matrix deposition would reveal the role of the remodeled scar on progressive ECM accumulation during fibrosis. Fibroblasts were cultured on nanoengineered platforms for 72 hours before fixation. Directionality of secreted matrix was investigated via custom written MATLAB code with fluorescently labeled collagen images to determine whether orientation of topographies governs the directionality of secreted ECM deposition. Whole coverslip-integrated multiwells were used for assessing collagen production by staining collagen with collagen type 1 antibody, then quantified through the color deconvolution function in ImageJ. Quantification of matrix secretion was complemented with RT-PCR of characteristic ECM proteins such as collagen 1A2, periostin, and ED-A fibronectin. Total RNA were extracted using Invetrogen's manufacturer's protocol. 2 μg of total RNA was used for cDNA synthesis, and RT-PCR was conducted with an automated thermal cycler CFX96 Real-Time System (BIO RAD). Reactions were run in triplicate. The signals were normalized to housekeeping gene GAPDH as an internal control. The primer sequences are provided in the Suppplemental Table 1. A $2^{\Delta\Delta CT}$ method was used to analyze each protein expression.

4.3 Results

4.3.1 Fibroblast transdifferentiation and proliferation are regulated by topographic cues

Previous fibrosis studies mainly focused on chemical regulation of myofibroblast transdifferentiation. However, as the Figure 4.1B, 4.1C and number of studies shows, microenvironment of infarct region is vastly different from healthy myocardium, and even within infarcted heart, border and infarct zone exhibited significantly altered geometry [50]. Moreover, myofibroblast population has been reported to be increased on the border of infarct zones [156]. Here we investigated whether *in vivo* topography-recapitulating platforms can regulate fibroblast transdifferentiation by altering topographic cues. Increased transdifferentiation and proliferation has been suggested to explain rise in myofibroblast population on the border of infarcts [156, 164, 165]. However, it is not clear how those factors are regulated. We attempted to investigate the effects of infarct topographies on myofibroblast transdifferentiation and proliferation and whether rise in myofibroblast population on the border after injury is from one particular results. MEF cells were cultured on each topographic platforms for 72 hours with or without TGFβ. Cells were fixed and stained for immunofluorescent imaging. Ki67 was used to distinguish proliferating cells, and αSMA was used to mark transdifferentiated myofibroblasts with positive actin stress fibers (Figure 4.2A). A closer observation of αSMA stress fiber expression suggested that aligned topographies resulted in polarized stress fiber expression which was absent in unpatterned and random platform (Figure 4.2B). A custom written MATLAB script was used to analyze the orientation of stress fibers (Figure 4.2C). A clear polarization of actin stress fiber organization was observed on aligned platform with 63.8% stress fibers aligned within 25 degree to the direction of topographies. Quantitative analysis of Ki67 positive cells has shown that cell proliferation was promoted on aligned topographies and was significantly higher with TGFβ treatment (Figure 4.2D). Topographic regulation on transdifferentiation was assessed by quantitatively analyzing αSMA positive cells after culturing MEF cells for 72 hours on each topographic platforms (Figure 4.2E).

As expected, MEF cells transdifferentiated significantly with TGFβ treatment on unpatterned platform. Notably, MEF cells exposed to aligned topographies displayed promoted transdifferentiation even without TGFβ treatment. The ratio of αSMA positive MEF cells on aligned topographies (6.56%) was comparable to that of unpatterned platform with TGFβ treatment (7.57%). The transdifferentiation was synergistically increased with TGFβ treatment on aligned topography (9.92%). MEF cells on random topography showed lower transdifferentiation when compared to unpatterned platform even with TGFβ treatment. As similar results were observed on cell proliferation, in order to check whether topographies affect both transdifferentiation and proliferation, the ratio of cells with both Ki67 positive and αSMA stress fiber positive were assessed. Notably, MEF cells did not exhibit Ki67 markers with αSMA stress fibers on unpatterned platform, but only on nanoengineered platform (Figure 4.2F). A representative image shows a MEF cell without both Ki67 and αSMA expression (Figure 4.2F orange), with both Ki67 and αSMA expression (Figure 4.2F yellow), Ki67 negative/ αSMA positive (Figure 4.2F cyan), and Ki67 positive/ αSMA negative (Figure 4.2F white) expression on aligned platform. Specifically, aligned topographies not only induced both proliferation and transdifferentiation, but also increased sensitivity to TGFβ treatment where significantly more cells displayed both Ki67 and αSMA stress fibers as representative image (Figure 4.2G).

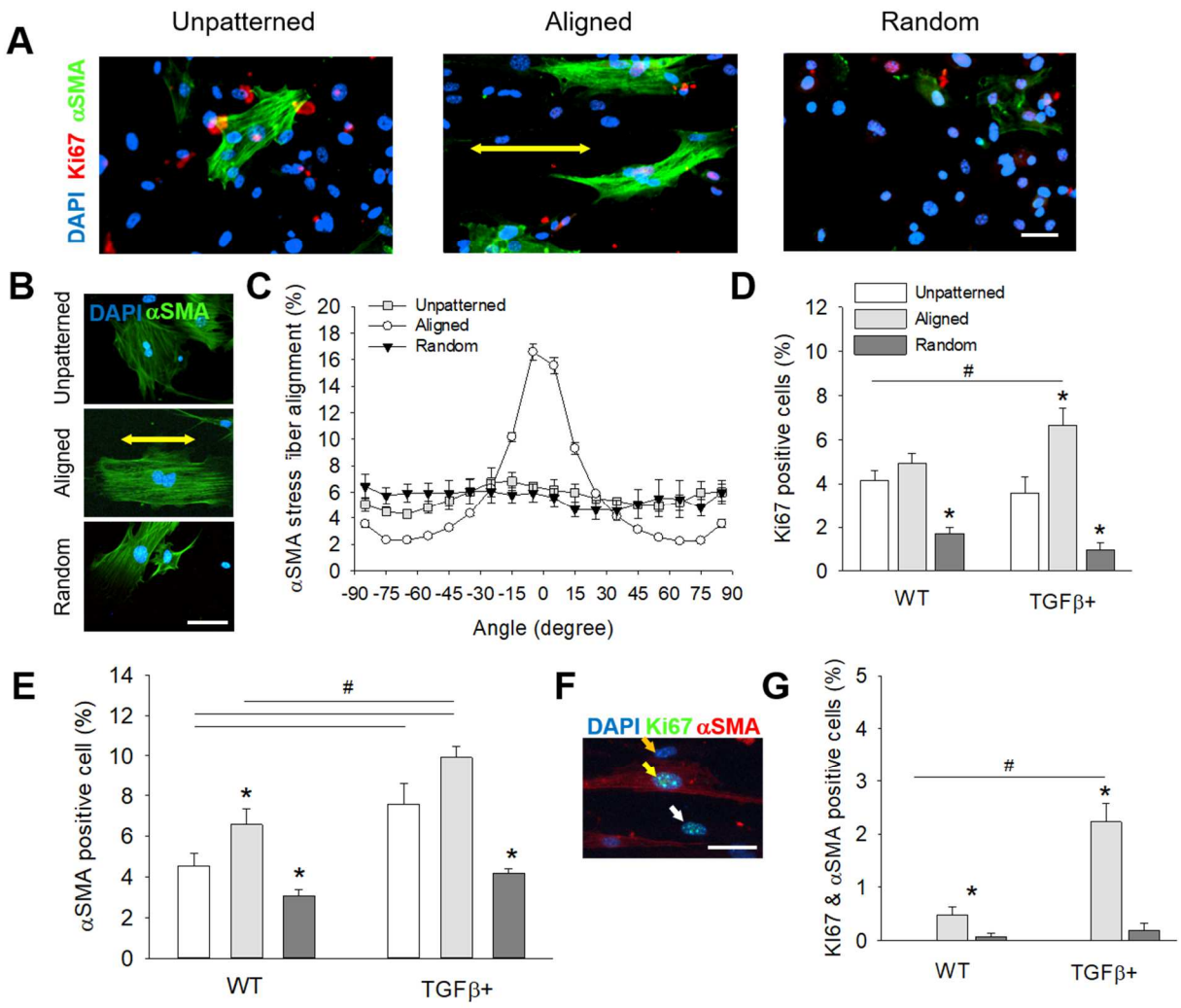

Figure 4.2. Fibroblast proliferation and transdifferentiation are regulated by topographic cues. (A) Immunofluorescent image of MEF cells after 72-hour culture in low serum condition on unpatterned (A, left), aligned (A, middle), and random (A, right) topographies. Green: αSMA. Red: Ki67. Blue: DAPI. (B) Representative images of actin stress fiber alignment on unpatterned (B, top), aligned (B, middle), and random (B, bottom) topography. (C) Aligned topography resulted in highly aligned actin stress fiber. (D) Quantitative analysis of the ratio of proliferating ki67 positive cells have shown directional topographies could modulate cell proliferation. (E) Quantitative analysis of the ratio of transdifferentiating αSMA positive cells exhibit significantly higher transdifferentiation with TGFβ treatment in all groups. Aligned topography significantly increased transdifferentiation whereas random topography resulted in inhibited transdifferentiation. (F) Representative image of Ki67 negative/αSMA negative (orange), Ki67 positive/αSMA positive (yellow), and Ki67 positive/αSMA negative (white) MEF cells on aligned platform. (G) Quantification of both Ki67 and αSMA positive cells revealed that MEF cells transdifferentiate and proliferate only on topographic platforms. Yellow arrow=Direction of topographic alignment. Scale bar: 100 μm.

4.3.2 ECM secretion direction is regulated by topographic cues

Myofibroblasts are identified by few factors such as αSMA expression, larger cell area, and contractility. However, the most important marker and phenotype of myofibroblast would be its ability to generate ECM accounting to their role in infarct formation. MEF cells were allowed to transdifferentiate and secrete ECM on unpatterned (Figure 4.3A left), aligned (middle), and random (right) platforms for 72 hours. Cells were fixed and stained with collagen type 1 antibody to observe ECM secreted by myofibroblasts. A custom made MATLAB code was used to analyze directionality of secreted collagen type I (Figure 4.3B). MEF cells provided with aligned topographic cues secreted collagen in the direction of the topographic cues (yellow arrow) whereas MEF cells on unpatterned and random topographies secreted collagen without distinguishable directionality. The results of aligned topographies inducing secretion of ECM congruent to underlying topography suggest that there may be a positive feedback loop in border zone formation. A previous study has revealed that fibroblasts secrete ECM in the direction of topographies it is exposed to [166], and ECM on the infarct border has been found to be aligned in the direction of pre-existing resident myocytes [50].

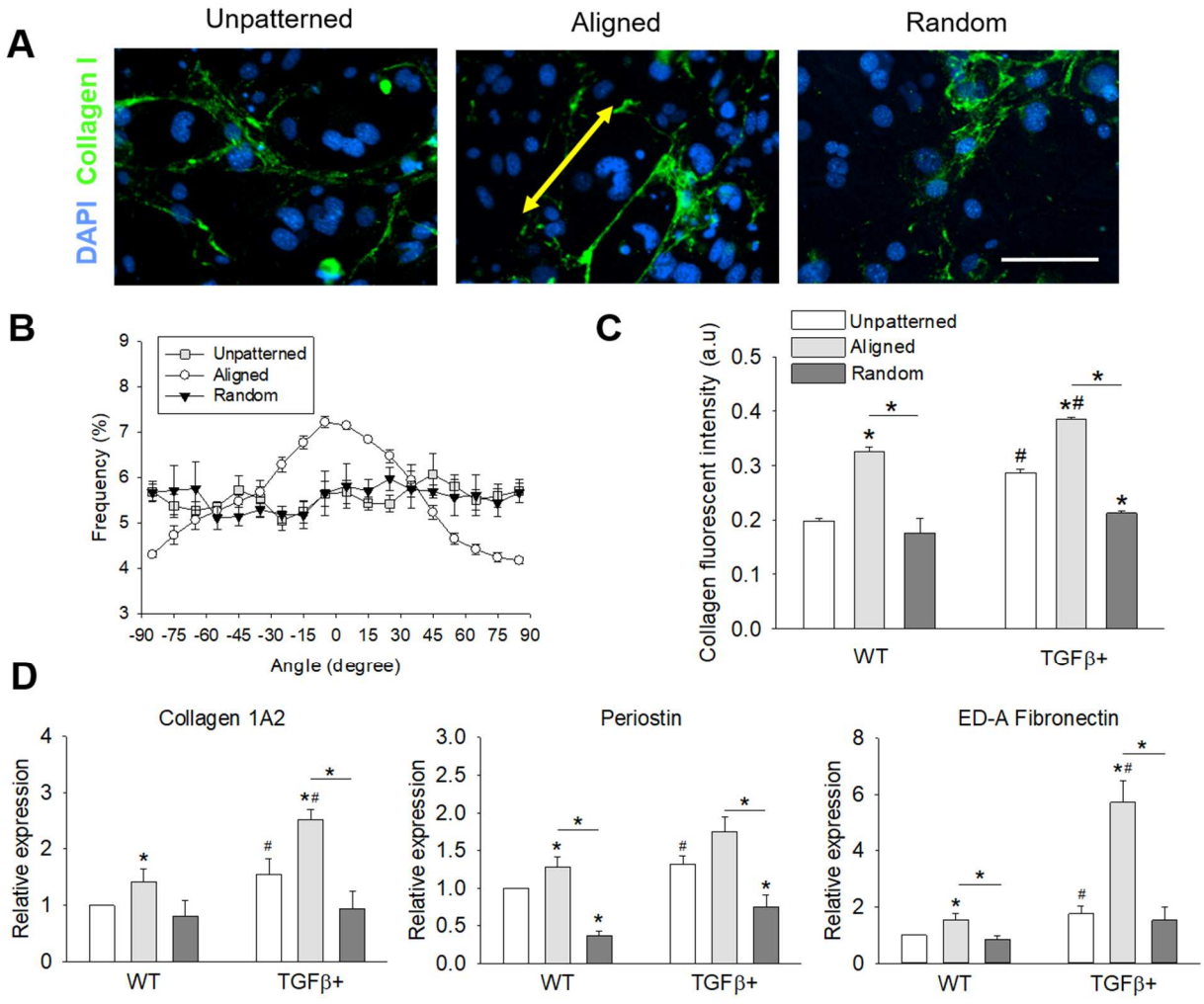

Figure 4.3. ECM secretion and synthesis are regulated by topographic cues. (A) MEF cell ECM secretion was assessed by staining collagen I after 72 hour of culture on unpattenred, aligned, and random platforms. Yellow arrow=Direction of topographic alignment (B) Directionality of secreted ECM was analyzed to observe topographic regulation of ECM orientation. (C) Quantity of secreted ECM was assessed by measuring fluorescent intensity on collagen I on unpatterned, aligned, and random platforms. (D) RT-PCR of myofibroblast characteristic ECM, collagen 1A2 (D, left), periostin (D, middle), and ED-A fibronectin (D, right). Scale bar: 100 μm

4.3.3 ECM secretion is regulated by topographic cues

A fluorescent intensity measurement was conducted to measure the amount of ECM secreted by MEF cells on each topographies (Figure 4.3C). Similar to the αSMA quantitative measurement result (Figure 4.2E), ECM secretion was promoted with TGFβ treatment. Interestingly, aligned topographies alone have significantly boosted the ECM secretion even higher than unpatterned

with TGFβ treatment ($p<0.05$). On aligned topographies, TGFβ treatment synergistically increased the secretion. Random topographies exhibited similar level of ECM secretion to unpatterned platform. In order to complement intensity measurement, RT-PCR was conducted to measure known ECM that are secreted by myofibroblasts. Collagen 1A2, periostin, and ED-A fibronectin are common matrix proteins that myofibroblasts secrete [158, 164, 167]. Periostin and ED-A fibronectin especially could be used to differentiate fibroblasts and myofibroblasts [99, 158]. RT-PCR was conducted on collagen 1A2 (Figure 4.3D left), periostin (Figure 4.3D middle), and ED-A fibronectin (Figure 4.3D right) and analyzed each gene expressions. All matrix gene expressions were increased with TGFβ treatment as expected from transdifferentiated MEF cells. When comparing each topographic platform, aligned topographies were enough to induce all collagen 1A2, periostin, and ED-A fibronectin expressions even without TGFβ treatment. Moreover, TGFβ effects were additive to aligned topography as relative expression of each gene was significantly higher with TGFβ treatment on aligned platform. On random topographies, such expression was similar to unpatterned or inhibited. This report would be the first case investigating the topographic regulation on fibroblast transdifferentiation, and the results revealed that alignment cue alone was capable of inducing transdifferentiation at a similar level to TGFβ.

4.4 Discussion

This Chapter has recapitulated the infarct ECM topographies through developing nanoengineered platforms and found that topographic orientations have significant regulatory effect on myofibroblast transdifferentiation. Our results showed that platforms that recapitulated a highly aligned, dense matrix was alone sufficient to transdifferentiate myofibroblasts along with increased matrix protein synthesis. Moreover, the direction of secreted matrix was sensitive to the topography cells were exposed to, suggesting that there may exist a positive feedback loop of pre-existing directionality. This could be stimulating fibroblasts to myofibroblast, and ECM

secreted by myofibroblasts in the direction, intensifying more transdifferentiation. Unexpectedly, cell proliferation was also altered by topographic cues which border zone recapitulating aligned topographies promoting higher proliferation rate, even resulting in proliferating myofibroblasts normally not observed for transdifferentiated cells. Proliferation was inhibited with random topographies suggesting cell division or proliferation may be correlated to directional cues it is exposed to. Such results may explain why population of myofibroblasts are concentrated on the border zone of infarcts where aligned matrix fibers are abundant and not in the core of infarcts where injury signals are still present, but packed with dense random matrix fibers. The increased sensitivity to TGFβ treatment and higher transdifferentiation on aligned pattern may also explain why myofibroblasts are populated mainly on the border zone. Altogether, results from this study may allow us to understand how the alignment in ECM fibers on the infarct border are generated and intensifies upon injury over time. Although majority of fibrosis has been focusing on chemical aspect of regulation, recent studies including our own suggests mechanical cues such as stretch, stiffness, and topographies also have a major impact on fibroblast fate and function. Future fibrosis studies will be able to incorporate mechanoregulation for understanding the dynamics of infarct scar development.

Chapter 5. Investigation of mechanotransduction pathways involved in myofibroblast transdifferentiation in response to post-infarct ECM topography.

5.1 Rationale

In order to overcome the current limitations for studying infarct scarring, we must understand how various environmental factors including topography affect cardiac cells. Understanding the

mechanisms of key regulators of fibroblast differentiation and the role of mechanical cues on fibroblast lineage determination would contribute to therapeutic approaches to prevent persistent myofibroblast transdifferentiation once the initial injury response has resolved. However, the steps in myofibroblast transdifferentiation are still not well understood, including the mechanistic regulation of transdifferentiation, as well as the interplay between chemical ligand and microenvironmental cues. Preliminary results showed anisotropic nanopatterns that recapitulate infarct border ECM topography resulted in pro-fibrotic response and randomly oriented nanopatterns that mimic the core of infarct scar suppressed myofibroblast transdifferentiation. Such findings may recapitulate *in vivo* myofibroblast transdifferentiation in response to ECM remodeling, and how the topographic cues are sensed by fibroblasts and signals are transduced must be investigated in depth. Previous studies have identified actin-mediated mechanotransduction pathways that may participate in myofibroblast transdifferentiation [27, 59, 77, 168]. Cyclic strain activated myofibroblast transdifferentiation was found to require a noncanonical pathway of TGFβ that involve p38 activity [169], which is a kinase in the mitogen-activated protein kinase (MAPK) signaling family. Mechanical perturbation such as perpendicular traction forces activates p38 via the integrin-actin cytoskeletal complex [55]. Inhibition of p38 via lox P-Cre deletion resulted in loss of tension-dependent actin remodeling that is an indicator of myofibroblast transformation. Previous *in vitro* study with fibroblast cultures on cyclic strain conditions suggests that myofibroblast transdifferentiation could be initiated mechanically without any secondary soluble growth factors [170]. This mechanical stimulation was not translated into αSMA expression and fibrotic response was significantly minimized when p38 was deleted. Our group has previously shown that the modulation of p38 has a critical role in myofibroblast transdifferentiation in conjuction with mechanical cues such as cyclic strain [59]. However, whether p38 is involved in topographic regulation has not been investigated. Another actin-mediated mechanosensitive pathway, RhoA/Rho-associated kinase (ROCK) has found to be

critical for development of fibrosis *in vivo* [77]. The role of ROCK in mechanotransduction for cell fate regulation has been well characterized previously [171, 172]. ROCK1 has been found to be critical for the development of cardiac fibrosis, and inhibition of ROCK1 activity is a promising anti-fibrotic therapeutic strategy [77]. ROCK has shown some regulatory effect in transducing topographic cues, but its role in myofibroblast transdifferentiation in response to fibrotic scar geometry has not been investigated. Actin-MRTF-SRF has also been identified to be critical in regulating cardiac remodeling [27, 168]. SRF is a downstream regulator of ROCK which is known to participate in actin regulation. Unlike ROCK, the role of SRF in mechanotransduction in fibrosis is has not been studied. As evidence suggests actin-mediated mechanotransducers participates in regulating external mechanical cues, our goal is to utilize a reductionist approach to isolate components of the complex regulatory mechanism of myofibroblast transdifferentiation in response to topographic cues of infarct scars in a well-controlled *in vitro* platform. Altogether, this Aim will investigate the identification regulators of mechanotransduction via modulating candidate pathways in order to broaden our understanding of mechanisms underlying myofibroblast transdifferentiation and fibrosis.

5.2 Scientific Methods

5.2.1 Investigation of p38 and YAP interactions through Immunoprecipitation

For immnunoprecipitation, cell were lysed in ice-cold lysis buffer (50 mM HEPES at pH 7.5, 150 mM NaCl, 1 mM EDTA, 1% NP-40, 10 mM pyrophosphate, 10 mM glycerophosphate, 50 mM NaF, 1.5 mM Na_3VO_4, protease inhibitor cocktail [Roche], 1 mM PMSF). Cell lysates were frozen down for 24 hours in -80 degree, and centrifuged for 10 min at 4°C to use supernatants. Quantify of protein was measured with nanodrop, and 1mg of total protein was mixed with 2.5 μg of antibody. Mixture was store at 4°C for overnight. Next day, 10μL of protein magnetic beads were added and beads for collected by using magnetic stand. Ice cold lysis buffer was used to wash

beads. After collecting and removing lysis buffer, laemmli buffer was added to denature at 100°C for 5 min. Samples were then loaded onto gradient gel for western blot.

5.2.2 Investigation of the role of p38 on mechanical transduction for myofibroblast transdifferentitaion

Adenovirus-mediated Cre deletion of lox P targeted p38 were utilized to generate a fibroblast knockout model. Primary MEFs were isolated from homozygous loxP targeted p38 mouse using the isolation protocol described above. Isolated p38 floxed MEF cells were seeded onto post-infarct model topographies to test whether p38 regulates topographic cues. Transdifferentiation of p38 knockout MEF was assessed by culturing p38 floxed MEF cells on nanotopographic platform at 100,000 cells/mL with Cre adenovirus at 1:100 ratio. Samples were fixed at 72 hours, and αSMA expression was analyzed from fluorescent images.

5.2.3 Constitutively active YAP modulation for investigating the role of YAP in mechanotransduction

In order to observe the role of YAP on topographic cue transduction and relationship with p38, FLAG tagged constitutively active YAP DNA was prepared from a plasmid (pCMV-Flag YAP, Addgene) as previously described [173]. Transfection was conducted with 0.01 μg/μL DNA and the protocol provided by Roche Applied Science with XTremeGene (Sigma). Transfection was confirmed with western blot for FLAG as normal cell type lacks FLAG.

5.2.4 Investigation of topographic cue transduction through focal adhesion via tensin 1 modulations

Tensin 1 was silenced using SiRNA (Santa Cruz). First, 50 μL OptiMEM (ThermoFisher) was mixed with 3 μL of siRNA at 10 μM. Then, mixture of 3 μL of RNAiMAX (ThermoFisher) and 50

μL of media was added. Mixture was incubated for 5 min in room temperature, and then added to the MEF culture media at 1:10 ratio. Immunofluorescence imaging for tensin 1 was conducted with tensin 1 primary antibody (Sigma) at 1:400 ratio.

5.3 Results

5.3.1 Mechanical cues from nanotopographies are transduced through p38 and YAP

Number of groups including our group has shown that p38 MAPK regulate myofibroblast transdifferentiation and fibrosis [25, 174-176]. As p38 mediates mechanical cues such as cyclic stretch and substrate stiffness, we hypothesized that it may have regulatory role in transducing topographic cues. To examine whether p38 also participate in mechanical signal transduction, we employed a lox P-Cre deletion of p38 on p38 floxed MEF cell as previously shown [174]. MEF cells were cultured on unpatterned (Figure 5.1A left), aligned (Figure 5.1A middle), and random (Figure 5.1A right) topographic platforms and adenoviral Cre was added for p38 knockout group to assess effects of p38 on topography transduction. Quantitative analysis of αSMA positive cell ratio has shown a significant inhibition on myofibroblast transdifferentiation for all platforms (Figure 5.1B). As p38 regulates TGFβ signal for transdifferentiation [174], we observed a reduction in αSMA stress fiber positive cell ratio and prohibited TGFβ response on unpatterned platform as expected. Interestingly, an increase in transdifferentiation on aligned pattern was also significantly decreased when p38 was knocked out. Such decrease could be interpreted as p38 being required to transduce aligned topographic cues. However, when compared to p38 knockout on unpatterned platform, MEF cells on aligned platform resulted in higher transdifferentiation ratio. The difference may suggest that although topographic cues are transduced through p38 pathway, other pathways may also transduce the signal. Addition of TGFβ did not promote transdifferentiation with p38 knockout on aligned platform either. MEF cells on random topographic platform displayed even more inhibited transdifferentiation with p38 knockout.

As YAP has been found to participate in mechanotransduction including topographic cues [87, 88, 157], we attempted to test our hypothesis of YAP transducing topographic cues from our infarct geometry-mimicking platform for myofibroblast transdifferentiation. YAP antibody was used to stain MEF cells after 72 hours of culture, and ratio of nucleus-localized YAP (Figure 5.1A yellow arrows) was quantitatively analyzed (Figure 5.1C). YAP activation was significantly higher on both aligned and random nanotopographic platforms with or without TGFβ treatment compared to unpatterned platforms. While TGFβ treatment effects were not noticeable on nanotopographic platforms, on unpatterned platforms, YAP activation was slightly promoted with TGFβ treatment. Interestingly, knocking out p38 significantly decreased topography-mediated YAP activations. Moreover, although the YAP activation was decreased with p38 knockout, the activation was still higher than that of unpatterned platforms. Inhibition of YAP activation with p38 knockout raises a possibility that p38 could be upstream of YAP. In order to test whether YAP activation and myofibroblast transdifferentiation were correlated, we analyzed cells with nuclear YAP positive with αSMA expression (Figure 5.1D). The results show greater transdifferentiation of cells with YAP positive in response to aligned topographies. When compared to unpatterned platform, both aligned and random platform resulted in more active YAP and αSMA positive cells, which may be due to the presence of some nanotopographies regardless of orientation. Significantly high active YAP and αSMA active cells on aligned platform compared to random platform suggest although nanotopographies were enough to increase YAP activation as shown in the Figure 5.1C, transdifferentiation required aligned cues. Similarly, knockout of p38 revealed that both activation of YAP and transdifferentiation were inhibited and were correlated. Notably, the ratio of transdifferentiated MEF with activated YAP were higher on both aligned and random nanotopographies even with p38 knockout group. An immunoprecipitation (IP) is a strong method to investigate whether two proteins are interacting together. Cell lysate collected from MEF cultured on unpatterned and aligned platform was collected, and were pulled down using p38

antibody with magnetic beads. A western blot was conducted with the pulled down proteins to stain for YAP (Figure 5.1F). A control group with no IP pull down has shown a clear YAP band from western. When compared to the IP group on unpatterned platform, aligned platform resulted in significantly more YAP that was bound to p38. MEF cells cultured on unpatterned surface exhibited a very low interaction between p38 and YAP, whereas aligned platform resulted in significantly more p38 and YAP interactions. IP control was confirmed with IgG heavy chain band shown in the bottom of the gel.

Results from the Figure 5.1A-F suggested that p38 and YAP were directly regulated together, and were both correlated to transdifferentiation. As knockout of p38 significantly reduced YAP activation, we examined whether p38 is upstream of YAP. To verify this, a constitutively active YAP plasmid with FLAG motif was transfected into MEF cells. The transfection was confirmed with western blot (Figure 5.1G) with FLAG only showing up on transfected group only. Transdifferentiation was assessed through αSMA stress fiber staining on wild type, constitutively active YAP, and p38 knockout with constitutively active YAP group (Figure 5.1H). First, on unpatterned platform, addition of constitutively active YAP has increased transdifferentiation significantly (Figure 5.1H left). Even with the p38 knockout, the transdifferentiation was rescued with active YAP which suggest that YAP is downstream of p38 in myofibroblast transdifferentiation. Throughout all platforms, MEF cells transdifferentiated more with constitutively active YAP compared to unpatterned control group. Strikingly, MEF cells were significantly more sensitive to aligned topographies with TGFβ response synergistically increased (Figure 5.1H middle). However the synergistic increase in transdifferentiation was not observed on random topographies (Figure 5.1H right). On all platforms, p38 knockout with YAP activation increased transdifferentiation compared to wild type, but TGFβ treatment did not increase transdifferentiation within the same group. Most importantly, the aligned topographies were able to transdifferentiate MEF cells more significantly even with p38 knockout if YAP was activated.

The transdifferentiation was still increased compared to wild type, but missing TGFβ response suggested p38 was required to mediate TGFβ signal, and topographic cues were able to induce transdifferentiation with active YAP.

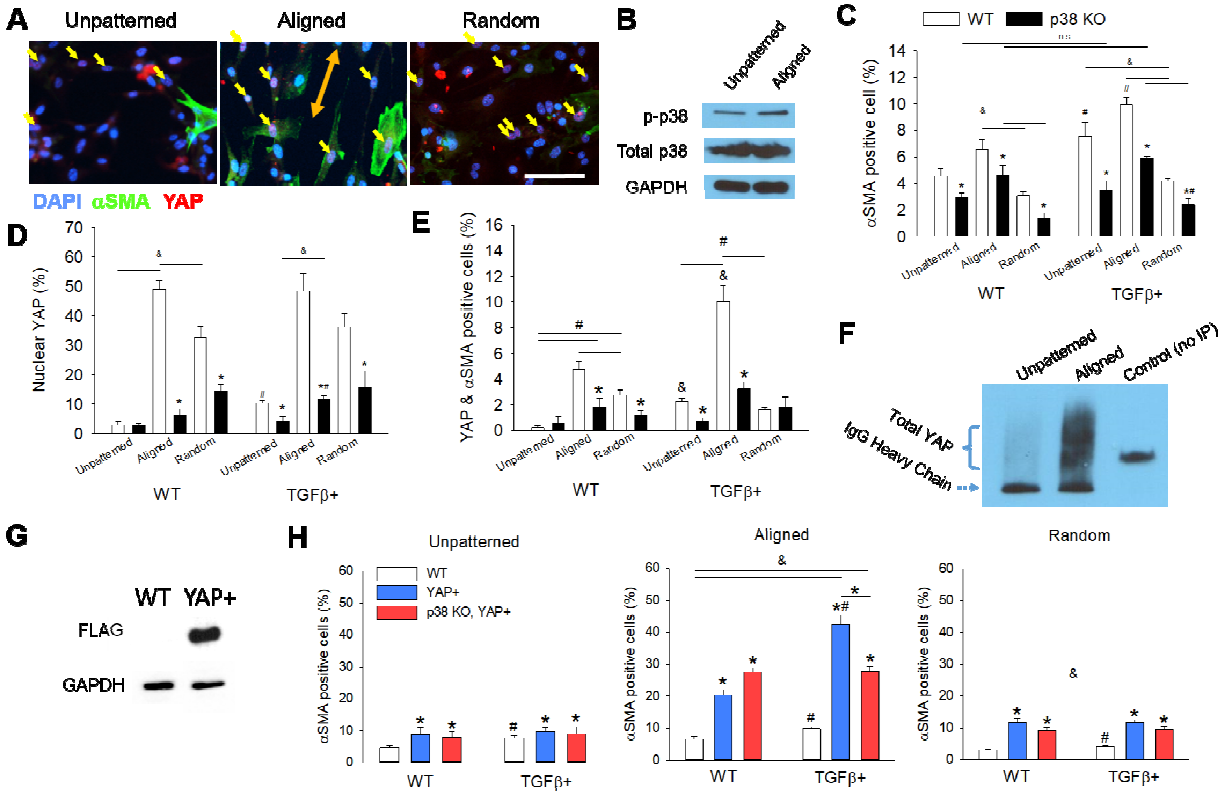

Figure 5.1. Topographic cues are transduced via p38 and YAP. (A) MEF cells were cultured on unpatterned (A, left), aligned (A, middle), and random (A, right) platform for 72 hours, then fixed and stained for aSMA and YAP. Orange arrow=direction of topographic alignment. (B) Western blot of phospho-p38, total p38, and GAPDH of MEF cells on unpatterned and aligned platform shows significantly more phosphor-p38 was expressed on aligned platform. (C) Transdifferentiation of MEF cells were quantified with p38 knockout via loxP-Cre deletion. Significant decrease in transdifferentiation with p38 knockout was observed on all conditions (D) Active YAP was measured by ratio of nuclear YAP. Nanotopographies significantly activated YAP. (E) Ratio of active YAP and αSMA positive cell was quantified to correlate YAP and transdifferentiation. (F) Immunoprecipitation of p38 pulling then YAP staining for western has confirmed that there exists a direct interaction between p38 and YAP on aligned platform. (G) Constitutively active YAP plasmid containing FLAG motif was introduced, and transfection was verified by western blot. (H) Activation of YAP with p38 knockout has revealed that YAP is downstream of p38, and mechanical cues are transduced via both p38 and YAP, but only p38 transduce TGFβ signal. Scale bar: 100 μm

5.3.2 Mechanical cues from nanotopographies are transduced through p38 and YAP

A protein found in focal adhesion complex of mature myofibroblast, tensin's role in myofibroblast transdifferentiation has not been investigated in depth. Previous studies have revealed that tensin 1 was required for fibroblast transdifferentiation and extracellular matrix formation [177]. Our group has shown the important role of focal adhesion on mechanotransduction of topographic cues [178]. Thus, a knockout of tensin 1 resulting in reduced transdifferentiation suggested that tensin 1 may contribute to topographic cue sensing process. To test whether tensin 1 has any correlation with myofibroblast transdifferentiation in response to topography, the MEF cells cultured on unpatterned, aligned, and random topography was stained with tensin 1 antibody at 72-hour time point (Figure 5.2A). The number of adhesions (Figure 5.2B), adhesion size (Figure 5.2C), and FA adhesion length (Figure 5.2D) were assessed. Generally, mature myofibroblasts would exhibit higher number of adhesions, bigger, and longer adhesions [177]. In order to examine whether tensin 1 in focal adhesion complex is required for MEF cells to sense topographic cues, a SiRNA was introduced to knockout tensin 1 as previously done [177]. The effectiveness of tensin 1 siRNA (SiTensin 1) was confirmed via western blot (Figure 5.2E). A clear silencing was obtained with high efficiency with GAPDH used as a control. In order to test whether tensin 1 have a regulatory role in transducing topographic cues for myofibroblast transdifferentiation, MEF cells were transfected with tensin 1 siRNA on each topographic platforms for 72 hours, and the ratios of αSMA stress fiber expression was quantified. Our results indicate that knockout of tensin 1 indeed resulted in lower transdifferentiation on all topographic platforms (Figure 5.2F) as expected from previous study [177]. On top of the regulatory effect of tensin 1, the topography-induced transdifferentiation observed on aligned platform was significantly reduced with tensin 1 knockout, suggesting that tensin 1 is required not only for myofibroblast transdifferentiation, but also for sensing topographic cues. To test the hypothesis of signaling pathway starting from tensin 1 in focal adhesion for topography sensing and

intracellular signaling of p38 and YAP, p38 and YAP was activated with knockout of tensin 1. AdMKK6 was introduced to activate p38 as MKK6 is a direct activator of p38 [179]. YAP was activated with constitutively active YAP plasmid as described above. A quantitative analysis of αSMA stress fiber positive cell ratio indicated that the activation of both p38 and YAP increase transdifferentiation even with tensin 1 knockout condition (Figure 5.2F). Notably, activation of p38 through AdMKK6 treatment was more effective in transdifferentiation of myofibroblast than YAP activation through constitutively active YAP plasmid transfection. We initially hypothesized that tensin 1 in focal adhesion complex upstream sensor of topographic cues that transduced intercellularly through p38 and YAP. The increased transdifferentiation in response to the activation of p38 and YAP was not affected by tensin 1 knockout (Figure 5.1G, Figure 5.2F).

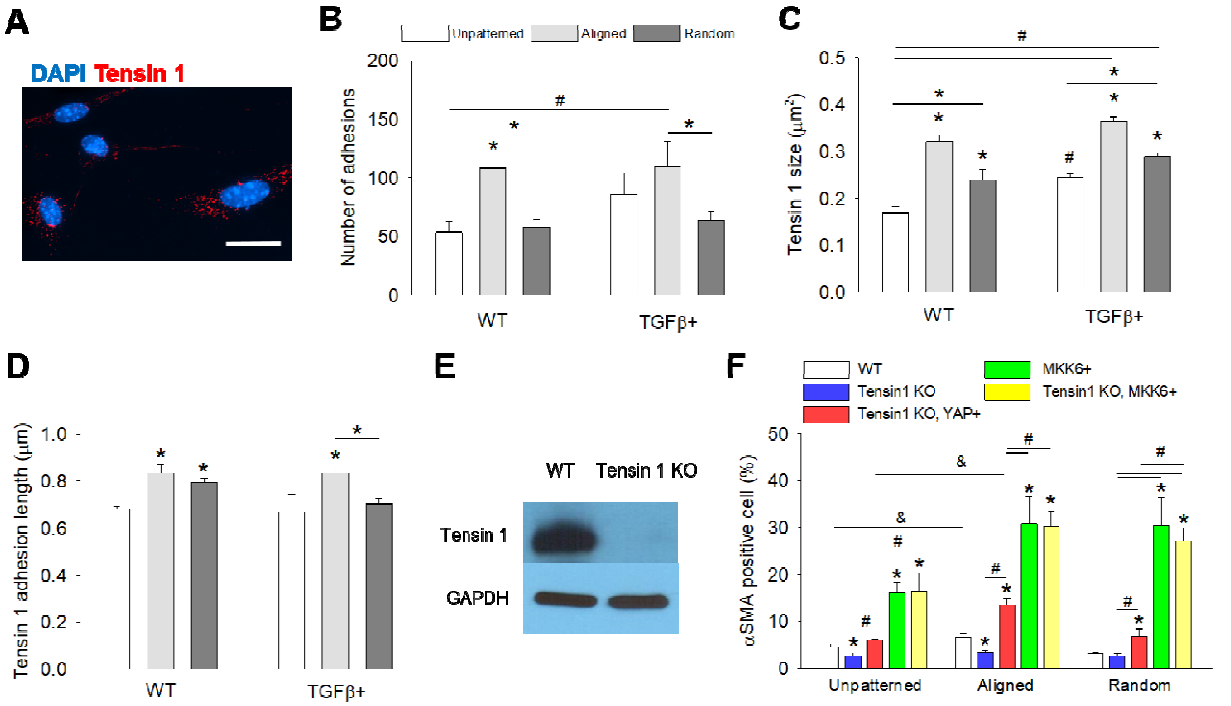

Figure 5.2. Topographic cues are sensed through tensin 1 in focal adhesion complex. (A) MEF cells cultured on aligned platform was fixed and stained for DAPI (blue) and tensin 1 (red). Tensin 1 staining image was analyzed for number (B), size (C), and length (D) of tensin 1. (E) SiRNA was introduced to knockout tensin 1 confirmed by western blot. (F) MEF cells were treated with tensin 1 SiRNA, constitutively active YAP, and AdMKK6 to knockout tensin 1, activate YAP, and activate p38 respectively. αSMA stress fiber positive cells were quantitatively analyzed to assess regulatory role of tensin 1, YAP, and p38 on topographic cue transduction. Scale bar: 30 μm

5.4 Discussion

In this chapter, a mechanotransduction of topographic cues was assessed through p38 and YAP modulations. In our previous studies, we have found that p38-MAPK pathway significantly govern myofibroblast transdifferentiation [174], which highlighted p38 as a major signal pathway transducing TGFβ signal over the canonical SMAD pathway. Our results suggested that p38 transduces topographic cues for myofibroblast transdifferentiation with TGFβ signal transduced synergistically. Such results strengthens a hypothesis that p38-MAPK is a master regulator for fibrosis development. YAP was also found to regulate topographic cues. Surprisingly, a strong activation of YAP was expressed on aligned topographies, and topography-induced transdifferentiation was significantly increased with addition of constitutively active YAP. A strong interaction between p38 and YAP on aligned platform was confirmed through immunoprecipitation, suggesting aligned topographies provided sufficient cues for p38 to interact with YAP. Two thick bands observed on aligned group on western gel may be due to phosphor-YAP and total YAP. In order to test whether p38-MAPK and YAP have any correlation and to investigate their hierarchy, constitutively active YAP plasmid was added to Cre-mediated p38 knockout MEF. We found that addition of YAP to the p38 knockout group successfully rescued transdifferentiation indicating that YAP is downstream of p38 for myofibroblast transdifferentiation. This may suggest that YAP is mainly regulated via topographic cues with aligned topography effectively inducing more YAP activation. TGFβ may have some effect on YAP activation as shown in the unpatterned platform case, but topographic cues were able to overwhelm any TGFβ effects.

Moreover, tensin 1 has been found to be essential in myofibroblast transdifferentiation previously [177]. Our results show that topographic cues were enough to regulate tensin 1 adhesion number, size, and length similar to the effect of TGFβ. To test whether focal adhesion, which has been reported to transduce extracellular mechanical cues, were related to p38 and YAP for topographic

cue transduction, we knocked tensin 1 by utilizing SiRNA as shown in the Figure 5.2E. As expected, knockout of tensin 1 decreased myofibroblast transdifferentiation. The amount of decrease was more significant on aligned topographies suggesting that tensin 1 is required not only to myofibroblast transdifferentiation as previously shown [177], but also to sense topographic cues. As we showed that p38 and YAP transduce topographic cues intercellularly, we hypothesized that there may be a crosstalk between tensin 1 and p38 and YAP. To test this, AdMKK6, a direct activator of p38, was introduced to activate p38 activity as previously shown [179]. Results from the Figure 5.2F exhibit that the decrease in transdifferentiation observed with tensin 1 knockout was rescued with p38 activation and YAP activation. Recently, it has been shown that YAP exerts its transcriptional control via TEAD mediated activation of enhancers [180], and p38 has shown to regulate Hippo pathway transcription factor TEAD [181]. Further studies on identifying master downstream regulator of pro-fibrotic cues may allow us to overhaul challenges of controlling cardiac fibrosis.

Taken together, this chapter provides insight into the mechanisms by which MEF cells respond to the topographic cues, recapitulating the geometry of the infarct scar ECM as shown in the schematic diagram in the Figure 5.3. A noncanonical p38-MAPK has been shown to participate in not only TGFβ signal transduction, but also in ECM topographic cue transduction. Relationship between p38 and YAP in topographic cue mediation suggests that YAP is downstream of p38. The role of tensin 1 and its relationship with p38 and YAP was also tested through tensin 1 modulations. The chapter stress the importance of understanding microenvironmental cues and how topographical cues are transduced and potentiate chemical cues such as TGFβ in cardiac fibrosis studies. Overall, the work opens up the avenue for a new paradigm for cardiac fibrosis modeling *in vitro*, and understanding the mechanistic regulation of post infarct heart.

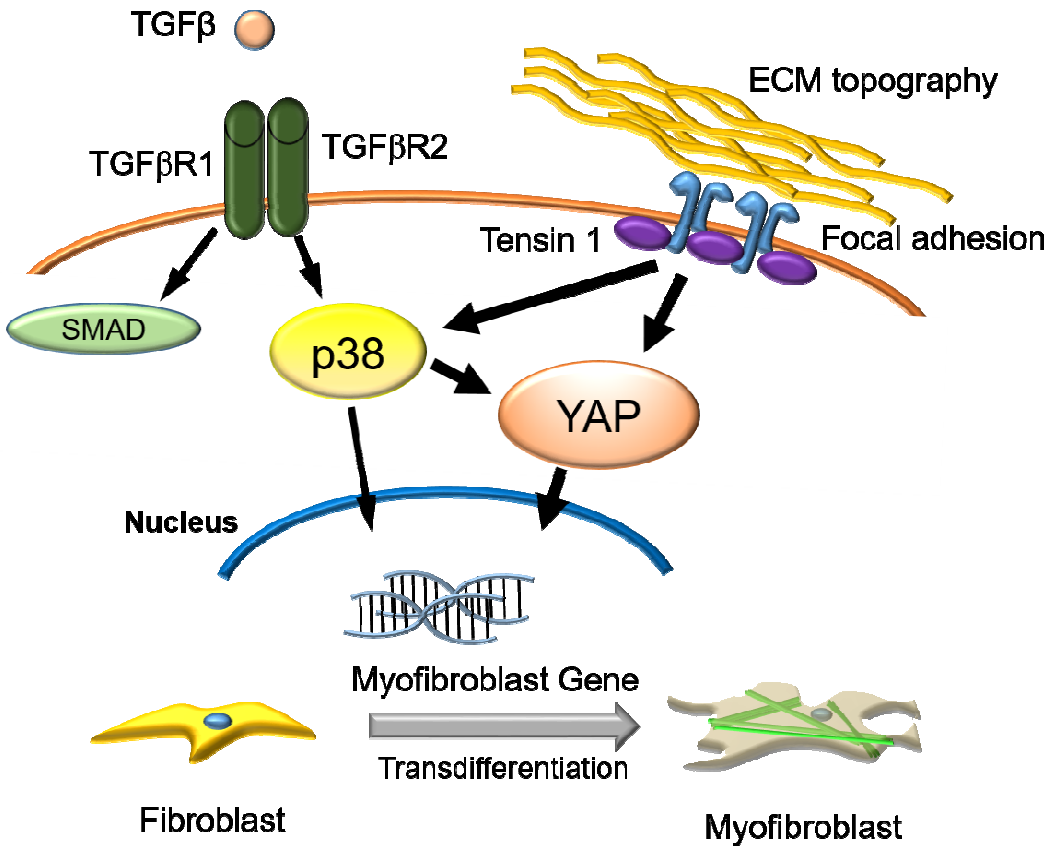

Figure 5.3 Schematics of mechanosensing of topographic cues for myofibroblast transdifferentiation.

Chapter 6. Summary and Future Directions

The above work addressed a novel approach to study myofibroblast transdifferentiation post-infarct condition via topographic regulation. In Aim 1, we explored the development and optimization of nanotopographic platform for cell culture model system. Topographic effects on various cell types including HUVEC, vSMC, and MEF were investigated. Results indicated that cells were able to sense topographic cues by aligning its morphology, skeletal structure, and activating intercellular pathways. Previously, ROCK/Rho pathway has been identified as a major mechanosensing pathway [182-184]. Although not discussed in the dissertation, the role of ROCK/Rho in topography sensing has been investigated. Preliminary data suggested promising

results that topographic cue transduction by ROCK/Rho for myofibroblast transdifferentiation may exist through regulating proteins participating in actin polymerization. Nanotopographic technique was then utilized to recapitulate mouse heart that has developed fibrosis. Therefore in Aim 2, we tested whether the developed platforms were able to regulate myofibroblast fate and function. Aligned topography induced aligned stress fiber as well as proliferation and transdifferentiation. Cell proliferation and transdifferentiation was assessed to address the question of what contribute to increased number of myofibroblasts on the border of infarct zone. Increased transdifferentiation on aligned topographies led to higher ECM synthesis in the direction of underlying topographies, suggesting a presence of positive feedback loop of deposited ECM alignment. In Aim 3, investigation of mechanotransduction pathway was conducted to identify p38, YAP, and tensin 1 as a key regulators of topographic cue transduction.

Our group has experiences in fabricating a 'smart polymer' which could change nanoscale shapes in response to external cues [185]. The material was used to investigate precursor cardiomyocyte differentiation over nanoscale topography changes previously [185]. Incorporating the material with the platform developed in this dissertation would allow a simulation of ECM topography change during fibrosis and observe how myofibroblast transdifferentiation is regulated over time. In addition to topography changes, the versatility of the developed platform would be able to simulate chemical changes as well, providing a combinatorial fibrosis model *in vitro*. Moreover, an optical transparency of the developed platform could be incorporated with luciferase assay or FRET microscopy to closer investigate how topographic cues are sensed by fibroblasts in real time in response to topography changes over time.

The dissertation focused on studying the myofibroblast transdifferentiation for first 72 hour exposure to topographic cues. Experimental conditions were designed to focus on the initial stage of fibrosis regulation as it has been reported that myofibroblast population rise quickly for first 3~4 days of injury and slowly decrease. However, a recent study has shown that the lineage tracing

of fibroblasts over 4 week period fibrosis revealed that fibroblasts expressed bone and cartilage signatures after 4 week period in fibrotic myocardium instead of protein synthesis, proliferation or ECM matrix genes [186]. As the developed platform could be utilized in long-term cultures as well as chemical treatments, it would be logical to investigate such time-related regulation of myofibroblast fate and function with the model developed. Moreover, it has been reported that YAP activity is increased with initial fibrosis as well as in developing heart which also goes through a dynamic ECM change. A deeper understanding of how this time-sensitive ECM change and pathway regulation would provide a better understanding of chronic fibrosis.

Although the proposed platform has strengths in decoupling topographic cues from confounding variables, an *in vivo* model will certain provide the field with stronger clinical relevance. Our group has successfully developed a transgenic mouse with various genetic modulations such as p38, MBNL, and MKK6. Such models could be used to study ECM topographic regulation of infarcts and remote region. Moreover, we recently developed a robust method to observe collagen fiber crosslinking and directionality through second harmonic microscopy system. Utilizing the fibroblast lineage tracking method as mentioned previously [186], a 3D mapping of ECM organization in fibrotic heart and an investigation of in vivo ECM organization in conjunction to myofibroblast transdifferentiation would be possible. Such approach will also bring the quasi-3D topographic cue used in this dissertation to full a 3D model to better portray *in vivo* conditions.

The research presented in this dissertation sets the stage for many immediate future studies that would have an immense impact in both cardiac fibrosis studies and *in vitro* model development. The immediate follow up study would dive the pathway mapping even deeper to identify converging transcription factors through co-immunoprecipitation for identifying possible therapeutic target for remediating fibrotic heart. Moreover, besides myocardial infarction modeling, our group has found that some genetic cardiac diseases that result in whole heart fibrosis exhibit altered myocardium ECM organization even without infarction or chemical stimuli.

Results from this dissertation could be incorporated to explain the phenomenon and assist in disease modeling. Additionally, current *in vitro* fibrosis studies are focused mostly on chemical or cellular interactions. We hope the results from this dissertation would allow a novel approach to study cardiac fibrosis, disease modeling *in vitro*, and understanding the mechanistic regulation of post infarct heart.

References

[1] Stempien-Otero A, Kim DH, Davis J. Molecular networks underlying myofibroblast fate and fibrosis. Journal of molecular and cellular cardiology. 2016;97:153-61.
[2] Meran S, Steadman R. Fibroblasts and myofibroblasts in renal fibrosis. International journal of experimental pathology. 2011;92:158-67.
[3] Grande MT, Lopez-Novoa JM. Fibroblast activation and myofibroblast generation in obstructive nephropathy. Nature reviews Nephrology. 2009;5:319-28.
[4] Serrano AL, Mann CJ, Vidal B, Ardite E, Perdiguero E, Munoz-Canoves P. Cellular and molecular mechanisms regulating fibrosis in skeletal muscle repair and disease. Current topics in developmental biology. 2011;96:167-201.
[5] van den Borne SW, Diez J, Blankesteijn WM, Verjans J, Hofstra L, Narula J. Myocardial remodeling after infarction: the role of myofibroblasts. Nature reviews Cardiology. 2010;7:30-7.
[6] Brown RD, Ambler SK, Mitchell MD, Long CS. The cardiac fibroblast: therapeutic target in myocardial remodeling and failure. Annual review of pharmacology and toxicology. 2005;45:657-87.
[7] Hinz B. Formation and function of the myofibroblast during tissue repair. The Journal of investigative dermatology. 2007;127:526-37.
[8] Suzuki J, Isobe M, Aikawa M, Kawauchi M, Shiojima I, Kobayashi N, et al. Nonmuscle and smooth muscle myosin heavy chain expression in rejected cardiac allografts. A study in rat and monkey models. Circulation. 1996;94:1118-24.
[9] Martin P, Tzanidis A, Stein-Oakley A, Krum H. Effect of a highly selective endothelin-converting enzyme inhibitor on cardiac remodeling in rats after myocardial infarction. Journal of cardiovascular pharmacology. 2000;36:S367-70.
[10] Swaney JS, Roth DM, Olson ER, Naugle JE, Meszaros JG, Insel PA. Inhibition of cardiac myofibroblast formation and collagen synthesis by activation and overexpression of adenylyl cyclase. Proceedings of the National Academy of Sciences of the United States of America. 2005;102:437-42.
[11] Micera A, Vigneti E, Pickholtz D, Reich R, Pappo O, Bonini S, et al. Nerve growth factor displays stimulatory effects on human skin and lung fibroblasts, demonstrating a direct role for this factor in tissue repair. Proceedings of the National Academy of Sciences of the United States of America. 2001;98:6162-7.
[12] Bogatkevich GS, Tourkina E, Abrams CS, Harley RA, Silver RM, Ludwicka-Bradley A. Contractile activity and smooth muscle alpha-actin organization in thrombin-induced human lung myofibroblasts. American journal of physiology Lung cellular and molecular physiology. 2003;285:L334-43.
[13] Liu T, Dhanasekaran SM, Jin H, Hu B, Tomlins SA, Chinnaiyan AM, et al. FIZZ1 stimulation of myofibroblast differentiation. The American journal of pathology. 2004;164:1315-26.
[14] Daskalopoulos EP, Hermans KC, Janssen BJ, Matthijs Blankesteijn W. Targeting the Wnt/frizzled signaling pathway after myocardial infarction: a new tool in the therapeutic toolbox? Trends in cardiovascular medicine. 2013;23:121-7.
[15] Kong P, Christia P, Frangogiannis NG. The pathogenesis of cardiac fibrosis. Cellular and molecular life sciences : CMLS. 2014;71:549-74.
[16] Shephard P, Hinz B, Smola-Hess S, Meister JJ, Krieg T, Smola H. Dissecting the roles of endothelin, TGF-beta and GM-CSF on myofibroblast differentiation by keratinocytes. Thrombosis and haemostasis. 2004;92:262-74.
[17] Santiago JJ, Dangerfield AL, Rattan SG, Bathe KL, Cunnington RH, Raizman JE, et al. Cardiac fibroblast to myofibroblast differentiation in vivo and in vitro: expression of focal adhesion components in neonatal and adult rat ventricular myofibroblasts. Developmental dynamics : an official publication of the American Association of Anatomists. 2010;239:1573-84.

[18] Tomasek JJ, Gabbiani G, Hinz B, Chaponnier C, Brown RA. Myofibroblasts and mechano-regulation of connective tissue remodelling. Nature reviews Molecular cell biology. 2002;3:349-63.
[19] Hinz B. The myofibroblast: paradigm for a mechanically active cell. Journal of biomechanics. 2010;43:146-55.
[20] Moore-Morris T, Guimaraes-Camboa N, Banerjee I, Zambon AC, Kisseleva T, Velayoudon A, et al. Resident fibroblast lineages mediate pressure overload-induced cardiac fibrosis. The Journal of clinical investigation. 2014;124:2921-34.
[21] Chrzanowska-Wodnicka M, Burridge K. Rho-stimulated contractility drives the formation of stress fibers and focal adhesions. The Journal of cell biology. 1996;133:1403-15.
[22] Gabbiani G. The myofibroblast in wound healing and fibrocontractive diseases. The Journal of pathology. 2003;200:500-3.
[23] Thompson SA, Copeland CR, Reich DH, Tung L. Mechanical coupling between myofibroblasts and cardiomyocytes slows electric conduction in fibrotic cell monolayers. Circulation. 2011;123:2083-93.
[24] Thompson SA, Blazeski A, Copeland CR, Cohen DM, Chen CS, Reich DM, et al. Acute slowing of cardiac conduction in response to myofibroblast coupling to cardiomyocytes through N-cadherin. Journal of molecular and cellular cardiology. 2014;68:29-37.
[25] Davis J, Burr AR, Davis GF, Birnbaumer L, Molkentin JD. A TRPC6-dependent pathway for myofibroblast transdifferentiation and wound healing in vivo. Developmental cell. 2012;23:705-15.
[26] Davis J, Salomonis N, Ghearing N, Lin SC, Kwong JQ, Mohan A, et al. MBNL1-mediated regulation of differentiation RNAs promotes myofibroblast transformation and the fibrotic response. Nature communications. 2015;6:10084.
[27] Small EM. The actin-MRTF-SRF gene regulatory axis and myofibroblast differentiation. Journal of cardiovascular translational research. 2012;5:794-804.
[28] Anderson KR, Sutton MG, Lie JT. Histopathological types of cardiac fibrosis in myocardial disease. The Journal of pathology. 1979;128:79-85.
[29] Wang X, Guo Z, Ding Z, Khaidakov M, Lin J, Xu Z, et al. Endothelin-1 upregulation mediates aging-related cardiac fibrosis. Journal of molecular and cellular cardiology. 2015;80:101-9.
[30] Russo I, Frangogiannis NG. Diabetes-associated cardiac fibrosis: Cellular effectors, molecular mechanisms and therapeutic opportunities. Journal of molecular and cellular cardiology. 2016;90:84-93.
[31] Upadhya B, Kitzman DW. Heart Failure with Preserved Ejection Fraction in Older Adults. Heart failure clinics. 2017;13:485-502.
[32] Robert V, Besse S, Sabri A, Silvestre JS, Assayag P, Nguyen VT, et al. Differential regulation of matrix metalloproteinases associated with aging and hypertension in the rat heart. Laboratory investigation; a journal of technical methods and pathology. 1997;76:729-38.
[33] Lopez B, Gonzalez A, Beaumont J, Querejeta R, Larman M, Diez J. Identification of a potential cardiac antifibrotic mechanism of torasemide in patients with chronic heart failure. Journal of the American College of Cardiology. 2007;50:859-67.
[34] Spinale FG. Myocardial matrix remodeling and the matrix metalloproteinases: influence on cardiac form and function. Physiological reviews. 2007;87:1285-342.
[35] von Gise A, Pu WT. Endocardial and epicardial epithelial to mesenchymal transitions in heart development and disease. Circulation research. 2012;110:1628-45.
[36] Zeisberg EM, Tarnavski O, Zeisberg M, Dorfman AL, McMullen JR, Gustafsson E, et al. Endothelial-to-mesenchymal transition contributes to cardiac fibrosis. Nature medicine. 2007;13:952-61.
[37] Souders CA, Bowers SL, Baudino TA. Cardiac fibroblast: the renaissance cell. Circulation research. 2009;105:1164-76.
[38] Carver W, Goldsmith EC. Regulation of tissue fibrosis by the biomechanical environment. BioMed research international. 2013;2013:101979.

[39] Fomovsky GM, Rouillard AD, Holmes JW. Regional mechanics determine collagen fiber structure in healing myocardial infarcts. Journal of molecular and cellular cardiology. 2012;52:1083-90.
[40] Klingberg F, Chow ML, Koehler A, Boo S, Buscemi L, Quinn TM, et al. Prestress in the extracellular matrix sensitizes latent TGF-beta1 for activation. The Journal of cell biology. 2014;207:283-97.
[41] Liu F, Lagares D, Choi KM, Stopfer L, Marinkovic A, Vrbanac V, et al. Mechanosignaling through YAP and TAZ drives fibroblast activation and fibrosis. American journal of physiology Lung cellular and molecular physiology. 2015;308:L344-57.
[42] Zong X, Bien H, Chung CY, Yin L, Fang D, Hsiao BS, et al. Electrospun fine-textured scaffolds for heart tissue constructs. Biomaterials. 2005;26:5330-8.
[43] Engler AJ, Carag-Krieger C, Johnson CP, Raab M, Tang HY, Speicher DW, et al. Embryonic cardiomyocytes beat best on a matrix with heart-like elasticity: scar-like rigidity inhibits beating. Journal of cell science. 2008;121:3794-802.
[44] Rouillard AD, Holmes JW. Mechanical regulation of fibroblast migration and collagen remodelling in healing myocardial infarcts. The Journal of physiology. 2012;590:4585-602.
[45] Kim DH, Lipke EA, Kim P, Cheong R, Thompson S, Delannoy M, et al. Nanoscale cues regulate the structure and function of macroscopic cardiac tissue constructs. Proceedings of the National Academy of Sciences of the United States of America. 2010;107:565-70.
[46] van Spreeuwel AC, Bax NA, Bastiaens AJ, Foolen J, Loerakker S, Borochin M, et al. The influence of matrix (an)isotropy on cardiomyocyte contraction in engineered cardiac microtissues. Integrative biology : quantitative biosciences from nano to macro. 2014;6:422-9.
[47] Ott HC, Matthiesen TS, Goh SK, Black LD, Kren SM, Netoff TI, et al. Perfusion-decellularized matrix: using nature's platform to engineer a bioartificial heart. Nature medicine. 2008;14:213-21.
[48] Sullivan KE, Quinn KP, Tang KM, Georgakoudi I, Black LD, 3rd. Extracellular matrix remodeling following myocardial infarction influences the therapeutic potential of mesenchymal stem cells. Stem cell research & therapy. 2014;5:14.
[49] Weber KT. Cardiac interstitium in health and disease: the fibrillar collagen network. Journal of the American College of Cardiology. 1989;13:1637-52.
[50] Goergen CJ, Chen HH, Sakadzic S, Srinivasan VJ, Sosnovik DE. Microstructural characterization of myocardial infarction with optical coherence tractography and two-photon microscopy. Physiological reports. 2016;4.
[51] Pang Y, Wang X, Lee D, Greisler HP. Dynamic quantitative visualization of single cell alignment and migration and matrix remodeling in 3-D collagen hydrogels under mechanical force. Biomaterials. 2011;32:3776-83.
[52] Tangkijvanich P, Santiskulvong C, Melton AC, Rozengurt E, Yee HF, Jr. p38 MAP kinase mediates platelet-derived growth factor-stimulated migration of hepatic myofibroblasts. Journal of cellular physiology. 2002;191:351-61.
[53] Wang JH, Yang G, Li Z, Shen W. Fibroblast responses to cyclic mechanical stretching depend on cell orientation to the stretching direction. Journal of biomechanics. 2004;37:573-6.
[54] Dickinson RB, Guido S, Tranquillo RT. Biased cell migration of fibroblasts exhibiting contact guidance in oriented collagen gels. Annals of biomedical engineering. 1994;22:342-56.
[55] Wang J, Chen H, Seth A, McCulloch CA. Mechanical force regulation of myofibroblast differentiation in cardiac fibroblasts. American journal of physiology Heart and circulatory physiology. 2003;285:H1871-81.
[56] Grinnell F. Fibroblast-collagen-matrix contraction: growth-factor signalling and mechanical loading. Trends in cell biology. 2000;10:362-5.
[57] Numaga-Tomita T, Kitajima N, Kuroda T, Nishimura A, Miyano K, Yasuda S, et al. TRPC3-GEF-H1 axis mediates pressure overload-induced cardiac fibrosis. Scientific reports. 2016;6:39383.

[58] Gould RA, Chin K, Santisakultarm TP, Dropkin A, Richards JM, Schaffer CB, et al. Cyclic strain anisotropy regulates valvular interstitial cell phenotype and tissue remodeling in three-dimensional culture. Acta biomaterialia. 2012;8:1710-9.
[59] Molkentin JD, Bugg D, Ghearing N, Dorn LE, Kim P, Sargent MA, et al. Fibroblast-specific genetic manipulation of p38 MAPK in vivo reveals its central regulatory role in fibrosis. Circulation. 2017.
[60] Blaauboer ME, Smit TH, Hanemaaijer R, Stoop R, Everts V. Cyclic mechanical stretch reduces myofibroblast differentiation of primary lung fibroblasts. Biochemical and biophysical research communications. 2011;404:23-7.
[61] Galie PA, Russell MW, Westfall MV, Stegemann JP. Interstitial fluid flow and cyclic strain differentially regulate cardiac fibroblast activation via AT1R and TGF-beta1. Experimental cell research. 2012;318:75-84.
[62] Hinz B, Mastrangelo D, Iselin CE, Chaponnier C, Gabbiani G. Mechanical tension controls granulation tissue contractile activity and myofibroblast differentiation. The American journal of pathology. 2001;159:1009-20.
[63] Hinz B. It has to be the alphav: myofibroblast integrins activate latent TGF-beta1. Nature medicine. 2013;19:1567-8.
[64] Atance J, Yost MJ, Carver W. Influence of the extracellular matrix on the regulation of cardiac fibroblast behavior by mechanical stretch. Journal of cellular physiology. 2004;200:377-86.
[65] Schroer AK, Merryman WD. Mechanobiology of myofibroblast adhesion in fibrotic cardiac disease. Journal of cell science. 2015;128:1865-75.
[66] Sawada Y, Nakamura K, Doi K, Takeda K, Tobiume K, Saitoh M, et al. Rap1 is involved in cell stretching modulation of p38 but not ERK or JNK MAP kinase. Journal of cell science. 2001;114:1221-7.
[67] Brault JJ, Pizzimenti NM, Dentel JN, Wiseman RW. Selective inhibition of ATPase activity during contraction alters the activation of p38 MAP kinase isoforms in skeletal muscle. Journal of cellular biochemistry. 2013;114:1445-55.
[68] Foster WH, Tidball JG, Wang Y. p38gamma activity is required for maintenance of slow skeletal muscle size. Muscle & nerve. 2012;45:266-73.
[69] MacKenna DA, Dolfi F, Vuori K, Ruoslahti E. Extracellular signal-regulated kinase and c-Jun NH2-terminal kinase activation by mechanical stretch is integrin-dependent and matrix-specific in rat cardiac fibroblasts. The Journal of clinical investigation. 1998;101:301-10.
[70] Hsu HJ, Lee CF, Locke A, Vanderzyl SQ, Kaunas R. Stretch-induced stress fiber remodeling and the activations of JNK and ERK depend on mechanical strain rate, but not FAK. PloS one. 2010;5:e12470.
[71] Wang J, Seth A, McCulloch CA. Force regulates smooth muscle actin in cardiac fibroblasts. American journal of physiology Heart and circulatory physiology. 2000;279:H2776-85.
[72] Buscemi L, Ramonet D, Klingberg F, Formey A, Smith-Clerc J, Meister JJ, et al. The single-molecule mechanics of the latent TGF-beta1 complex. Current biology : CB. 2011;21:2046-54.
[73] Wipff PJ, Rifkin DB, Meister JJ, Hinz B. Myofibroblast contraction activates latent TGF-beta1 from the extracellular matrix. The Journal of cell biology. 2007;179:1311-23.
[74] Jenkins RG, Su X, Su G, Scotton CJ, Camerer E, Laurent GJ, et al. Ligation of protease-activated receptor 1 enhances alpha(v)beta6 integrin-dependent TGF-beta activation and promotes acute lung injury. The Journal of clinical investigation. 2006;116:1606-14.
[75] Tomasek JJ, Martin MD, Vaughan MB, Cowan RL, Kropp BP. Myofibroblast contraction in granulation tissue is dependent on Rho kinase. Mol Biol Cell. 2000;11:88a-a.
[76] Li Q, Xu Y, Li X, Guo Y, Liu G. Inhibition of Rho-kinase ameliorates myocardial remodeling and fibrosis in pressure overload and myocardial infarction: role of TGF-beta1-TAK1. Toxicology letters. 2012;211:91-7.

[77] Zhang YM, Bo J, Taffet GE, Chang J, Shi J, Reddy AK, et al. Targeted deletion of ROCK1 protects the heart against pressure overload by inhibiting reactive fibrosis. FASEB journal : official publication of the Federation of American Societies for Experimental Biology. 2006;20:916-25.
[78] Godbout C, Follonier Castella L, Smith EA, Talele N, Chow ML, Garonna A, et al. The mechanical environment modulates intracellular calcium oscillation activities of myofibroblasts. PloS one. 2013;8:e64560.
[79] Huang C, Fu X, Liu J, Qi Y, Li S, Wang H. The involvement of integrin beta1 signaling in the migration and myofibroblastic differentiation of skin fibroblasts on anisotropic collagen-containing nanofibers. Biomaterials. 2012;33:1791-800.
[80] Meyer-ter-Vehn T, Han H, Grehn F, Schlunck G. Extracellular matrix elasticity modulates TGF-beta-induced p38 activation and myofibroblast transdifferentiation in human tenon fibroblasts. Investigative ophthalmology & visual science. 2011;52:9149-55.
[81] Huang X, Yang N, Fiore VF, Barker TH, Sun Y, Morris SW, et al. Matrix stiffness–induced myofibroblast differentiation is mediated by intrinsic mechanotransduction. American Journal of Respiratory Cell and Molecular Biology. 2012;47:340-8.
[82] Pelham RJ, Jr., Wang Y. Cell locomotion and focal adhesions are regulated by substrate flexibility. Proceedings of the National Academy of Sciences of the United States of America. 1997;94:13661-5.
[83] Ko KS, Arora PD, McCulloch CA. Cadherins mediate intercellular mechanical signaling in fibroblasts by activation of stretch-sensitive calcium-permeable channels. The Journal of biological chemistry. 2001;276:35967-77.
[84] Goffin JM, Pittet P, Csucs G, Lussi JW, Meister JJ, Hinz B. Focal adhesion size controls tension-dependent recruitment of alpha-smooth muscle actin to stress fibers. The Journal of cell biology. 2006;172:259-68.
[85] Bell E, Ivarsson B, Merrill C. Production of a tissue-like structure by contraction of collagen lattices by human fibroblasts of different proliferative potential in vitro. Proceedings of the National Academy of Sciences of the United States of America. 1979;76:1274-8.
[86] Tomasek JJ, Haaksma CJ, Eddy RJ, Vaughan MB. Fibroblast contraction occurs on release of tension in attached collagen lattices: dependency on an organized actin cytoskeleton and serum. The Anatomical record. 1992;232:359-68.
[87] Yang C, Tibbitt MW, Basta L, Anseth KS. Mechanical memory and dosing influence stem cell fate. Nature materials. 2014;13:645-52.
[88] Mosqueira D, Pagliari S, Uto K, Ebara M, Romanazzo S, Escobedo-Lucea C, et al. Hippo pathway effectors control cardiac progenitor cell fate by acting as dynamic sensors of substrate mechanics and nanostructure. ACS nano. 2014;8:2033-47.
[89] Lin Z, von Gise A, Zhou P, Gu F, Ma Q, Jiang J, et al. Cardiac-specific YAP activation improves cardiac function and survival in an experimental murine MI model. Circulation research. 2014;115:354-63.
[90] Xin M, Kim Y, Sutherland LB, Murakami M, Qi X, McAnally J, et al. Hippo pathway effector Yap promotes cardiac regeneration. Proceedings of the National Academy of Sciences of the United States of America. 2013;110:13839-44.
[91] Kshitiz, Park J, Kim P, Helen W, Engler AJ, Levchenko A, et al. Control of stem cell fate and function by engineering physical microenvironments. Integrative biology : quantitative biosciences from nano to macro. 2012;4:1008-18.
[92] Chaterji S, Kim P, Choe SH, Tsui JH, Lam CH, Ho DS, et al. Synergistic effects of matrix nanotopography and stiffness on vascular smooth muscle cell function. Tissue engineering Part A. 2014;20:2115-26.
[93] Beussman KM, Rodriguez ML, Leonard A, Taparia N, Thompson CR, Sniadecki NJ. Micropost arrays for measuring stem cell-derived cardiomyocyte contractility. Methods. 2016;94:43-50.

[94] Kim P, Yuan A, Nam KH, Jiao A, Kim DH. Fabrication of poly(ethylene glycol): gelatin methacrylate composite nanostructures with tunable stiffness and degradation for vascular tissue engineering. Biofabrication. 2014;6:024112.
[95] Kim DH, Han K, Gupta K, Kwon KW, Suh KY, Levchenko A. Mechanosensitivity of fibroblast cell shape and movement to anisotropic substratum topography gradients. Biomaterials. 2009;30:5433-44.
[96] Rouillard AD, Holmes JW. Mechanical boundary conditions bias fibroblast invasion in a collagen-fibrin wound model. Biophysical journal. 2014;106:932-43.
[97] Booth AJ, Hadley R, Cornett AM, Dreffs AA, Matthes SA, Tsui JL, et al. Acellular normal and fibrotic human lung matrices as a culture system for in vitro investigation. American journal of respiratory and critical care medicine. 2012;186:866-76.
[98] Ali SR, Ranjbarvaziri S, Talkhabi M, Zhao P, Subat A, Hojjat A, et al. Developmental heterogeneity of cardiac fibroblasts does not predict pathological proliferation and activation. Circulation research. 2014;115:625-35.
[99] Kanisicak O, Khalil H, Ivey MJ, Karch J, Maliken BD, Correll RN, et al. Genetic lineage tracing defines myofibroblast origin and function in the injured heart. Nature communications. 2016;7:12260.
[100] Pagliari S, Mosqueira D, Escobedo-lucea C, Goumans MJ, Pinto-do-o P, Aoyagi T, et al. Hippo pathway effectors YAP/TAZ control cardiac progenitor cell fate by acting as dynamic sensors of substrate mechanics and nanostructure. J Tissue Eng Regen M. 2014;8:178-.
[101] Nichol JW, Koshy ST, Bae H, Hwang CM, Yamanlar S, Khademhosseini A. Cell-laden microengineered gelatin methacrylate hydrogels. Biomaterials.31:5536-44.
[102] Van den Bulcke AI, Bogdanov B, De Rooze N, Schacht EH, Cornelissen M, Berghmans H. Structural and rheological properties of methacrylamide modified gelatin hydrogels. Biomacromolecules. 2000;1:31-8.
[103] Hutson CB, Nichol JW, Aubin H, Bae H, Yamanlar S, Al-Haque S, et al. Synthesis and characterization of tunable poly(ethylene glycol): gelatin methacrylate composite hydrogels. Tissue Eng Part A.
[104] Kim DH, Lipke EA, Kim P, Cheong R, Thompson S, Delannoy M, et al. Nanoscale cues regulate the structure and function of macroscopic cardiac tissue constructs. Proc Natl Acad Sci U S A.107:565-70.
[105] Kopycinska-Muller M, Geiss RH, Hurley DC. Contact mechanics and tip shape in AFM-based nanomechanical measurements. Ultramicroscopy. 2006;106:466-74.
[106] Derjaguin BV, Muller VM, Toporov YP. Effect of contact deformations on the adhesion of particles. Journal of Colloid and Interface Science. 1975;53:314-26.
[107] Benton JA, DeForest CA, Vivekanandan V, Anseth KS. Photocrosslinking of gelatin macromers to synthesize porous hydrogels that promote valvular interstitial cell function. Tissue Eng Part A. 2009;15:3221-30.
[108] Harms BD, Bassi GM, Horwitz AR, Lauffenburger DA. Directional persistence of EGF-induced cell migration is associated with stabilization of lamellipodial protrusions. Biophysical journal. 2005;88:1479-88.
[109] Jeong HE, Kwak R, Khademhosseini A, Suh KY. UV-assisted capillary force lithography for engineering biomimetic multiscale hierarchical structures: From lotus leaf to gecko foot hairs. Nanoscale. 2009;1:331-8.
[110] Suh KY, Kim YS, Lee HH. Capillary force lithography. Advanced Materials. 2001;13:1386-9.
[111] Wong HC, Tang WC. Finite element analysis of the effects of focal adhesion mechanical properties and substrate stiffness on cell migration. J Biomech.44:1046-50.
[112] Wells RG. The role of matrix stiffness in regulating cell behavior. Hepatology. 2008;47:1394-400.
[113] Engler A, Bacakova L, Newman C, Hategan A, Griffin M, Discher D. Substrate compliance versus ligand density in cell on gel responses. Biophys J. 2004;86:617-28.

[114] Georges PC, Janmey PA. Cell type-specific response to growth on soft materials. J Appl Physiol. 2005;98:1547-53.
[115] Engler AJ, Griffin MA, Sen S, Bonnemann CG, Sweeney HL, Discher DE. Myotubes differentiate optimally on substrates with tissue-like stiffness: pathological implications for soft or stiff microenvironments. J Cell Biol. 2004;166:877-87.
[116] Discher DE, Janmey P, Wang YL. Tissue cells feel and respond to the stiffness of their substrate. Science. 2005;310:1139-43.
[117] Albuquerque ML, Waters CM, Savla U, Schnaper HW, Flozak AS. Shear stress enhances human endothelial cell wound closure in vitro. American journal of physiology Heart and circulatory physiology. 2000;279:H293-302.
[118] Mericskay M, Parlakian A, Porteu A, Dandré F, Bonnet J, Paulin D, et al. An overlapping CArG/octamer element is required for regulation of desmin gene transcription in arterial smooth muscle cells. Developmental biology. 2000;226:192-208.
[119] Gonschior P, Gerheuser F, Gonschior G-M, Maier GR, Mack B, Nerlich A, et al. Experimental directional atherectomy injury in arterial vessels: impact of trauma depth on cellular response. American heart journal. 1995;129:1067-77.
[120] Dunn SA, Mohteshamzadeh M, Daly AK, Thomas TH. Altered Tropomyosin Expression in Essential Hypertension. Hypertension. 2003;41:347-54.
[121] van der Loop FT, Gabbiani G, Kohnen G, Ramaekers FC, van Eys GJ. Differentiation of smooth muscle cells in human blood vessels as defined by smoothelin, a novel marker for the contractile phenotype. Arteriosclerosis, thrombosis, and vascular biology. 1997;17:665-71.
[122] Egashira K. Molecular Mechanisms Mediating Inflammation in Vascular Disease: Special Reference to Monocyte Chemoattractant Protein-1. Hypertension. 2003;41:834-41.
[123] Weber KT. From inflammation to fibrosis: a stiff stretch of highway. Hypertension. 2004;43:716-9.
[124] Kim HR, Gallant C, Leavis PC, Gunst SJ, Morgan KG. Cytoskeletal remodeling in differentiated vascular smooth muscle is actin isoform dependent and stimulus dependent. American Journal of Physiology - Cell Physiology. 2008;295:C768-C78.
[125] Fukata Y, Amano M, Kaibuchi K. Rho-Rho-kinase pathway in smooth muscle contraction and cytoskeletal reorganization of non-muscle cells. Trends in pharmacological sciences. 2001;22:32.
[126] McBeath R, Pirone DM, Nelson CM, Bhadriraju K, Chen CS. Cell shape, cytoskeletal tension, and RhoA regulate stem cell lineage commitment. Developmental cell. 2004;6:483-95.
[127] Noma K, Oyama N, Liao JK. Physiological role of ROCKs in the cardiovascular system. American Journal of Physiology - Cell Physiology. 2006;290:C661-C8.
[128] Halayko AJ, Solway J. Invited Review: Molecular mechanisms of phenotypic plasticity in smooth muscle cells. Journal of Applied Physiology. 2001;90:358-68.
[129] Gunn J, Arnold N, Chan K, Shepherd L, Cumberland D, Crossman D. Coronary artery stretch versus deep injury in the development of in-stent neointima. Heart. 2002;88:401-5.
[130] Xie Z, Gong MC, Su W, Xie D, Turk J, Guo Z. Role of Calcium-independent Phospholipase A2β in High Glucose-induced Activation of RhoA, Rho Kinase, and CPI-17 in Cultured Vascular Smooth Muscle Cells and Vascular Smooth Muscle Hypercontractility in Diabetic Animals. Journal of Biological Chemistry. 2010;285:8628-38.
[131] Nohria A, Prsic A, Liu P-Y, Okamoto R, Creager MA, Selwyn A, et al. Statins inhibit Rho kinase activity in patients with atherosclerosis. Atherosclerosis. 2009;205:517-21.
[132] Bongalon S, Dai YP, Singer CA, Yamboliev IA. PDGF and IL-1β Upregulate Cofilin and LIMK2 in Canine Cultured Pulmonary Artery Smooth Muscle Cells. Journal of vascular research. 2004;41:412-21.
[133] Dai Y-P, Bongalon S, Tian H, Parks SD, Mutafova-Yambolieva VN, Yamboliev IA. Upregulation of profilin, cofilin-2 and LIMK2 in cultured pulmonary artery smooth muscle cells and in pulmonary arteries of monocrotaline-treated rats. Vascular Pharmacology. 2006;44:275-82.

[134] Lin T, Zeng L, Liu Y, DeFea K, Schwartz MA, Chien S, et al. Rho-ROCK-LIMK-Cofilin Pathway Regulates Shear Stress Activation of Sterol Regulatory Element Binding Proteins. Circulation Research. 2003;92:1296-304.
[135] Loirand G, Guérin P, Pacaud P. Rho Kinases in Cardiovascular Physiology and Pathophysiology. Circulation Research. 2006;98:322-34.
[136] Hardin CD, Vallejo J. Caveolins in vascular smooth muscle: Form organizing function. Cardiovascular research. 2006;69:808-15.
[137] Aravamudan B, VanOosten SK, Meuchel LW, Vohra P, Thompson M, Sieck GC, et al. Caveolin-1 knockout mice exhibit airway hyperreactivity. American Journal of Physiology-Lung Cellular and Molecular Physiology. 2012;303:L669-L81.
[138] Grande-García A, Echarri A, de Rooij J, Alderson NB, Waterman-Storer CM, Valdivielso JM, et al. Caveolin-1 regulates cell polarization and directional migration through Src kinase and Rho GTPases. The Journal of cell biology. 2007;177:683-94.
[139] Mouneimne G, Hansen SD, Selfors LM, Petrak L, Hickey MM, Gallegos LL, et al. Differential Remodeling of Actin Cytoskeleton Architecture by Profilin Isoforms Leads to Distinct Effects on Cell Migration and Invasion. Cancer cell. 2012;22:615-30.
[140] Nemir S, West JL. Synthetic materials in the study of cell response to substrate rigidity. Annals of biomedical engineering. 2010;38:2-20.
[141] Yeung T, Georges PC, Flanagan LA, Marg B, Ortiz M, Funaki M, et al. Effects of substrate stiffness on cell morphology, cytoskeletal structure, and adhesion. Cell Motility and the Cytoskeleton. 2005;60:24-34.
[142] Lee SK, Jung JM, Lee JS, Jung HT. Fabrication of complex patterns with a wide range of feature sizes from a single line prepattern by successive application of capillary force lithography. Langmuir.26:14359-63.
[143] Choi SS, Hong JP, Seo YS, Chung SM, Nah C. Fabrication and characterization of electrospun polybutadiene fibers crosslinked by UV irradiation. Journal of Applied Polymer Science. 2006;101:2333-7.
[144] Gupta P, Trenor SR, Long TE, Wilkes GL. In situ photo-cross-linking of cinnamate functionalized poly(methyl methacrylate-co-2-hydroxyethyl acrylate) fibers during electrospinning. Macromolecules. 2004;37:9211-8.
[145] Seunarine K, Gadegaard N, Tormen M, Meredith DO, Riehle MO, Wilkinson CD. 3D polymer scaffolds for tissue engineering. Nanomedicine (Lond). 2006;1:281-96.
[146] Zhang K, Liu T, Li JA, Chen JY, Wang J, Huang N. Surface modification of implanted cardiovascular metal stents: From anti-thrombosis and anti-restenosis to endothelialization. Journal of biomedical materials research Part A. 2013.
[147] Lowe HC, Oesterle SN, Khachigian LM. Coronary in-stent restenosis: current status and future strategies. Journal of the American College of Cardiology. 2002;39:183-93.
[148] Shirota T, Yasui H, Shimokawa H, Matsuda T. Fabrication of endothelial progenitor cell (EPC)-seeded intravascular stent devices and in vitro endothelialization on hybrid vascular tissue. Biomaterials. 2003;24:2295-302.
[149] Hu X, Ma L, Wang C, Gao C. Gelatin hydrogel prepared by photo-initiated polymerization and loaded with TGF-beta1 for cartilage tissue engineering. Macromol Biosci. 2009;9:1194-201.
[150] Fomovsky GM, Thomopoulos S, Holmes JW. Contribution of extracellular matrix to the mechanical properties of the heart. Journal of molecular and cellular cardiology. 2010;48:490-6.
[151] Kim P, Yuan A, Nam K-H, Jiao A, Kim D-H. Fabrication of poly(ethylene glycol): gelatin methacrylate composite nanostructures with tunable stiffness and degradation for vascular tissue engineering. Biofabrication. 2014;6:024112.

[152] Kim P, Kim DH, Kim B, Choi SK, Lee SH, Khademhosseini A, et al. Fabrication of nanostructures of polyethylene glycol for applications to protein adsorption and cell adhesion. Nanotechnology. 2005;16:2420-6.
[153] Kim DH, Seo CH, Han K, Kwon KW, Levchenko A, Suh KY. Guided Cell Migration on Microtextured Substrates with Variable Local Density and Anisotropy. Adv Funct Mater. 2009;19:1579-86.
[154] Kim DH, Kim P, Song I, Cha JM, Lee SH, Kim B, et al. Guided three-dimensional growth of functional cardiomyocytes on polyethylene glycol nanostructures. Langmuir : the ACS journal of surfaces and colloids. 2006;22:5419-26.
[155] Kim DH, Kshitiz, Smith RR, Kim P, Ahn EH, Kim HN, et al. Nanopatterned cardiac cell patches promote stem cell niche formation and myocardial regeneration. Integrative biology : quantitative biosciences from nano to macro. 2012;4:1019-33.
[156] Dhanjal TS, Lellouche N, von Ruhland CJ, Abehsira G, Edwards DH, Dubois-Rande JL, et al. Massive Accumulation of Myofibroblasts in the Critical Isthmus Is Associated With Ventricular Tachycardia Inducibility in Post-Infarct Swine Heart. JACC Clinical electrophysiology. 2017;3:703-14.
[157] van Putten S, Shafieyan Y, Hinz B. Mechanical control of cardiac myofibroblasts. Journal of molecular and cellular cardiology. 2016;93:133-42.
[158] Kim P, Chu N, Davis J, Kim D-H. Mechanoregulation of Myofibroblast Fate and Cardiac Fibrosis. Advanced Biosystems. 2018;2:1700172.
[159] Biernacka A, Frangogiannis NG. Aging and Cardiac Fibrosis. Aging and disease. 2011;2:158-73.
[160] Pinto AR, Ilinykh A, Ivey MJ, Kuwabara JT, D'Antoni ML, Debuque R, et al. Revisiting Cardiac Cellular Composition. Circulation research. 2016;118:400-9.
[161] Hinz B. The extracellular matrix and transforming growth factor-beta1: Tale of a strained relationship. Matrix biology : journal of the International Society for Matrix Biology. 2015;47:54-65.
[162] Klingberg F, Hinz B, White ES. The myofibroblast matrix: implications for tissue repair and fibrosis. The Journal of pathology. 2013;229:298-309.
[163] Carson D, Hnilova M, Yang X, Nemeth CL, Tsui JH, Smith AS, et al. Nanotopography-Induced Structural Anisotropy and Sarcomere Development in Human Cardiomyocytes Derived from Induced Pluripotent Stem Cells. ACS applied materials & interfaces. 2016;8:21923-32.
[164] Chen W, Frangogiannis NG. Fibroblasts in post-infarction inflammation and cardiac repair. Biochimica et biophysica acta. 2013;1833:945-53.
[165] Ma Y, de Castro Bras LE, Toba H, Iyer RP, Hall ME, Winniford MD, et al. Myofibroblasts and the extracellular matrix network in post-myocardial infarction cardiac remodeling. Pflugers Archiv : European journal of physiology. 2014;466:1113-27.
[166] Xing Q, Vogt C, Leong KW, Zhao F. Highly Aligned Nanofibrous Scaffold Derived from Decellularized Human Fibroblasts. Advanced functional materials. 2014;24:3027-35.
[167] Segura AM, Frazier OH, Buja LM. Fibrosis and heart failure. Heart failure reviews. 2014;19:173-85.
[168] Velasquez LS, Sutherland LB, Liu Z, Grinnell F, Kamm KE, Schneider JW, et al. Activation of MRTF-A-dependent gene expression with a small molecule promotes myofibroblast differentiation and wound healing. Proceedings of the National Academy of Sciences of the United States of America. 2013;110:16850-5.
[169] Meyer-Ter-Vehn T, Gebhardt S, Sebald W, Buttmann M, Grehn F, Schlunck G, et al. p38 inhibitors prevent TGF-beta-induced myofibroblast transdifferentiation in human tenon fibroblasts. Investigative ophthalmology & visual science. 2006;47:1500-9.
[170] Kessler D, Dethlefsen S, Haase I, Plomann M, Hirche F, Krieg T, et al. Fibroblasts in mechanically stressed collagen lattices assume a "synthetic" phenotype. The Journal of biological chemistry. 2001;276:36575-85.

[171] Kim J, Kim HN, Lim KT, Kim Y, Seonwoo H, Park SH, et al. Designing nanotopographical density of extracellular matrix for controlled morphology and function of human mesenchymal stem cells. Scientific reports. 2013;3:3552.
[172] Dalby MJ, Gadegaard N, Oreffo RO. Harnessing nanotopography and integrin-matrix interactions to influence stem cell fate. Nature materials. 2014;13:558-69.
[173] Zhao B, Li L, Tumaneng K, Wang CY, Guan KL. A coordinated phosphorylation by Lats and CK1 regulates YAP stability through SCF(beta-TRCP). Genes & development. 2010;24:72-85.
[174] Molkentin JD, Bugg D, Ghearing N, Dorn LE, Kim P, Sargent MA, et al. Fibroblast-Specific Genetic Manipulation of p38 Mitogen-Activated Protein Kinase In Vivo Reveals Its Central Regulatory Role in Fibrosis. Circulation. 2017;136:549-61.
[175] Corradetti A, Saccucci F, Emanuelli M, Vagnoni G, Cecati M, Sartini D, et al. The role of p38alpha mitogen-activated protein kinase gene in the HELLP syndrome. Cell stress & chaperones. 2010;15:95-100.
[176] Wang L, Ma R, Flavell RA, Choi ME. Requirement of mitogen-activated protein kinase kinase 3 (MKK3) for activation of p38alpha and p38delta MAPK isoforms by TGF-beta 1 in murine mesangial cells. The Journal of biological chemistry. 2002;277:47257-62.
[177] Bernau K, Torr EE, Evans MD, Aoki JK, Ngam CR, Sandbo N. Tensin 1 Is Essential for Myofibroblast Differentiation and Extracellular Matrix Formation. Am J Respir Cell Mol Biol. 2017;56:465-76.
[178] Ray A, Lee O, Win Z, Edwards RM, Alford PW, Kim DH, et al. Anisotropic forces from spatially constrained focal adhesions mediate contact guidance directed cell migration. Nature communications. 2017;8:14923.
[179] Remy G, Risco AM, Inesta-Vaquera FA, Gonzalez-Teran B, Sabio G, Davis RJ, et al. Differential activation of p38MAPK isoforms by MKK6 and MKK3. Cellular signalling. 2010;22:660-7.
[180] Stein C, Bardet AF, Roma G, Bergling S, Clay I, Ruchti A, et al. YAP1 Exerts Its Transcriptional Control via TEAD-Mediated Activation of Enhancers. PLoS genetics. 2015;11:e1005465.
[181] Lin KC, Moroishi T, Meng Z, Jeong HS, Plouffe SW, Sekido Y, et al. Regulation of Hippo pathway transcription factor TEAD by p38 MAPK-induced cytoplasmic translocation. Nature cell biology. 2017;19:996-1002.
[182] Dostal DE, Feng H, Nizamutdinov D, Golden HB, Afroze SH, Dostal JD, et al. Mechanosensing and Regulation of Cardiac Function. Journal of clinical & experimental cardiology. 2014;5:314.
[183] Ohashi K, Fujiwara S, Mizuno K. Roles of the cytoskeleton, cell adhesion and rho signalling in mechanosensing and mechanotransduction. Journal of biochemistry. 2017;161:245-54.
[184] Nardone G, Oliver-De La Cruz J, Vrbsky J, Martini C, Pribyl J, Skladal P, et al. YAP regulates cell mechanics by controlling focal adhesion assembly. Nature communications. 2017;8:15321.
[185] Uto K, Ebara M, Aoyagi T. Temperature-responsive poly(epsilon-caprolactone) cell culture platform with dynamically tunable nano-roughness and elasticity for control of myoblast morphology. International journal of molecular sciences. 2014;15:1511-24.
[186] Fu X, Khalil H, Kanisicak O, Boyer JG, Vagnozzi RJ, Maliken BD, et al. Specialized fibroblast differentiated states underlie scar formation in the infarcted mouse heart. The Journal of clinical investigation. 2018;128:2127-43.

VITA

Peter Kim was born and raised in Ann Arbor, MI. He received his Bachelor of Science degree in Department of Biomedical Engineering, and Department of Applied Mathematics and Statistics from Johns Hopkins University in 2012. He earned his PhD in Department of Bioengineering from the University of Washington in 2018.